NAVAL POSTGRADUATE SCHOOL

Monterey, California

AD-A261 721

DTIC
S **ELECTE**
MAR 2 3 1993
C **D**

THESIS

AN EXPERIMENTAL STUDY
OF THE RESPONSE OF SMALL TUNNEL THRUSTERS
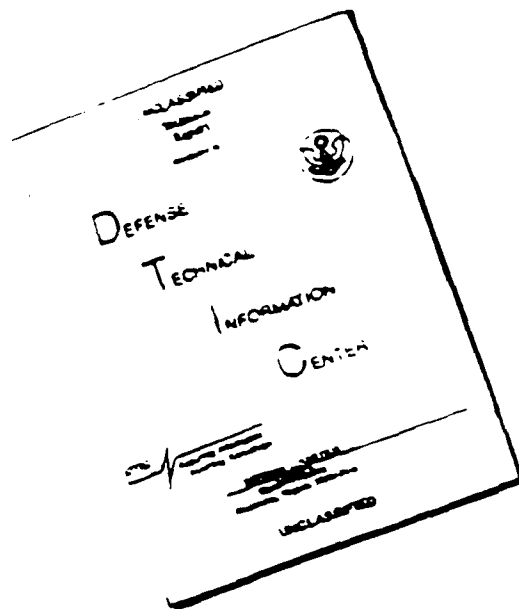TO TRIANGULAR AND SQUARE WAVE INPUTS

by

Steven E. Cody

December, 1992

Thesis Advisor: Anthony J. Healey

Approved for public release; distribution is unlimited

93-05924

93 3 22 016

DISCLAIMER NOTICE

THIS DOCUMENT IS BEST QUALITY AVAILABLE. THE COPY FURNISHED TO DTIC CONTAINED A SIGNIFICANT NUMBER OF PAGES WHICH DO NOT REPRODUCE LEGIBLY.

REPORT DOCUMENTATION PAGE

1a. REPORT SECURITY CLASSIFICATION UNCLASSIFIED	1b. RESTRICTIVE MARKINGS

2a. SECURITY CLASSIFICATION AUTHORITY	3. DISTRIBUTION/AVAILABILITY OF REPORT
2b. DECLASSIFICATION/DOWNGRADING SCHEDULE	Approved for public release; distribution is unlimited.

4. PERFORMING ORGANIZATION REPORT NUMBER(S)	5. MONITORING ORGANIZATION REPORT NUMBER(S)

6a. NAME OF PERFORMING ORGANIZATION Naval Postgraduate School	6b. OFFICE SYMBOL (If applicable) 34	7a. NAME OF MONITORING ORGANIZATION Naval Postgraduate School

6c. ADDRESS (City, State, and ZIP Code) Monterey, CA 93943-5000	7b. ADDRESS (City, State, and ZIP Code) Monterey, CA 93943-5000

8a. NAME OF FUNDING/SPONSORING ORGANIZATION	8b. OFFICE SYMBOL (If applicable)	9. PROCUREMENT INSTRUMENT IDENTIFICATION NUMBER

8c. ADDRESS (City, State, and ZIP Code)	10. SOURCE OF FUNDING NUMBERS			
	Program Element No.	Project No.	Task No.	Work Unit Accession Number

11. TITLE (Include Security Classification)
AN EXPERIMENTAL STUDY OF THE RESPONSE OF SMALL TUNNEL THRUSTERS TO TRIANGULAR AND SQUARE WAVE INPUTS

12. PERSONAL AUTHOR(S) CODY, STEVEN E.

13a. TYPE OF REPORT Master's Thesis	13b. TIME COVERED From To	14. DATE OF REPORT (year, month, day) DECEMBER 1992	15. PAGE COUNT 116

16. SUPPLEMENTARY NOTATION
The views expressed in this thesis are those of the author and do not reflect the official policy or position of the Department of Defense or the U.S. Government.

17. COSATI CODES			18. SUBJECT TERMS (continue on reverse if necessary and identify by block number)
FIELD	GROUP	SUBGROUP	THRUSTERS, DYNAMIC RESPONSE
			AUTONOMOUS UNDERWATER VEHICLES (AUV)

19. ABSTRACT (continue on reverse if necessary and identify by block number)

The response of small tunnel thrusters to triangular and square wave changes in applied voltages to the thruster motor is studied. Previous mathematical models have attempted to identify the dynamic characteristics in thruster responses in order to minimize limit cycling in underwater vehicle position control. These experiments validate the effect of fluid inertia in the tunnel for long and shorter period commands. Additionally, the presence of a transient lag between changes in propeller speed and affected water column velocity has been identified which delays and reduces the transient peak thrust for shorter period triangular waves and square wave input signals.

20. DISTRIBUTION/AVAILABILITY OF ABSTRACT ☒ UNCLASSIFIED/UNLIMITED ☐ SAME AS REPORT ☐ DTIC USERS	21. ABSTRACT SECURITY CLASSIFICATION UNCLASSIFIED	
22a. NAME OF RESPONSIBLE INDIVIDUAL Anthony J. Healey	22b. TELEPHONE (Include Area code) (408) 646-3462	22c. OFFICE SYMBOL ME/HY

DD FORM 1473, 84 MAR 83 APR edition may be used until exhausted SECURITY CLASSIFICATION OF THIS PAGE
All other editions are obsolete UNCLASSIFIED

An Experimental Study
of the Response of Small Tunnel Thrusters
to Triangular and SquareWave Inputs

by

Steven E. Cody
Lieutenant Commander, United States Navy
B.S., College of William and Mary in Virginia, 1978

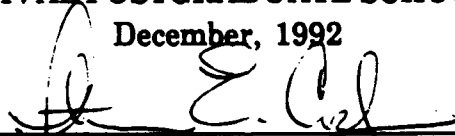Submitted in partial fulfillment
of the requirements for the degree of

MASTER OF SCIENCE IN MECHANICAL ENGINEERING

from the

NAVAL POSTGRADUATE SCHOOL
December, 1992

Author: _____
Steven E. Cody

Approved by: _____
Anthony J. Healey, Thesis Advisor

_____
Matthew D. Kelleher, Chairman
Department of Mechanical Engineering

ABSTRACT

The response of small tunnel thrusters to triangular and square wave changes in applied voltages to the thruster motor is studied. Previous mathematical models have attempted to identify the dynamic characteristics in thruster responses in order to minimize limit cycling in underwater vehicle position control. These experiments validate the effect of fluid inertia in the tunnel for long and shorter period commands. Additionally, the presence of a transient lag between changes in propeller speed and affected water column velocity has been identified which delays and reduces the transient peak thrust for shorter period triangular waves and square wave input signals.

iii

TABLE OF CONTENTS

LIST OF FIGURES

NOMENCLATURE

A	cross sectional area of the thruster
C_M	motor shaft viscous friction coefficient
C_P	propeller shaft viscous friction coefficient
C_{PM}	combined propeller and motor shaft viscous friction coefficients applied to the motor
i	current
J_{DG}	polar mass moment of inertia for the pinion
J_M	polar mass moment of inertia for the motor
J_P	polar mass moment of inertia for the propeller
J_{PM}	polar mass moment of inertia for the propeller, ring gear, motor and pinion
Ka	added mass coefficient
K_M	motor back EMF constant
K_T	motor torque constant
L	length of the thruster tunnel
L_a	added length factor
L_B	effective length of propeller blade
N	reduction gear ratio
p	propeller pitch
T	thrust
t_c	time constant for water column velocity response
U	water column velocity

$\Delta\alpha$	kinetic energy correction factor
$\Delta\beta$	momentum flux correction factor
η	propeller slip efficiency
ω_M	motor angular velocity
ω_P	propeller angular velocity
ρ	fluid density
σ	propeller torque/thrust conversion factor
τ_H	propeller torque (hydrodynamic)
τ_M	motor torque
τ_P	propeller torque (inertial)

ACKNOWLEDGEMENTS

I would like to take this opportunity to thank several individuals who have significantly contributed to the preparation of this thesis.

- Dr. Anthony J. Healey, my thesis advisor, who was always available, for his inspiration and generous assistance.

- Mr. David Marco, Department of Mechanical Engineering, Naval Postgraduate School, who designed the thruster and and laid the basic material ground work for this thesis.

- Mr. Mike Lee and Mr. Dick Burton of the Monterey Bay Aquarium Research Institute for their outstanding technical advice and ready material support.

- Mr. Tom McCord, Mr. Jim Selby, Mr. Tom Christian, Mr. Charles Crow and Mr. Tom Smottlatch, all of the Department of Mechanical Engineering, Naval Postgraduate School, for their outstanding cooperation and superb technical and material assistance.

- and lastly but most importantly, my wife Jayne and daughter Eryn, without whose love, continuous moral support and personal sacrifices I would not have been able to complete this work.

I. INTRODUCTION

A. BACKGROUND

As the use of Remotely Operated Vehicles (ROV's) has become more widespread, their tasking more complex and the emergence of Autonomous Underwater Vehicles (AUV's) as a potentially viable platform for a multitude of subsea operations, the need for precise vehicle control has become paramount. The maneuvering and control of vehicles at moderate to high speeds is well documented and reasonably well understood. The slow speed control and dynamic positioning, however, involve many nonlinearities and modeling uncertainties. The generally accepted method of maneuvering ROV's and AUV's is through the use of thrusters mounted on or otherwise attached to the vehicles. A thorough understanding of the behavior of these thrusters and their interaction with the surrounding water column is required in order to provide a control system with an accurate model on which to base responses and provide optimum control.

Work performed by Yoerger and Cooke at the Massachusetts Institute of Technology/Woods Hole Oceanographic Institute (WHOI) noted that thruster dynamics dominate the behavior of closed loop controlled vehicles and produce limit cycles or

1

positioning hysteresis problems, even in the absence of external disturbances [Refs. 1 and 2].

McLean of the Naval Postgraduate School (NPGS), however, investigating the dynamics of tunnel thrusters for the NPGS AUV II, noted an initial peak thrust with decay to steady state following a step voltage input which would indicate a leading system, conducive to system stabilization [Ref.3]. The difference between the WHOI model was the acceleration of the added mass of the water column in the tunnel.

Further investigation of the dynamics problem by Miles of the Monterey Bay Aquarium Research Institute and Stanford Aerospace Research Laboratory (MBARI/SARL) indicated that neither of the previous two models accurately described a rapid transient condition and attributed this to arising from sudden start motion dynamics in the angle of attack of the water column on the accelerating propeller blades [Ref. 4].

B. SCOPE OF THESIS

The intent of this thesis is to build on the modeling begun by McLean in 1990 and to provide the necessary corrections to update the models to account for the water column velocity lag in response to propeller acceleration. Additionally, the effects of tunnel length and propeller pitch on the mathematical model are quantified by new carefully instrumented experiments to verify their effects on the models. An experimental apparatus based on an actual AUV II

tunnel thruster has been utilized to provide data under various dynamic conditions. The ultimate product of this research is to provide an accurate model for the tunnel thrusters onboard the AUV II to be used for and verified during slow speed maneuvering and hovering trials.

Chapter II will, in depth, cover the derivations of the mathematical model of this system. Chapter III will describe the experimental apparatus and procedures utilized to obtain the data. This will include block diagrams of the system and calibration procedures. Chapter IV will discuss the results of the raw data and how the variables influenced the results. Chapter V will present a comparison between the modeled simulations and actual laboratory responses. Chapter VI will summarize the results of this thesis, present conclusions and make recommendations for further research. Appendicies will be included to provide computer programs utilized in the course of this research.

II. THRUSTER MODELING

A. AUV II TUNNEL THRUSTERS

The NPS AUV II employs four tunnel thrusters for slow speed maneuvering and hovering/station keeping. These thrusters are mounted in pairs athwartships, both horizontally and vertically, located forward and aft of the center of gravity of the vehicle. This is to reduce drag during forward flight and is contrasted to externally mounted, pivoting ducted thrusters typically found on most Remotely Operated Vehicles (ROVs). The thruster assemblies for the NPS AUV II are basically composed of a DC servomotor, a set of reduction gears, a propeller and thruster tunnels. The relatively small size of the AUV and subsequent small diameter of the horizontal and vertical thruster tunnels, required that the thruster motors be mounted external to the tunnels (within the body of the AUV) and that some special arrangement for driving the propellers be employed. This contrasts with the normal configuration for thrusters of ROVs, which have a drive motor directly in line with the propeller. This configuration did two things; first, it provided the potential for the thruster to be equally efficient in either direction by removing the motor body from either the suction or discharge side of the propeller. Secondly, it required that the propeller be

mounted in a ring gear such that the servomotor, coupled directly to a pinion gear, could drive the propeller from the outside. Figure 1 shows a cross section view of the thruster assembly. This is essentially the same configuration modeled by McLean [Ref. 3] with minor modifications and will be repeated here for clarity.

1. Servomotor

The servomotors are Pittman PITMO DC Model 14202[1] series with a nominal outside diameter of 2.125 inches and 3.40 inches in length, not including the length of the shaft. They have a stall torque of 106 ounce-inches, a no load speed of 3820 RPM and a peak power draw of 333 watts. Operating at 24 volts (winding number 3), the motor has a no load current rating of 0.230 amps. Motor speed is adjusted through an Advance Motion Controls PWM Servo Amplifier Model 30A8DD[2]. The PWM servo amplifier utilizes a zero to ten volt control signal to modulate the pluse width of a 24 volt, 5 - 45 KHz (load dependent) output signal to the motor. This effectively provides a zero to 24 volt averaged signal to supply the motor with a bandwidth well beyond the bandwidth of the motor. Direction of the motor operation is controlled by changing the polarity of the control signal.

---

[1] Manufactured by Pittman Division of Penn Engineering and Manufacturing Corporation, Harleysville, PA.

[2] Manufactured by Advanced Motion Controls, Camarillo, CA.

Reduction Gear Housing

Pinion Gear

Seal

3.0 inch I.D. PVC Pipe

Propeller Shaft Bearing

Ring Gear

Motor Housing

Servomotor

Speed Sensor

Propeller

Propeller Shaft Strut
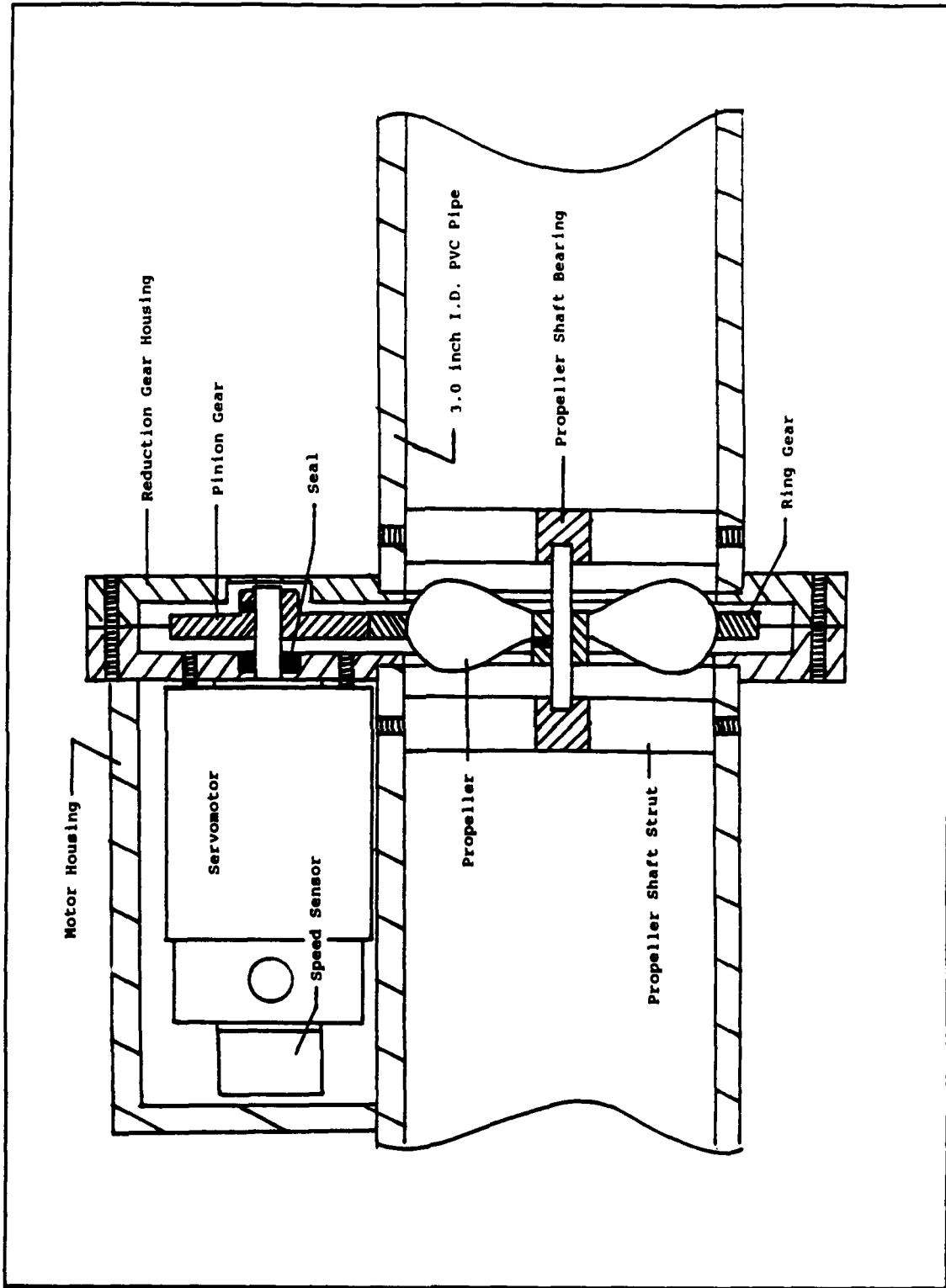
Figure 1 Cross Section View of Thruster Assembly

6

2. Reduction Gears

The gearing that connects the motor to the propeller is a set of spur gears, a pinion and gear, made of Delrin[3]. Both the pinion and the gear have a pitch of 24 teeth per inch; the pinion with 45 teeth and a pitch diameter of 1.875 inches and the gear with 90 teeth and a pitch diameter of 3.750 inches. This results in a reduction ratio of 2:1. As indicated above, the gear was converted to a ring gear by removing a three inch diameter disk from the center of the gear. The propeller was then inserted in the opening and rigidly affixed to the ring gear.

3. Propeller

Two different propellers were fabricated locally in the machine shop for this experiment. They were of a Kaplan type with four blades and pitch angles of approximately 30 and 45 degrees respectively. The pitch angle remained relatively constant along the entire length of the blade and this quality, along with a zero camber, permitted them to be equally effective in either forward or reverse directions. The thrust from the propeller is transferred to the vehicle via a thrust/journal bearing, made of PVC, located in two struts mounted axially in the tunnels on either side of the reduction gear housing to support the propeller shaft.

---

[3] Registered Trademark, Winfred M. Berg Company, East Rockaway, NY.

4. Thruster Tunnels

The tunnels for the thrusters are constructed of 3.0 inch inside diameter, schedule 40 PVC plastic pipe. The overall lengths of the tunnels are 16.5 and 10.0 inches for the horozontal and vertical thrusters respectively. These dimensions correspond to the outside dimensions of the AUV II body in the horozontal and vertical planes. The reduction gear housing, containing the propeller, is located at the mid-point of each tunnel.

B. THRUSTER MODELING

There exist two basic models for describing thruster dynamics; one developed at the Woods Hole Oceanographic Institute (WHOI) by Yoerger, Cooke, and Slotine [Ref. 1] and one by McLean at the Naval Postgraduate School (NPGS) [Ref. 3]. The WHOI model was based on experimentation with a shrouded thruster whereas McLean's model reflected that of a tunnel thruster. Both of these models were based on a lumped mass, one dimensional technique, the McLean model, however, included the acceleration of a cylinder of water through the thruster tunnel. The models are summarized in Figure 2.

Adams, of the Monterey Bay Aquarium Research Institute and Stanford Aerospace Robotics Laboratory (MBARI/SARL) evaluated both models for a step torque input and noted that the WHOI model predicted a lag response and the NPGS model predicted a lead response. The difference in the thrust response of the

8

Torque: $\tau = K_I \dot{\omega} + K_{II}\omega|\omega|$

Thrust: $T = K_{III}\dot{\omega} + K_{IV}\omega|\omega|$

WHOI MODEL

$K_I = (\eta p)^2 \rho V$
$K_{II} = 0.5(\eta p)^3 \rho A$
$K_{III} = 0$
$K_{IV} = (\eta p)^2 \rho A$

McLEAN MODEL

$K_I = (\eta p)^2 \rho AL(Ka+1)\Delta\beta$
$K_{II} = 0.5(\eta p)^3 \rho A\Delta\alpha$
$K_{III} = (\eta p)\rho AL(Ka+1)$
$K_{IV} = (\eta p)^2 \rho A\Delta\beta$

Figure 2 Previous Thruster Dynamics Models in Response to Propeller Speed Changes

two models is the result of a water column acceleration term in the NPGS model. Adams went on to say that the models could be further simplified by identifying four constants (K_I, K_{II}, K_{III} and K_{IV}) using the nomenclature of McLean as follows;

$$\tau = K_I\dot{\omega} + K_{II}\omega|\omega|$$

and

$$T = K_{III}\dot{\omega} + K_{IV}\omega|\omega|$$

where the constants could be found from empirical thruster tests for steady state and step torque responses [Ref. 5].

Recent research by Miles, also of MBARI/SARL, indicates that a deficiency exists in both models, in that they fail to take into account lags in the effective angle of attack of the

9

propeller on the thrust. These may be significant when extremely rapid propeller speed changes are commanded. It is intuitive that as the propeller accelerates, the velocity of the water column will lag and the angle of attack of the propeller will increase until the water column can accelerate. As the velocity of the water column increases, the angle of attack will decrease and, at a steady state torque input, the thrust will eventually become proportional to the square of the propeller speed. The previous models relate the volumetric flow rate of the water column directly to the speed of the propeller without taking into account this lag.

In order to provide continuity for the presentation of this paper and since the thruster is essentially identical to the thruster evaluated by McLean, the derivation of most of the mathematical model will be repeated here based on McLean's model. In order to construct this model, however, the thruster will be divided into three simple physical subsystems; electrical, mechanical and hydrodynamic. These three areas will then be related through system constraints and a combined model will be produced.

1. Electrical Model

The electrical portion of this model consists of a voltage source connected to a motor as depicted in Figure 3. The motor law relates the torque generated by the motor as a function of the current applied;

$$\tau_M = K_T i$$

and the generator law relates the back EMF as a function of motor angular velocity;

$$e = K_M \omega_M$$

Solving for the current utilizing Kirchoff's voltage law and neglecting winding inductance yields:

$$i = \frac{Vs - K_M \omega_M}{R}$$

Substituting the current into the motor torque equation provides torque as a function of the voltage applied and the motor speed;

$$\tau_M = \frac{K_T}{R} Vs - \frac{K_T K_M}{R} \omega_M$$

2. Mechanical Model

For the mechanical portion, three distinct subsections will be evaluated; the motor shaft, the propeller shaft and the connecting gear box. The mechanical torque loading on the motor shaft is a combination of the inertial, friction and applied loads as represented by;
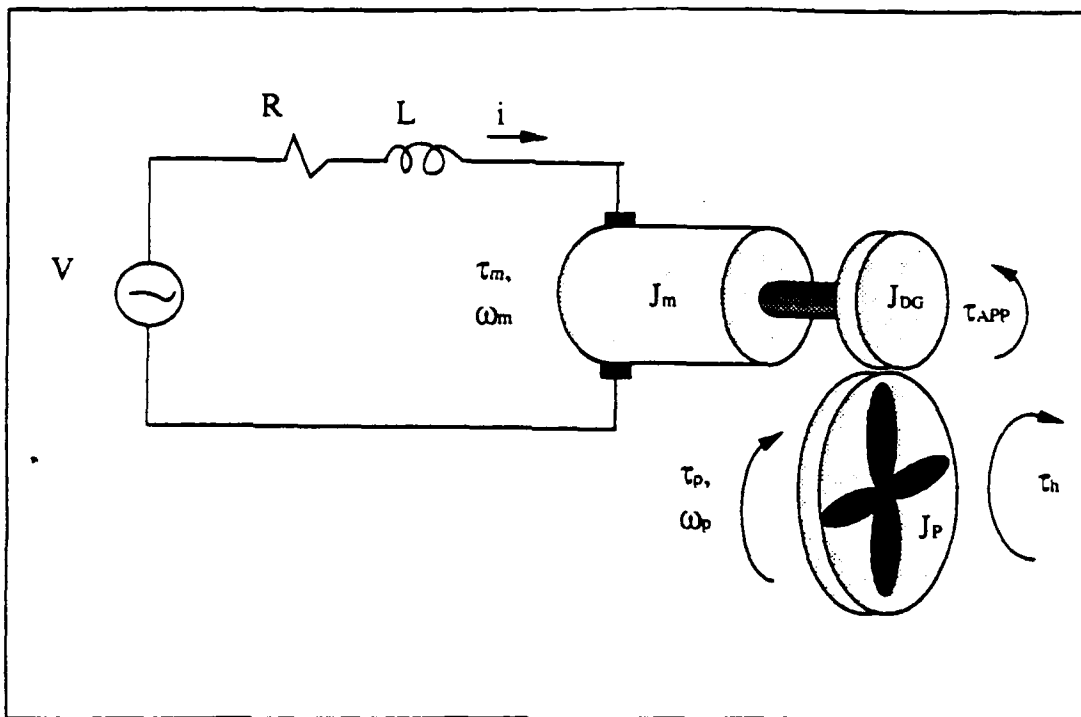
Figure 3 Lumped Mass Thruster Model

$$\tau_M = (J_M + J_{DG})\, \dot{\omega}_M + C_M \omega_M + \tau_{APPL}$$

where the torque applied (τ_{APPL}) by the pinion is equated to the inertial, damping and hydrodynamic load torques on the propeller:

$$\tau_{APPL} \approx \frac{\tau_P + \tau_H}{N}$$

The inertial and damping torque on the propeller is given by;

$$\tau_P = J_P \dot{\omega}_P + C_P \omega_P$$

and the mechanical relationship between the pinion and the propeller gear is;

$$\omega_M = N\omega_P$$

Combining the above equations and solving for the motor torque in terms of the motor speed yeilds;

$$\tau_M = (J_M + J_{DG} + \frac{J_P}{N^2})\dot{\omega}_M + (C_M + \frac{C_P}{N^2})\omega_M + \frac{\tau_H}{N}$$

3. Hydrodynamic Load Model

From McLean's model the hydrodynamic loading on the propeller is expressed as;

$$\tau_H = (\eta p)^2 \rho AL(Ka+1)\Delta\beta\dot{\omega}_P + \frac{(\eta p)\rho A}{2}\Delta\alpha\omega_P|\omega_P|$$

If we let

$$K_I = (\eta p)^2 \rho AL(Ka+1)\Delta\beta$$

and

$$K_{II} = \frac{(\eta p)}{2}\rho A\Delta\alpha$$

13

then the expression reduces to;

$$\tau_H = \frac{K_I}{N}\dot{\omega}_M + \frac{K_{II}}{N^2}\omega_M|\omega_M|$$

Again from McLean's model we obtain an expression for the thrust as;

$$T = \eta p A \rho L (Ka+1)\dot{\omega}_P + (\eta p)^2 A \rho (\Delta\beta)\omega_P|\omega_P|$$

If we let

$$K_{III} = (\eta p)\rho A L (Ka+1)$$

and

$$K_{IV} = (\eta p)^2\rho A \Delta\beta$$

the equation reduces to;

$$T = \frac{K_{III}}{N}\dot{\omega}_M + \frac{K_{IV}}{N^2}\omega_M|\omega_M|$$

4. Combined Model

Substituting the expression for the hydrodynamic loading on the propeller into the mechanical model yields the following expression for motor torque:

$$\tau_M = (J_M + J_{DG} + \frac{J_P + K_I}{N^2})\dot{\omega}_M + (C_M + \frac{C_P}{N^2})\omega_M + \frac{K_{II}}{N^3}\omega_M|\omega_M|$$

14

Setting the electrical model and hydromechanical models for motor torque equal to each other and solving in terms of motor speed yields the following first order differential equation:

$$\dot{\omega}_M = -\frac{(J_M + J_{DG} + \frac{J_P + K_I}{N^2})}{(C_M + \frac{C_P}{N^2} + \frac{K_T K_M}{R})} \omega_M - \frac{K_{II}}{K_2 N^3} \omega_M |\omega_M| + \frac{\frac{K_T}{R}}{(J_M + J_{DG} + \frac{J_P + K_I}{N^2})} V_S$$

If we let

$$K_2 = (J_M + J_{DG} + \frac{J_P + K_I}{N^2})$$

and

$$K_1 = \frac{K_T}{R}$$

and

$$K_0 = (C_M + \frac{C_P}{N^2} + \frac{K_T K_M}{R})$$

the differential equation simplifies to;

$$\dot{\omega}_M = (-\frac{K_0}{K_2}) \omega_M - \frac{K_{II}}{K_2 N^3} \omega_M |\omega_M| + \frac{K_1}{K_2} V_S$$

Substituting this equation into the hydrodynamic equation for thrust yeilds a quadratic equation in terms of ω_M, ω_M^2 and Vs:

$$T = -\frac{K_{III}K_0}{NK_2}\omega_M + (\frac{K_{IV}}{N^2} - \frac{K_{III}K_{II}}{K_2 N^4})\omega_M|\omega_M| + \frac{K_{III}K_1}{NK_2}Vs$$

5. Extension of Model to include Blade--Flow Speed Lags

In order to take into account and model the lag between the propeller speed changes and the resulting water column velocity change, portions of the above model need to be modified. Recall that the mechanical torque on the motor can be expressed as a function of the inertial, friction and hydrodynamic loads;

$$\tau_M = J_{PM}\dot{\omega}_M + C_{PM}\omega_M + \frac{\tau_H}{N}$$

where

$$J_{PM} = (J_M + J_{DG} + \frac{J_P}{N^2})$$

and

$$C_{PM} = (C_M + \frac{C_P}{N^2})$$

16

Also recall that the electrical torque on the motor can be expressed as;

$$\tau_M = K_T i$$

where

$$i = \frac{Vs - K_M \omega_M}{R}$$

Setting the electrical and mechanical torques equal to each other, substituting for the current and solving for angular acceleration yields;

$$\dot{\omega}_M = -\frac{(C_{PM} + \frac{K_T K_M}{R})}{J_{PM}} \omega_M + \frac{K_T}{R J_{PM}} Vs - \frac{\tau_H}{N J_{PM}}$$

We can also relate the thrust of the propeller to the torque using a conversion factor, σ, and an effective blade length, L_B as follows;

$$\tau_H = \sigma L_B T$$

where the thrust or force generated by the blades can be approximated as proportional to the acceleration of the water column and the square of its velocity by;

$$T = \rho L A (Ka+1) \dot{U} + \rho A \Delta \beta U |U|$$

17

If we assume a first order lag exists between the angular velocity of the propeller and the acceleration of the water column, it can be expressed as follows;

$$\dot{U} = \frac{-U + (\eta p)\dfrac{\omega_M}{N}}{t_c}$$

where t_c is the time constant.

We now have two first order differential equations to solve for in terms of ω_M and U.

6. **Summary**

In order to simulate the response of the model to given input voltage signals, two coupled first order differential equations which describe the thruster system dynamics need to be solved;

$$\dot{\omega}_M = f_1(\omega_M, U, Vs)$$

$$\dot{U} = f_2(\omega_M, U)$$

18

In addition to the above equations, two other equations are required to provide output data to compare with the measureable parameters of the experimental data;

$$T = g_1(\omega_M, U)$$

$$i = g_2(\omega_M, Vs)$$

III. EXPERIMENTAL APPARATUS

A. GENERAL

The test apparatus for the AUV II tunnel thruster consisted of four basic components:

- The thruster assembly consisting of the servomotor, reduction gear, propeller, gear housing and tunnel.

- The test stand frame and load cell on which the thruster assembly was mounted.

- The instrumentation for controlling the thruster and collecting data.

- The tank of water for immersing the thruster assembly.

1. Thruster Assembly

The test thruster assembly was a specially modified unit of that described in Chapter II. The modification consisted of encasing the servomotor in a water--tight enclosure (an extra section of PVC pipe) and providing an extension of the gear housing to allow the thruster assembly to be rigidly mounted in the test stand. This enabled the thruster assembly, mounted in the test stand, to be immersed without shorting out the motor while keeping the load cell dry. See Figures 4 and 5 for photographs of the thruster assembly.
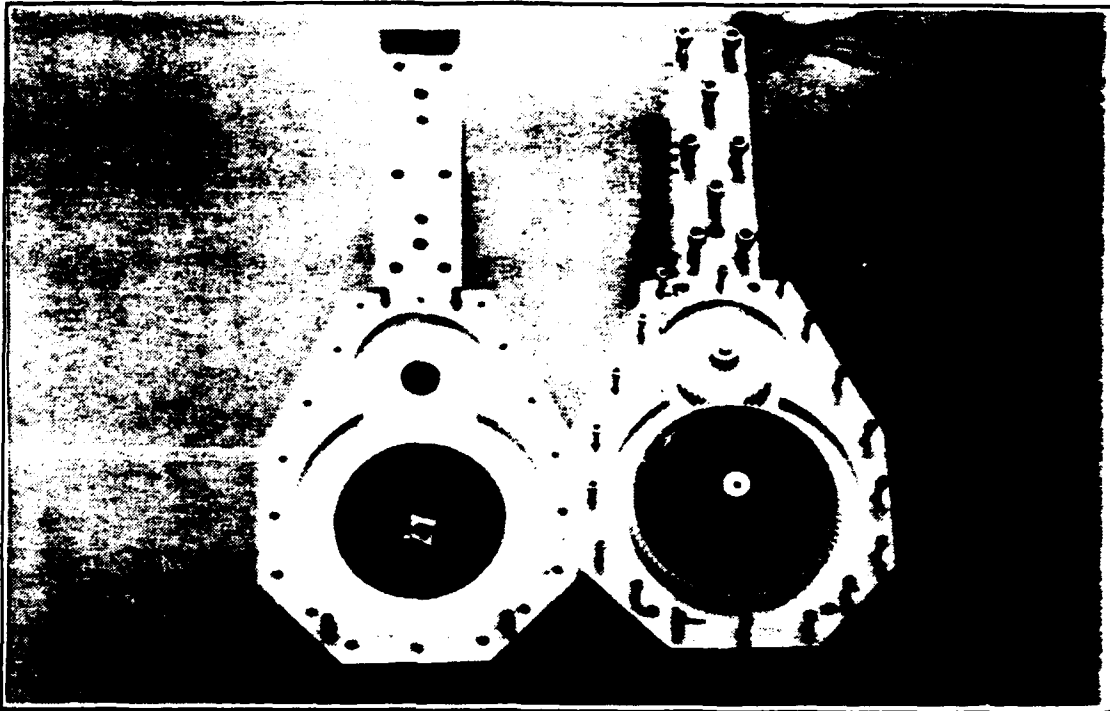
Figure 4 Thruster Assembly
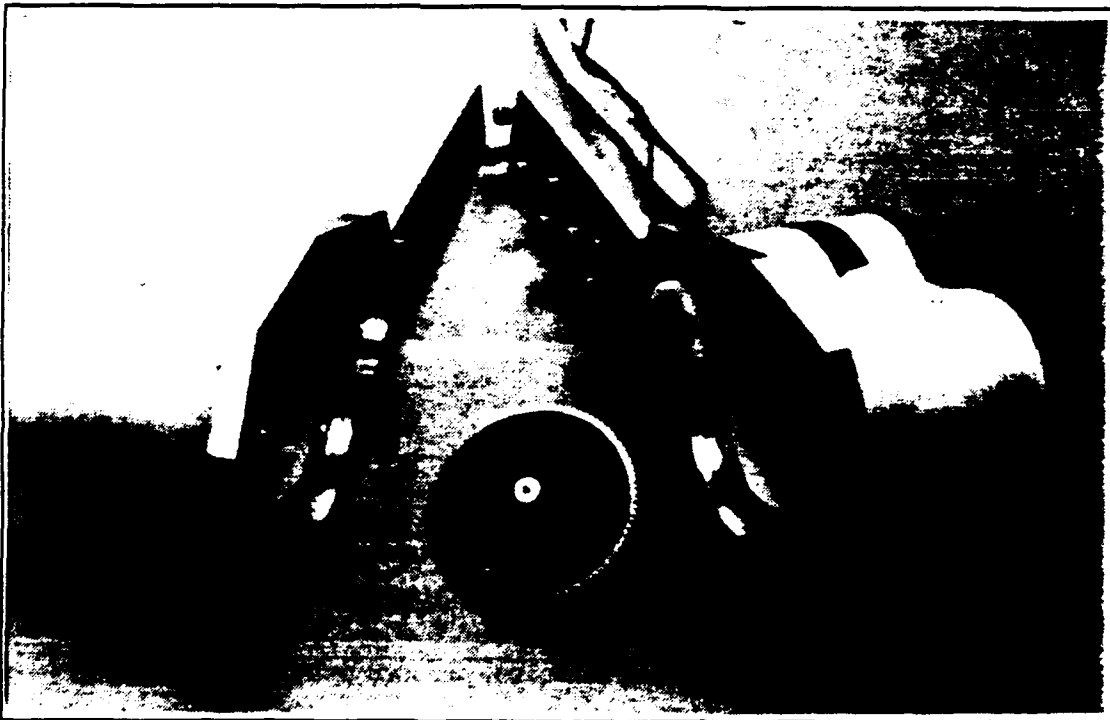
Figure 5 Thruster Assembly

2. Test Stand Frame and Load Cell

The test stand used to measure thrust was a triangular frame assembly that had a load cell placed in--line on the tension/compression leg shown in Figure 6. All of the joints were flexible to reduce cross axis loading from the thruster assembly, while providing stiff support to reduce structural dynamic corruption of the thrust response data. This frame was rigidly mounted to an overhead beam or truss and suspended over the test tank as shown in Figures 7 and 8.

3. Instrumentation and Measurements

In order to be able to verify the accuracy of the model derived in Chapter II, experiments needed to be conducted to obtain data under appropriate conditions. The
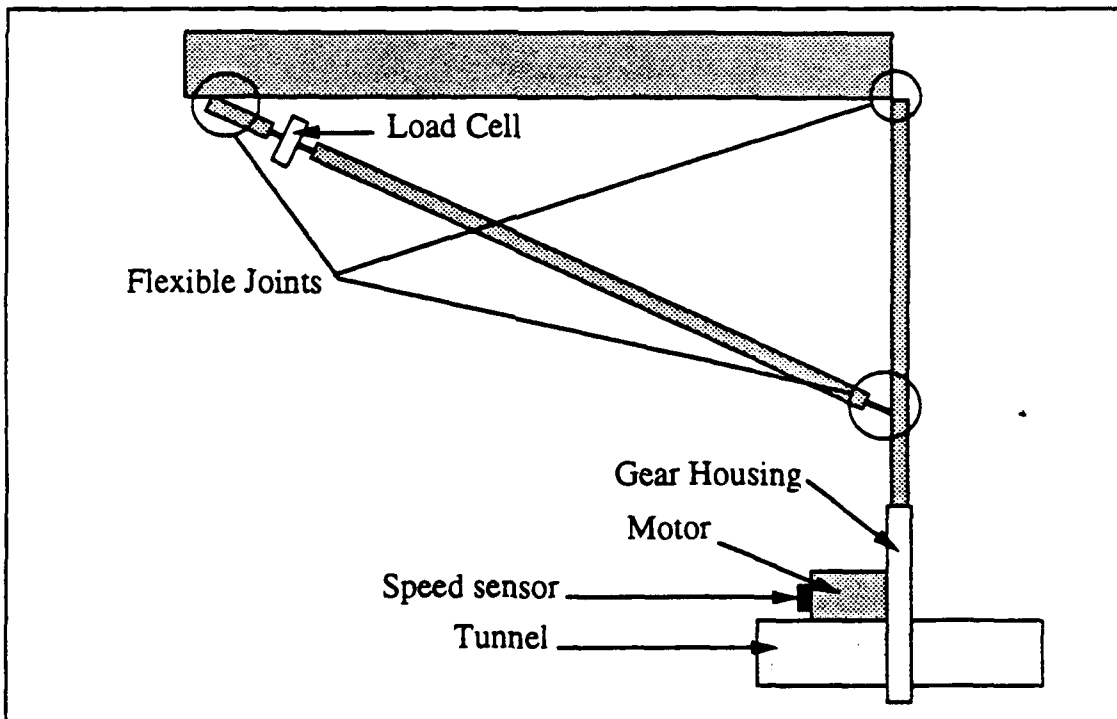
Figure 6 Test Frame Assembly
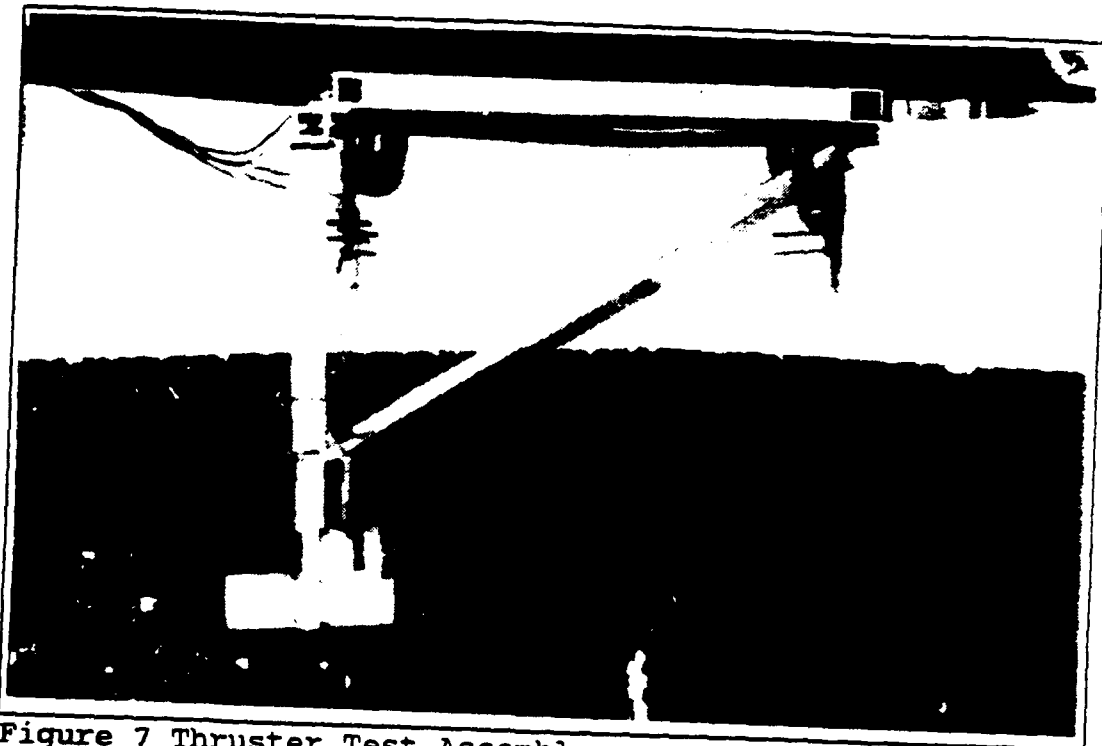
Figure 7 Thruster Test Assembly suspended from beam
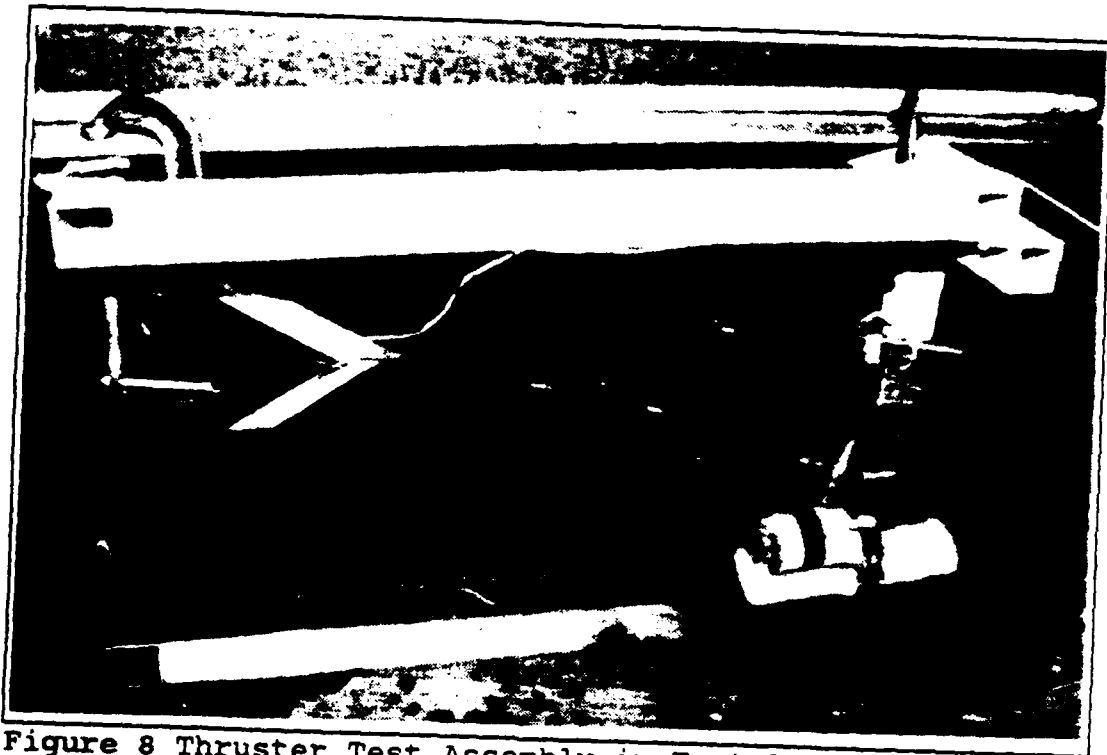
Figure 8 Thruster Test Assembly in Test Tank

model was specifically tailored to variables that were readily measurable; thruster force response, motor speed, applied voltage and motor current. Water column velocity and blade flow parameters, although desirable, were not measureable.

To achieve the detail of data required to verify the model, instrumentation was required to not only record the experimental data but also to provide control for the experiment. The following equiment was utilized:

- Personal Computer: MS-DOS, 286 microprocessor; utilized to run the data acquisition program and record data

- Analog to Digital Converter (ADC): Data Translation DT 2801; utilized to convert raw analog data to digital data suitable for recording

- Signal/Function Generator(s):
  (1) Wavetek 20 MHz Pulse/Function Generator, Model 145; utilized to provide signal functions of desired voltage and frequency for input to PWM servo amplifier
  (2) BK Precision 3025 Sweep/Function Generator; utilized to provide trigger signal to activate ADC card

- Filter: Krohn--Hite Model 3343; utilized to filter raw data signals for both load cell and motor current output

- DC Power Supply(s):
  (1) Lambda Regulated Power Supply, Model LK 345A FM; utilized to provide 24.0 VDC source voltage for PWM amplifier
  (2) Lambda Regulated Power Supply, Model LP 411 FM; utilized to provide 5.0 VDC for optical encoder (motor speed sensor)

- PWM Servo Amplifier: Advanced Motion Controls Model 30A8DD; utilized to provide +/- 0 to 24 volts PWM per +/- 0 to 10 volts input signal, also provide voltage signal output proportional to motor current

- Tachometer Module Card: of local maunfacture for this application; utilized to convert input signal of counts per second (cps) to an output voltage signal proportional

24

to cps, through a LM2917 tachometer chip with a charge pump circuit

- Motor speed encoder: <u>Hewlett--Packard</u> Incremental Optical Shaft Encoder Model 50xx; utilized to provide output signal of counts per second of motor revolution to tachometer module card, capable of definition of 500 counts per revolution

- Digital Voltmeters: <u>BK Precision</u> DVM; utilized to monitor voltages throughout the measurement apparatus

- Universal Counter: <u>Hewlett--Packard</u> 5315A; utilized to calibrate tachometer module card output voltage

- Oscilloscope: <u>Iwatsu</u> SS--5702 Oscilloscope DC--20 MHz; utilized to provide real time observation of output signals and monitor progress of data taking sessions

- Load Cell and Bridge/Amplifier: utilized to provide an output voltage signal proportional to sensed thruster force

Please refer to Figure 9 for a block diagram of the instrumentation and Figure 10 for a photograph of the equipment set up in the lab.

B.   EXPERIMENTAL DATA

This section will describe the procedures used to calibrate the test equipment and collect the experimental data.

1. Calibration

Three separate calibrations were required for the laboratory set--up; the load cell output, applied motor current and resulting motor speed. Data was recorded for
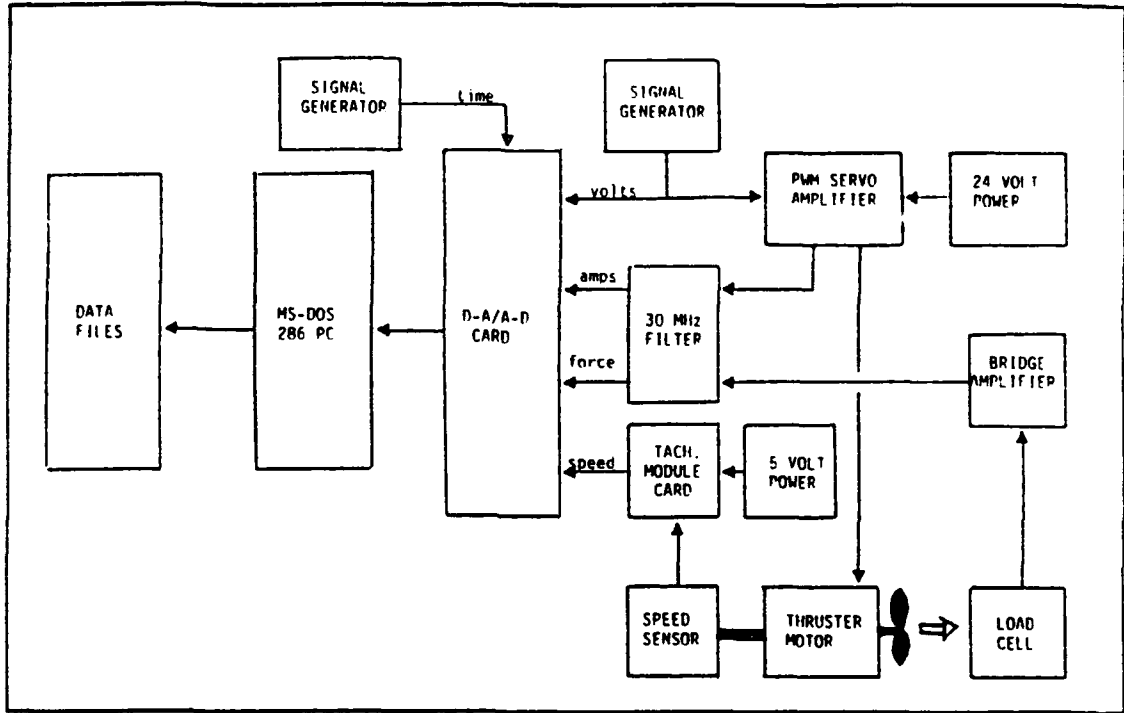
Figure 9 Block Diagram of Experimental Setup
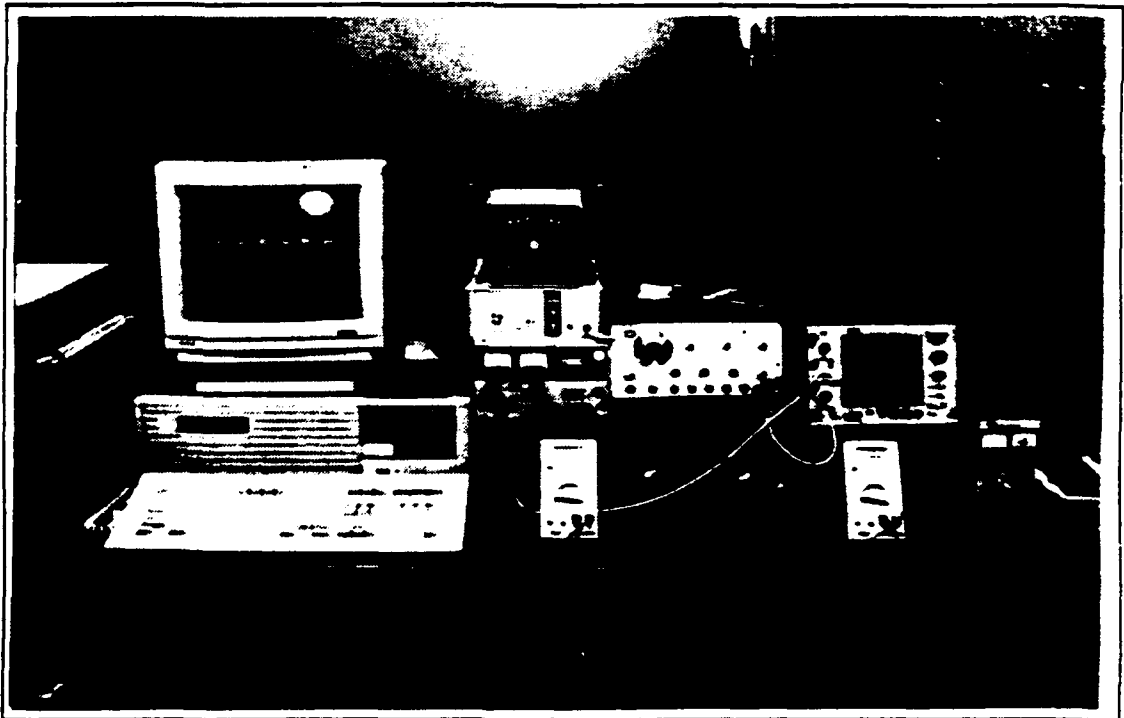
Figure 10 Instrumentation Setup in Lab

26

each calibration series and plotted utilizing MATLAB[1]. A least squares first order equation was obtained in each case through the POLYFIT function.

a. Load Cell

The calibration of the load cell, mounted in the test stand, required determining the force exerted by the thruster on the load cell per output voltage of the load cell. With the thruster assembly mounted in the test stand, a line was attached to the center of the thrust bearing supports on the discharge side of the propeller. This line was then passed around a low friction pulley (fairlead) placed in direct line with the thruster tunnel. Known weights were suspended from the line and corresponding load cell output voltages were recorded. This procedure was repeated for the opposite discharge tunnel for reverse thrust conditions. A linear relationship was observed between force and output voltage. See Figure 11 for the load cell calibration curve.

b. Motor Current

The PWM Servo Amplifier was equipped with terminals that provided an output voltage signal as a measure of the current draw of the system, say 'Vc'. In order to calibrate this voltage, Ohm's Law, $v = iR$, was employed utilizing a known resistor in line with the thruster motor

---

[1] MATLAB is a registered trademark of The Math Works Incorporated, Nantick, MA.
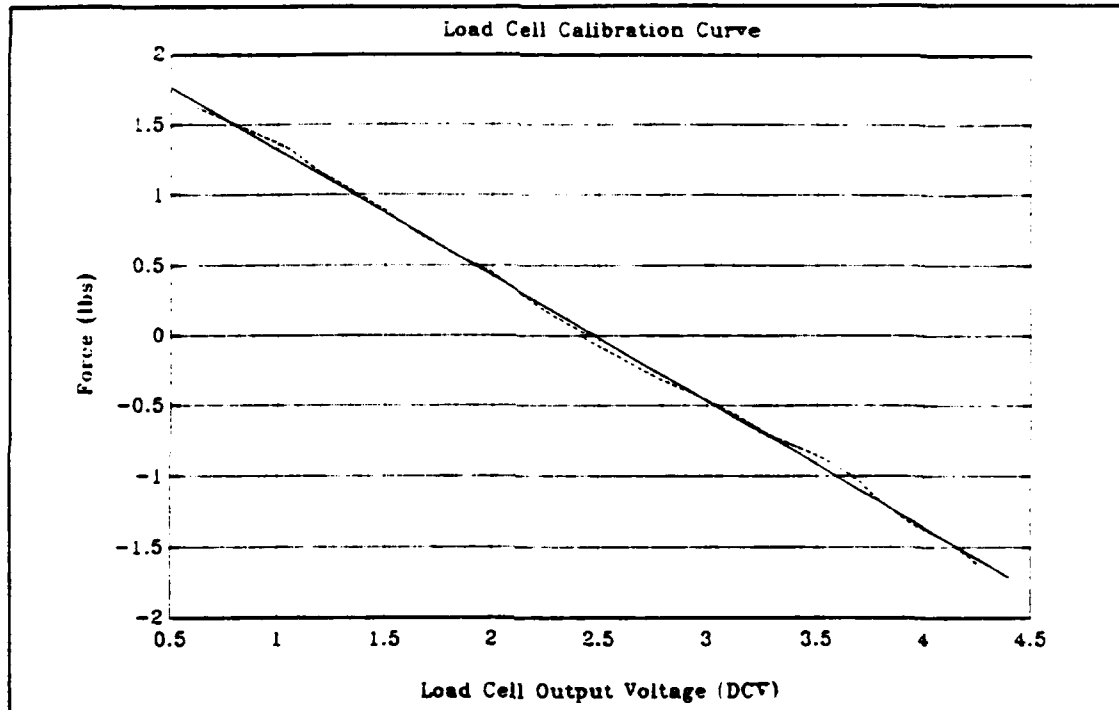
Figure 11 Load Cell Calibration Curve

circuit. Measuring the voltage drop across this resistor at
several different control voltages for the thruster motor
provided data to construct Figure 12, the motor current versus
sensed voltage, 'Vc', calibration curve. This also proved to
be a linear relationship.

c. Motor Speed

An optical encoder attached to the motor shaft
provided a pulse frequency to a tachometer module card which
converted this signal into an output voltage proportional to
the pulse frequency. Measuring the pulse frequency/time
period and the associated tachometer module card output
voltage at various intervals throughout the operating range
gave the linear calibration curve in Figure 13. The optical

28
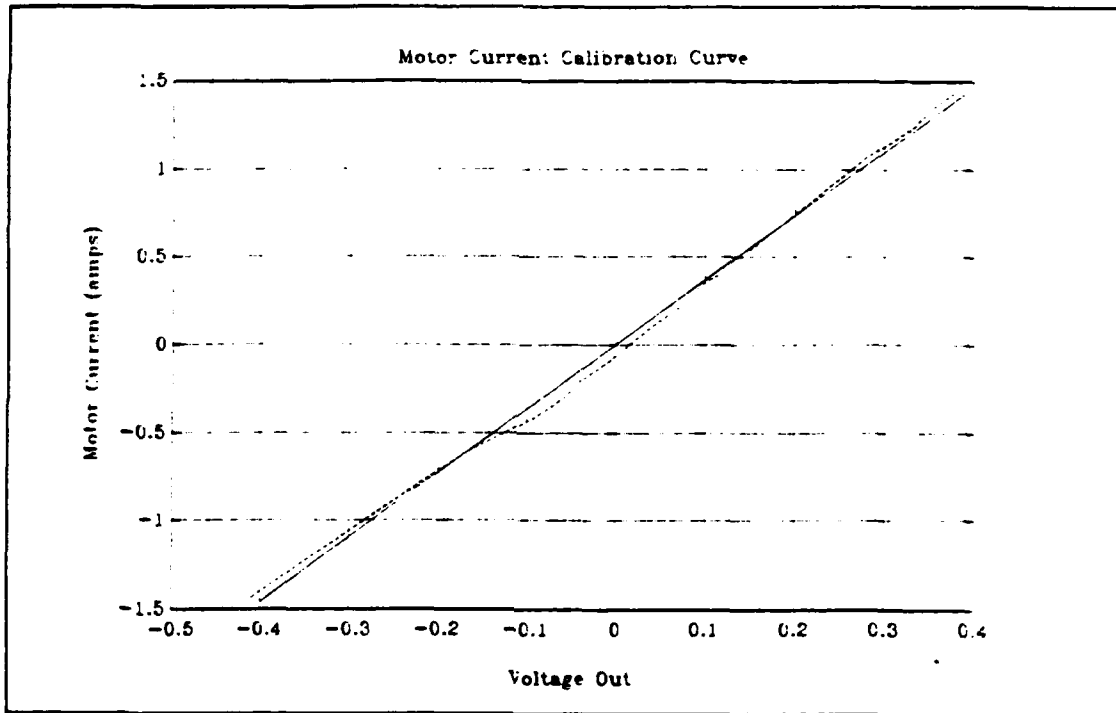
Figure 12 Motor Current Calibration Curve

encoder signal saturated the circuit card at approximately 3100 counts per second. The frequency to analog converter utilized a smoothing filter with a 50 Hz bandwidth.

2. Data Collection

In order to obtain as much meaningful data in the fewest data runs as possible, regularly varying control voltage input signals of a triangular wave configuration was applied to the thruster motor. The time periods of these signals were varied incrementally from 50 seconds (to approximate steady state conditions and still provide analysis of speed dominant characteristics) to 0.5 seconds (to observe the dynamics of the system). Additionally, square waves of +/- 9.0, 6.75, 4.50 and 3.00 volts were utilized to observe

29
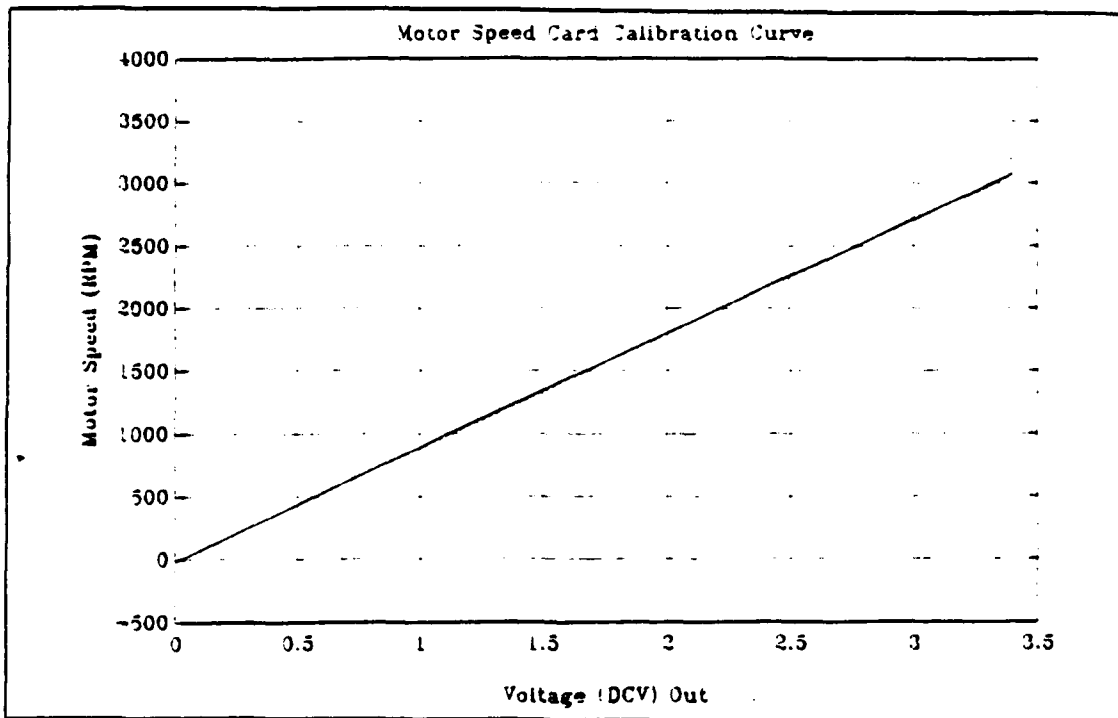
Figure 13 Motor Speed Calibration Curve

the dynamic effects of step input control voltages of varying magnitude.

In order to validate the effects of propeller pitch and tunnel lengths on the mathematical model (provided the remaining variables remained relatively constant), the above experiments were conducted for both 30 and 45 degree pitched propellers each connected to the 10.0 and 16.5 inch tunnels.

A TURBO PASCAL[2] computer program was written to interface with the ADC card for data aquisition. It was to record five separate channels of data; a time/step counter, load cell output voltage, motor controller circuit card

---

[2] TURBO PASCAL is a registered trademark of BORLAND International, Scotts Valley, CA.

input/control voltage, motor speed output voltage and motor current output voltage, and convert these output voltages to useable values utilizing the calibration data obtained above. These channels were first written to a RAM resident array and then, following the collection of all the data points, down loaded to a file of five column vectors. Sample rates of up to 160 Hz were possible using this technique. Sampling was initiated using an external source square wave provided by a signal generator. This initiated a timed trigger signal to the DT 2801 ADC card resident in the MS-DOS 286 personal computer.

a. Time/Step Counter

The time counter was generated by the data acquisition program by first interactively quierying the user for the number of data points desired and the sampling frequency at which they were to be obtained. The time step was calculated and at each successive iteration added to the previous time. The result was written into a vector array.

b. Load Cell Output

Following the calibration of the load cell at a known bias for the bridge/amplifier, the data aquisition program was coded to quiery the user for the bias of the bridge/amplifier at the start of each successive data taking run. This was required due to the fact that the bias drifted. This bias was compared with the calibration bias and the

31

difference used to compensate the load cell output and correct the corresponding thruster force calibration. The load cell output voltage from the bridge/amplifier was first passed through a 30 Hz, max flat low pass filter prior to reaching the ADC card, so that excessive high bandwidth noise was eliminated.

c. PWM Servo Amplifier Input/Output Voltage

This voltage was recorded directly from the input terminals of the servo amplifier. It had a linear relationship with the voltage to the motor of 1:2.27.

d. Motor Speed

Motor speed was sensed as an output voltage signal from the tachometer module card, converted to RPM units by the data management program and recorded. This signal was soley a signal of magnitude and had no polarity. In order for the recorded speed to reflect the proper direction, the speed vector data was post processed to reflect appropriate sign prior to plotting.

e. Motor Current

Motor current was sensed as the output voltage signal from the PWM servo amplifier and converted to amperes by the data management program utilizing the calibration data obtained above and recorded. This signal was also passed through a 30 Hz, max flat low pass filter prior to reaching the ADC card.

IV. ANALYSIS OF EXPERIMENTAL DATA

A. GENERAL

The intent of this chapter is to make observations regarding the nature of the experimental data collected for triangular and square wave inputs. Within the sections for the responses to both triangular and square wave inputs, specific comments will be made with respect to the effects of period (triangular wave only), control voltage (square wave only), different tunnel lengths and different propeller pitches on thruster force, motor current and motor speed responses.

B. TRIANGULAR WAVE RESPONSE

As described in Chapter III, a control voltage signal in the form of a triangular wave with a voltage range of +/- 9.0 volts DC (which corresponds to an applied motor voltage of approximately +/- 20.4 volts or 85% of the rated value for the motor) was utilized to excite the thruster motor. Data was recorded for waves with periods of 50, 20, 10, 5, 2, 1 and 0.5 seconds. This was done for propellers of 45° and 30° pitch, and at tunnel lengths of 10.0 and 16.5 inches for each propeller.

33

1. Long Period (50 second) Waves

As indicated in Chapter III, the long period wave was utilized to approximate steady state conditions, and as such will be used as the basis for comparison of subsequent data. Data from the shorter periods can reasonably be assumed to be dominated by strong dynamic phenomena.

a.   Thruster Force Response

The general shape of the force response for the 50 second period wave reflected that of the square of the propeller's angular velocity, as expected from the model. This was observed for both propeller pitches and both tunnel lengths as shown in Figures 14, 15, 16 and 17. It was noted that as the force approached zero, the response dropped quickly to zero and remained there for a few seconds before rapidly increasing to follow the regular form of the curve. This is associated with the motor stiction; where the motor cannot overcome the static friction of the system and stops until the applied voltage becomes sufficient to overcome it again; and the current goes through a sharp change, as described later below.

Comparing the force response of the two different propellers at the same tunnel length (10.0 inches) showed that the 45° propeller provided significantly higher thrust than that of the 30° propeller, as expected. The maximum thrust observed was approximately 1.5 lbs versus 1.0 lbs respectively

34
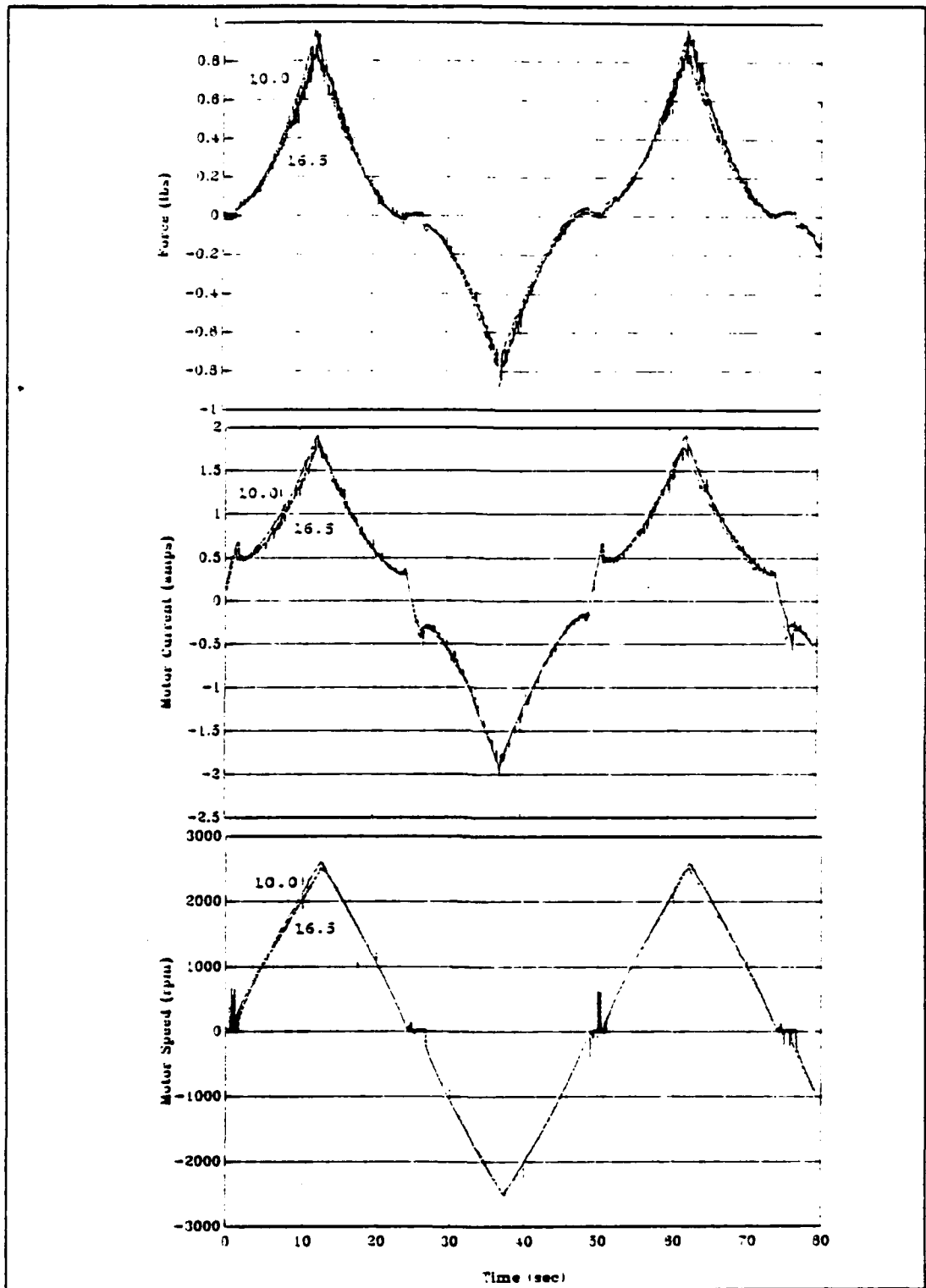
Figure 14 50 second period triangular wave, +/- 20.4 volts, 30° pitch propeller, 10.0 and 16.5 inch tunnel lengths

35
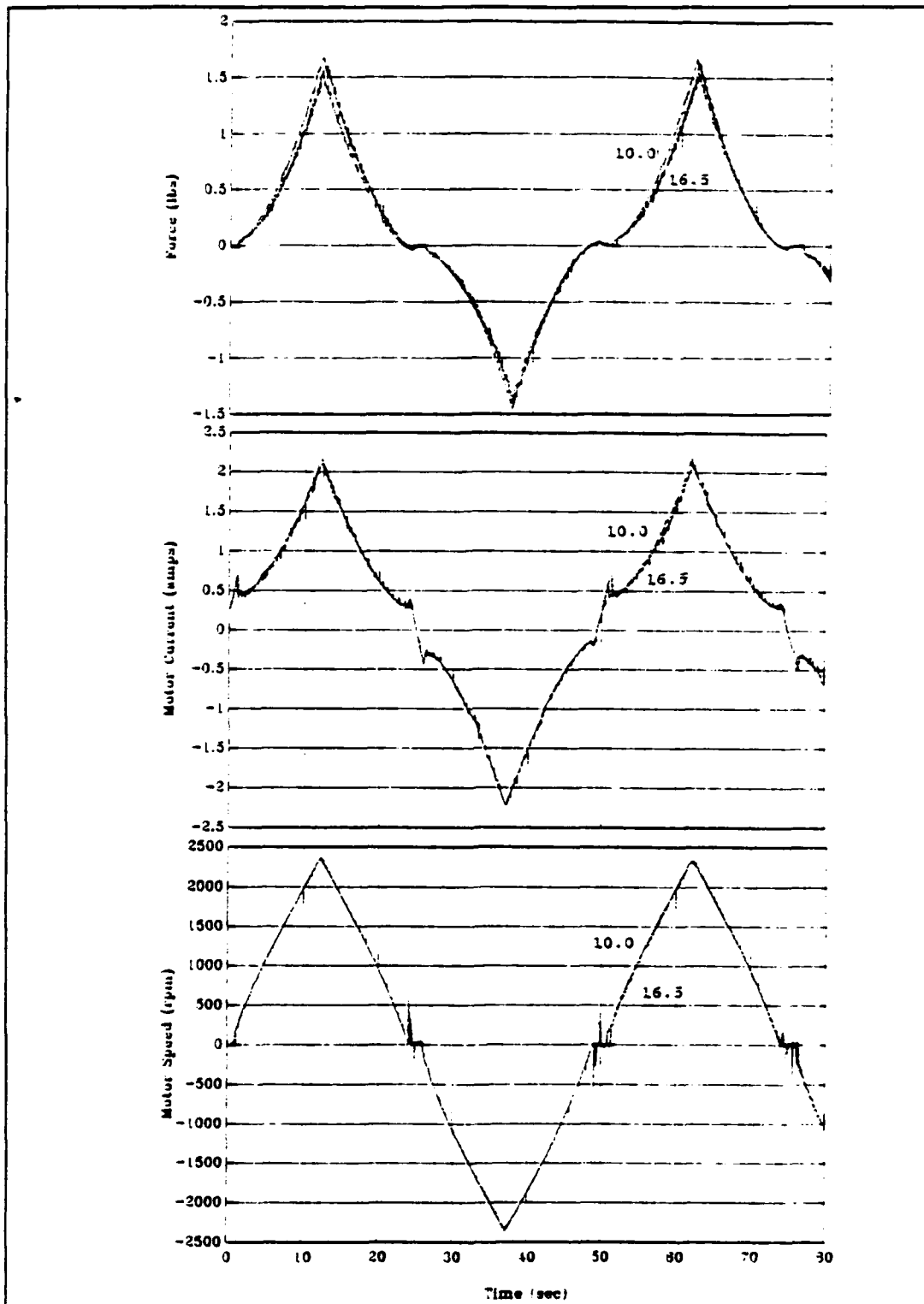
Figure 15 50 second period triangular wave, +/- 20.4 volts, 45° pitch propeller, 10.0 and 16.5 in tunnel lengths

36
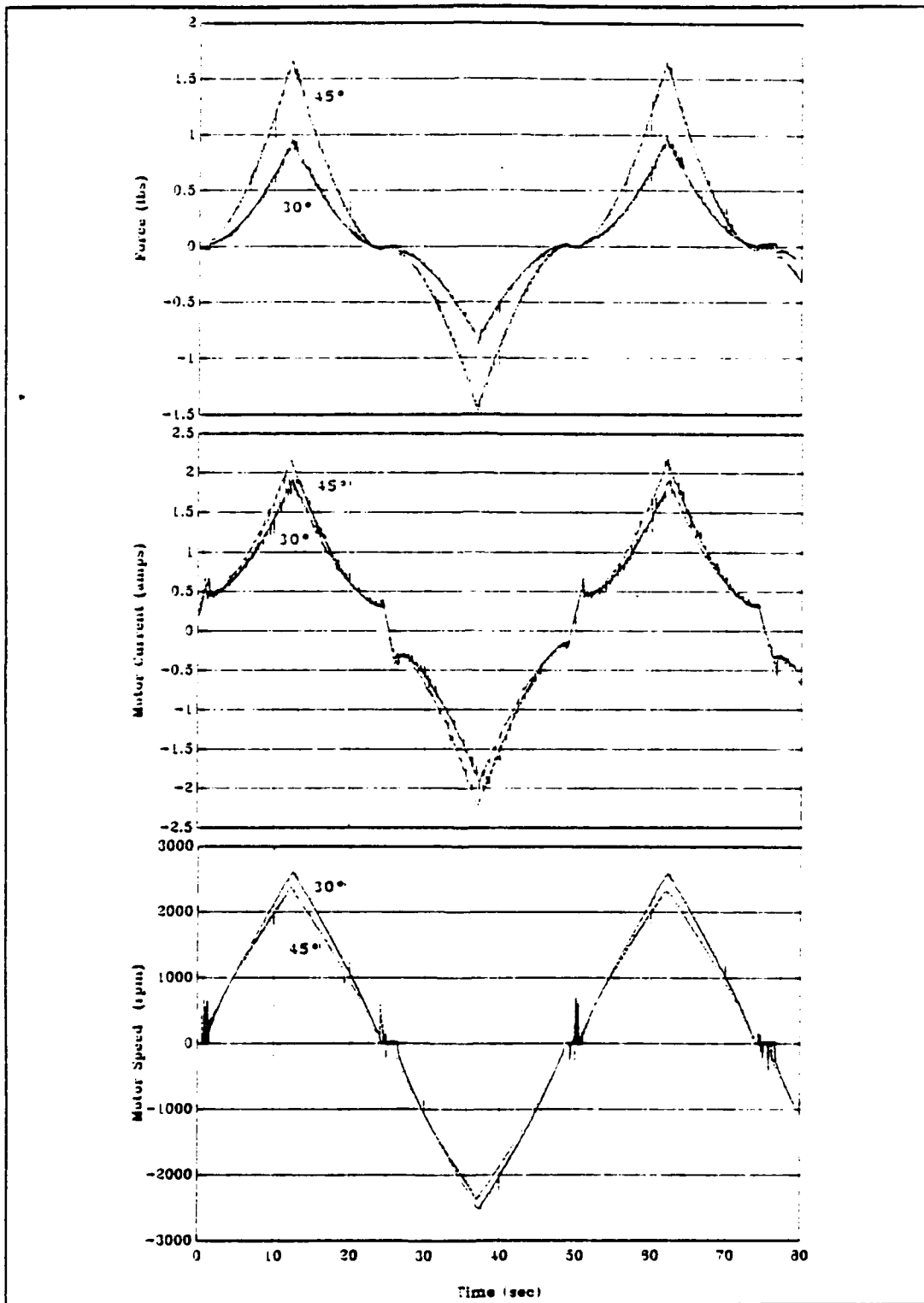
Figure 16 50 second period triangular wave, +/- 20.4 volts, 30° and 45° pitch propellers, 10.0 inch tunnel length

37
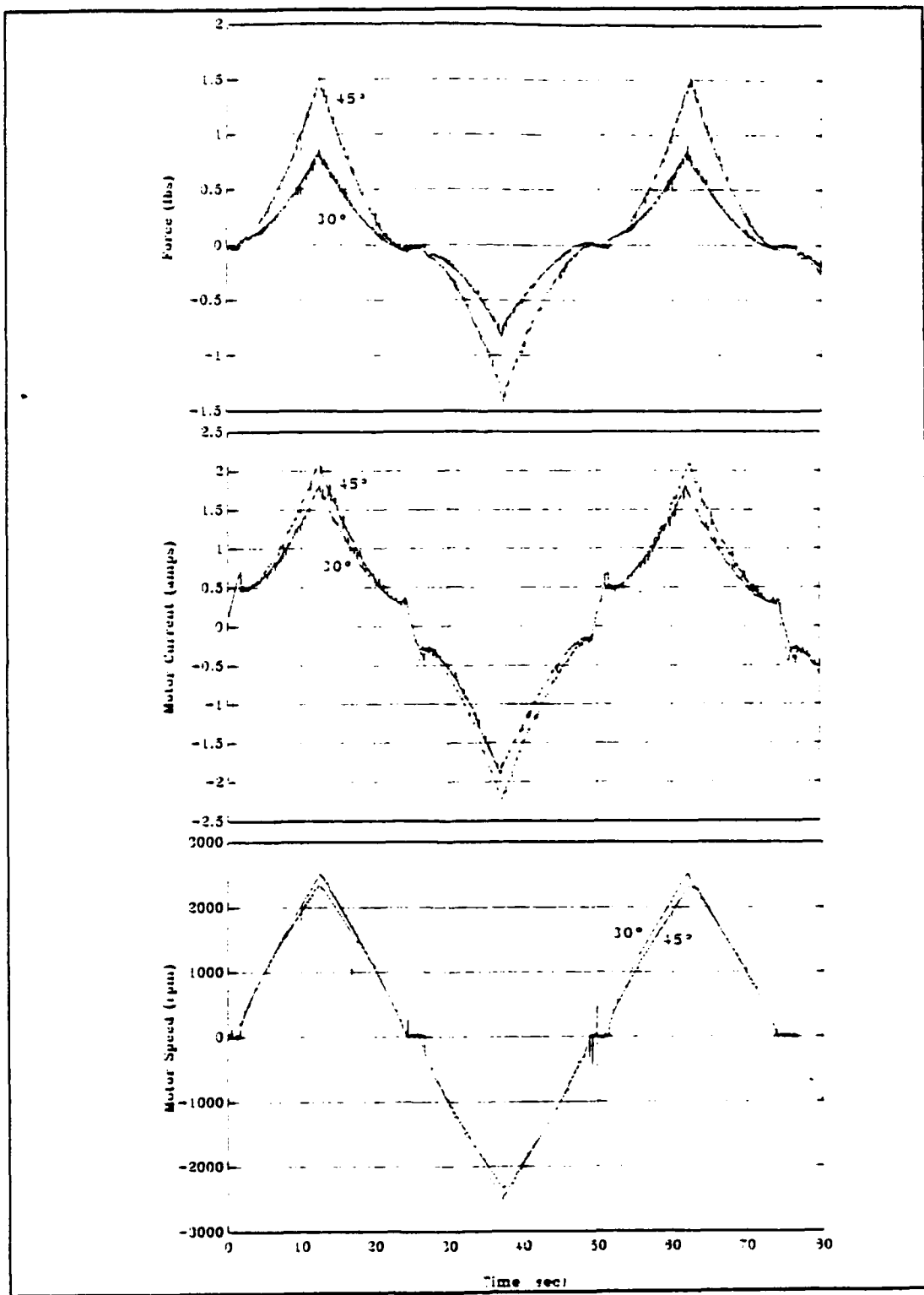
Figure 17 50 second period triangular wave, +/- 20.4 volts, 30° and 45° pitch propellers, 16.5 inch tunnel length

as can be seen in Figure 16. For increased tunnel lengths, the thrust for each propeller was slightly reduced as shown in Figures 14 and 15 and by comparing Figures 16 and 17. This is evidence of the loss in thrust due to friction between the moving water column and the longer tunnel walls. It should also be noted that the propellers may not have been equally efficient in both directions as originally hoped. Figures 16 and 17 show differences in the peak forces in opposite thrust directions for the same propellers.

b. Motor Current Response

Plots of the current drawn by the thruster motor, Figures 16 and 17, closely followed that of the force response plots as expected, with the 45° propeller drawing more current than the 30°; approximately 2.2 versus 1.9 amperes. Tunnel length appeared to have no significant effect on current response as can be seen in Figures 14 and 15. The discontinuities in the curves occur in the region of stiction, where the amperage increased slightly as the motor, responding to a decrease in applied voltage, was slowed, and finally stopped by friction. It then changed linearly, passing through zero, until it overcame the friction again when it decreased slightly before assuming the regular shape of the curve. The difference in the current levels at the onset of subsequent stiction regions can be explained by the differences in the static friction from one direction of

39

rotation to the other.

c. Motor Speed Response

Motor speed (angular velocity), closely followed that of the applied voltage triangular wave. The stiction regions can clearly be seen as regions of zero rpm's. The shape of the curve was not quite linear, due in part to both the friction of the system and the load torque speed dependency of the propeller. As can be seen in Figures 16 and 17, the 30° propeller reached higher speeds than did the 45° propeller because of the increased loading on the 45° propeller, approximately 2600 versus 2350 rpms respectively. Again, tunnel length appeared to have no significant effect on motor speed response as shown in Figures 14 and 15.

2. Shorter Time Period Waves

Since the length of the thruster tunnels has been shown to only have an effect on the steady state force of the thruster by decreasing the force for an increase in tunnel length, and even though the data was recorded, a single tunnel length of 16.5 inches will be utilized to illustrate the effect of decreasing time periods of the applied voltage triangular wave input signals. The responses of the 45° and 30° propellers will be plotted on the same graph for comparison.

a. Thruster Force Response

As the period of the triangular wave was incrementally reduced from 50 seconds, the more skewed the force responses became as evident in Figures 18 and 19. This is attributable to the increased influence of fluid inertia on the affected water column as compared to the modified squared speed component in the total thrust. The shorter the period, the more effect the inertia had on the force response. It effectively slowed down the response, or increased the response time, to a change in propeller speed. This was observed for both propeller pitches. As the period was reduced even further, Figures 20 and 21, the skew shape became less noticable and virtually disappeared as shown in Figure 22 for a time period of 0.5 seconds where the thrust response is dominated by the linear term in $\dot{\omega}$.

Also, as the period was decreased, the peaks of the force responses became less distinct, or more rounded, indicating a smoother transition between the acceleration and deceleration of the water column. Additionally, the discontinuities associated with the regions of motor stiction became less apparent.

It was also noted that as the periods were reduced below 10 seconds, the peak forces increased over those of the long periods. Between time periods of 10 and 5 seconds we see, by comparing Figures 18 and 19, that the peak forces for the 45° and 30° propellers increased from approximately 1.5

and 1.0 to 1.75 and 1.2 lbs respectively. This trend of increasing peak force responses for decreasing period triangular wave inputs was observed to continue from the 5 second period to the 2 and 1 second periods as seen by comparing the force response of Figures 19, 20 and 21. The difference between the peak forces of the 45° and 30° propellers remained fairly constant at approximately 0.5 lbs as the period decreased until a period of 0.5 seconds was reached. At this point both propellers produced almost identical force response plots with a peak force of approximately 3.3 lbs as can be seen in Figure 22.

b. Motor Current Response

As before for the long period wave, the motor current response basically followed that of the force response. When the force response became skewed with decreasing periods, so did the motor current response. Stiction effects became less noticable earlier in the motor current responses than in the force responses. Figure 20 shows the responses for a 2 second period triangular wave with discontinuities in the force response as compared to very little deviation of the motor current response.

Additionally, as was seen in the force response for decreasing periods, the peak motor current also increased. However, this occurred for the motor current response between the 5 and 2 second periods versus the 10 and 5 second periods

Figure 18 10 second period triangular wave, +/- 20.4 volts, 30° & 45° pitch propellers, 16.5 inch tunnel length

43

Figure 19 5 second period triangular wave, +/- 20.4 volts, 30° & 45° pitch propellers, 16.5 inch tunnel length
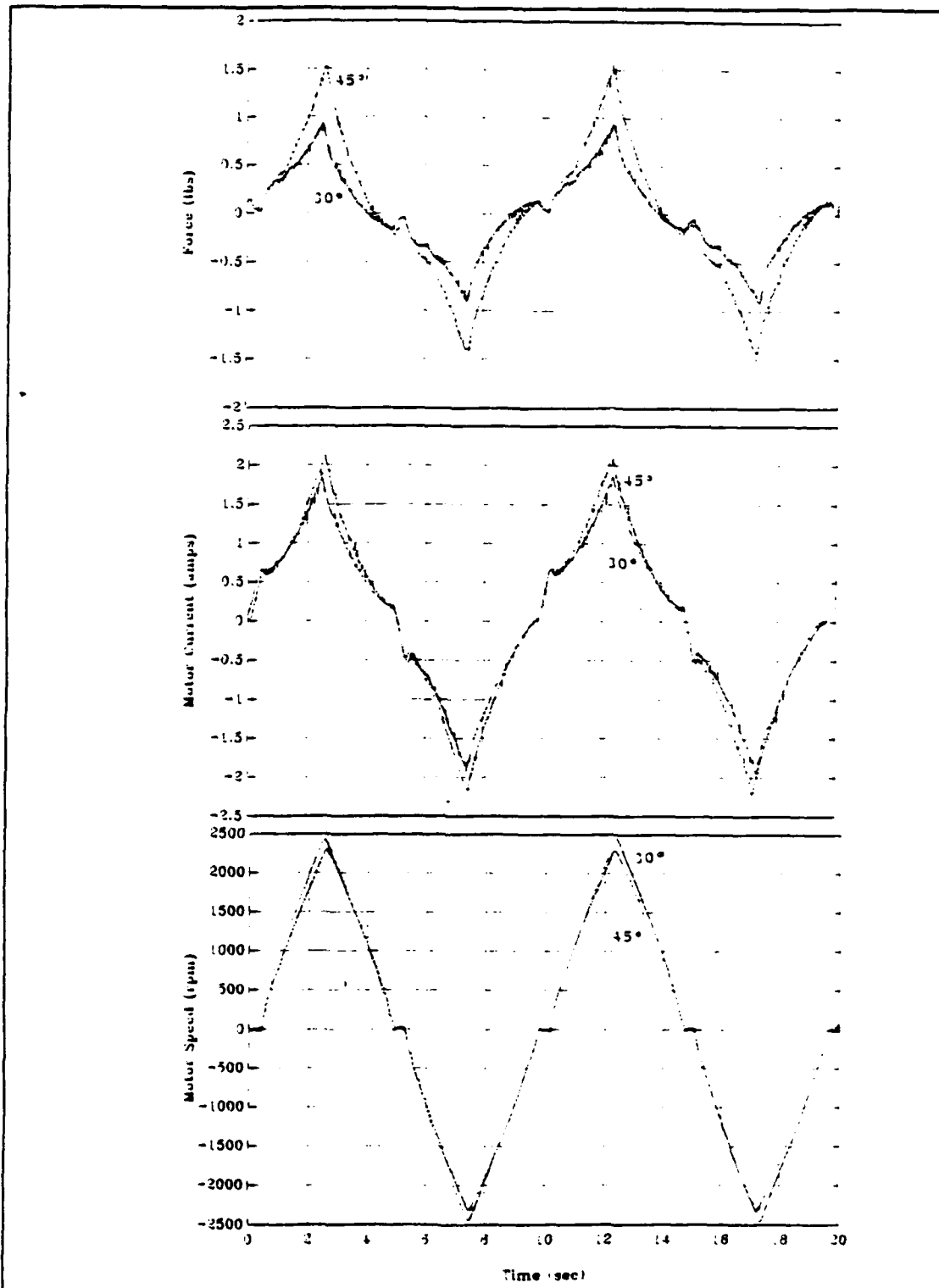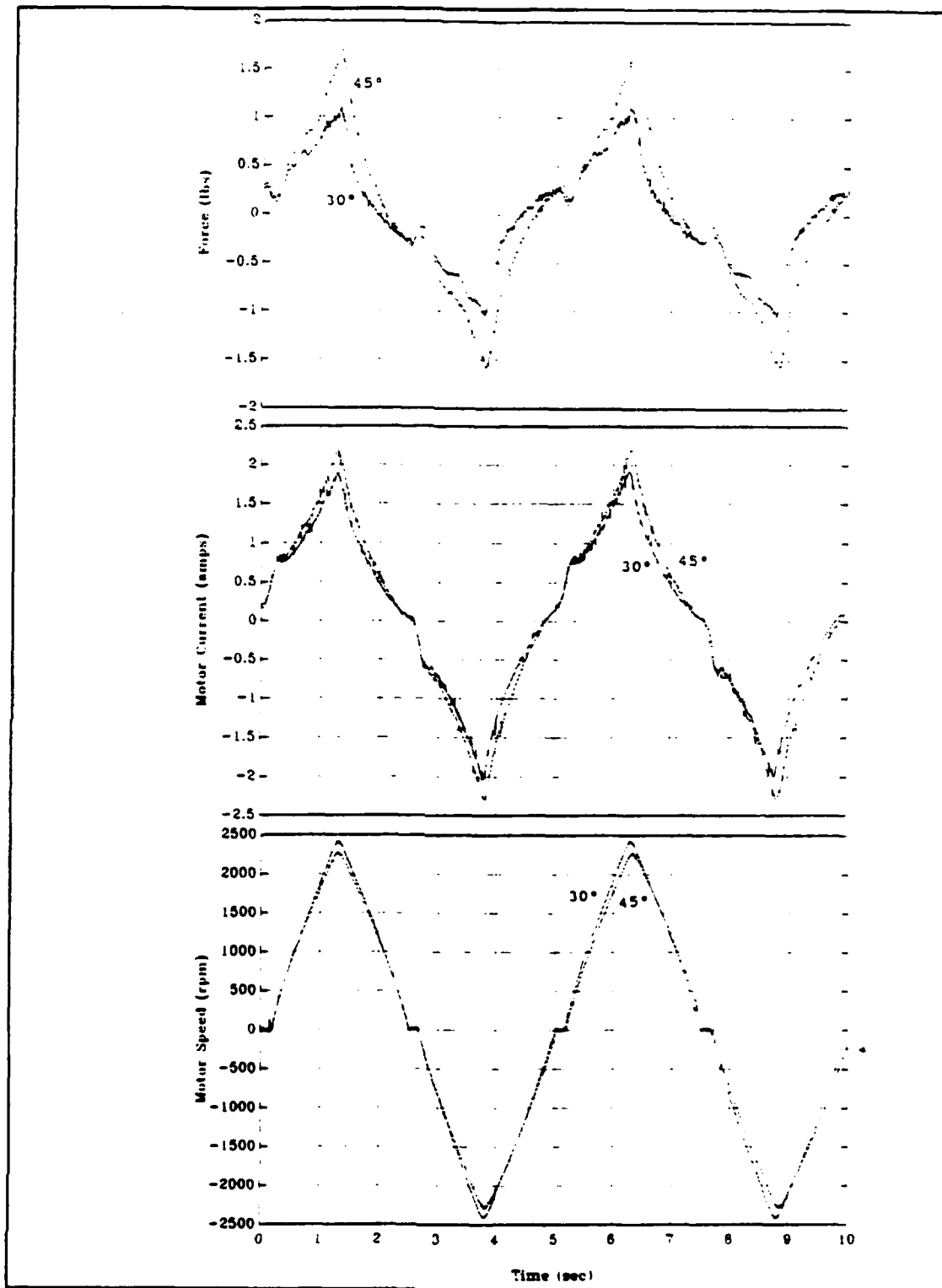
Figure 20 2 second period triangular wave, +/- 20.4 volts, 30° & 45° pitch propellers, 16.5 inch tunnel length

Figure 21 1 second period triangular wave, +/- 20.4 volts, 30° & 45° pitch propellers, 16.5 inch tunnel length

Figure 22 0.5 second period triangular wave, +/-20.4 volts,
30° & 45° pitch propellers, 16.5 inch tunnel length

for the force responses. The motor current peak response increased from approximately 2.2 and 1.9 amperes, for the 45° and 30° propellers respectively, from the 5 second period to the 2 second period where the peak current levels were approximately 2.5 and 2.2 amperes respectively. Again the same difference of about 0.3 amperes between the two propellers peak current responses was maintained until the 0.5 second period when motor current response for both propellers became practically identical. The above trends can be observed in Figures 18, 19, 20, 21 and 22.

c. Motor Speed Response

With the decreasing period of the applied voltage triangular wave input signals, the motor speed response was similar to that of the longer period waves, in that it also resembled the triangular input signal. In all cases, the peak motor speed of the 30° propeller remained approximately 200 to 250 rpm higher than that of the 45° propeller. As the period of the wave decreased from 10 seconds to 0.5 seconds, Figures 18, 19, 20, 21 and 22, so did the peak motor speed from approximately 2450 rpm for the 30° propeller and 2250 rpm for the 45° propeller to approximately 1950 and 1700 rpms respectively.

Additionally, as the period of the input signal decreased so did the amount of time the motor spent at zero rpm to where the extra inertia of the accelerating

48

/decelerating thruster motor assisted in passing through the null zone in a continuous manner as can be seen in Figures 21 and 22. Also of note was that as the period decreased the peaks of the motor speed response became less distinct and more of a continuous curve indicative of a less abrupt change in angular acceleration.

3. Normalized Thruster Responses

Normalizing the force responses for the 45° and 30° propellers at the same tunnel lengths provided Figures 23 and 24. The responses were virtually identical for the long period (50 second) waves. However, as the period decreased, Figures 25, 26 and 27, the normalized force response of the 45° propeller lagged behind that of the 30° propeller. When the period reached 0.5 seconds the force responses for both propellers were almost identical again, as can be seen in Figures 27, 28 and 29.

C. SQUARE WAVE INPUTS

Control voltage signals in the form of square waves with amplitudes of +/- 9.0, 6.75, 4.5 and 3.0 volts (corresponding to applied motor voltages of approximately +/- 20.4, 18.4, 12.2 and 8.2 volts or 85.0, 76.7, 50.8 and 34.2 percent of the rated value of the motor) were utilized to excite the motor. Data was recorded for each of the above listed wave amplitudesfor both the 45° and 30° propellers, each at tunnel lengths of 10.0 and 16.5 inches. The periods of the waves
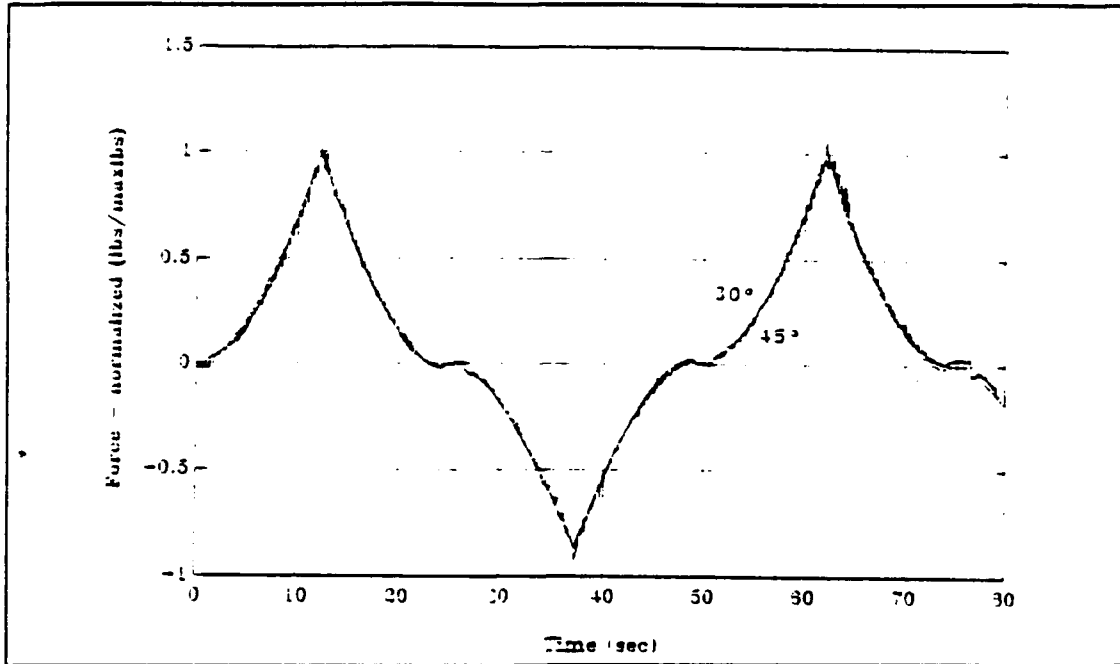
Figure 23 50 second period triangular wave, +/- 20.4 volts 30° & 45° pitch propellers, 10.0 inch tunnel length
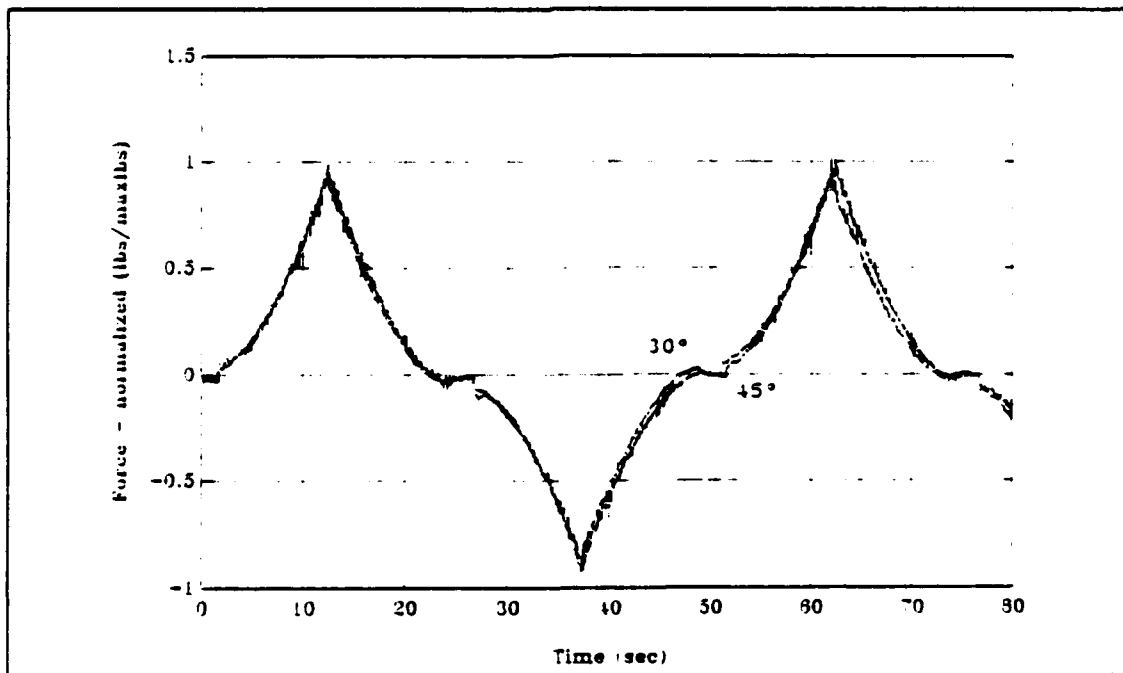
Figure 24 50 second period triangular wave, +/- 20.4 volts 30° & 45° pitch propellers, 16.5 inch tunnel length
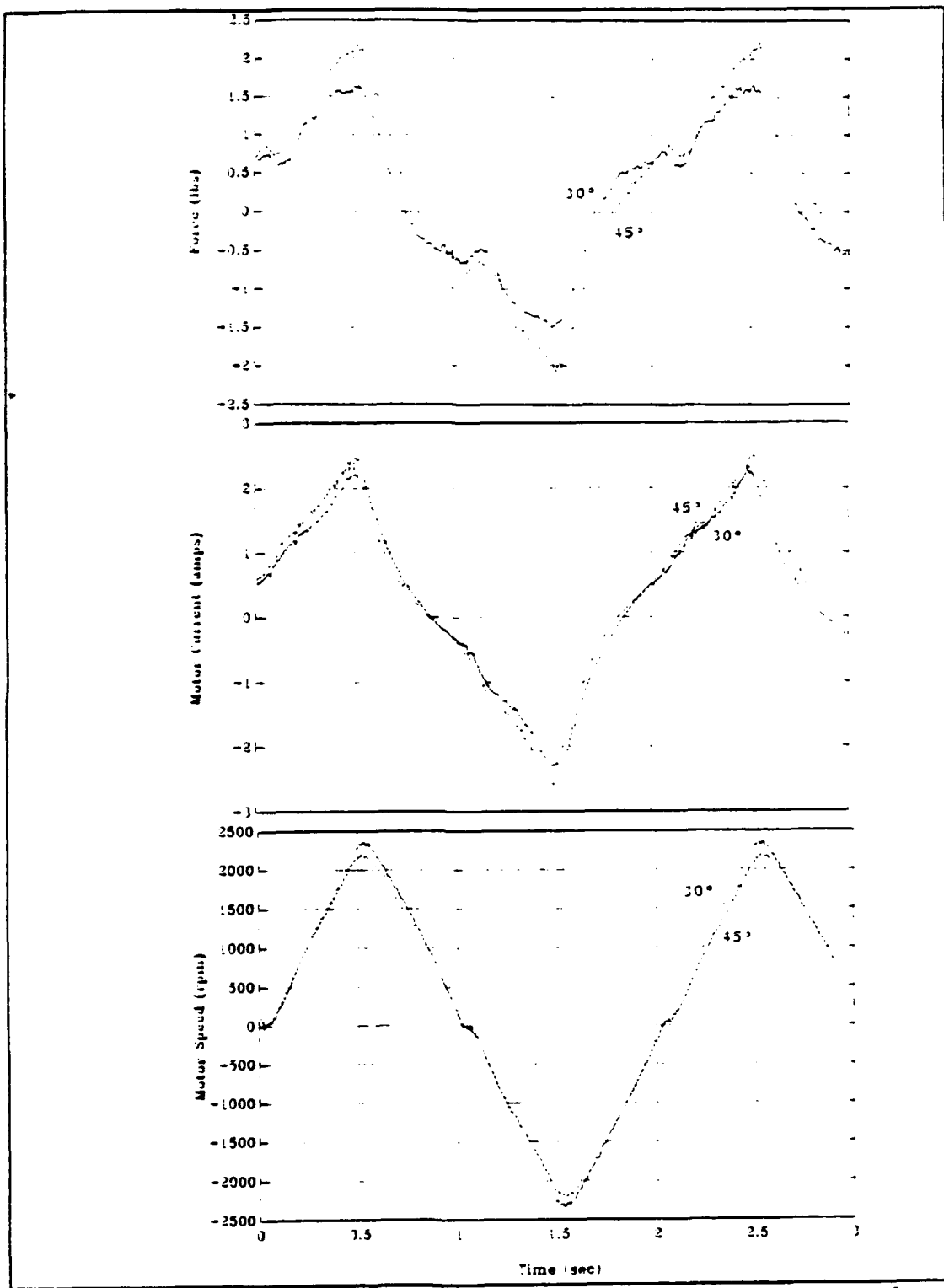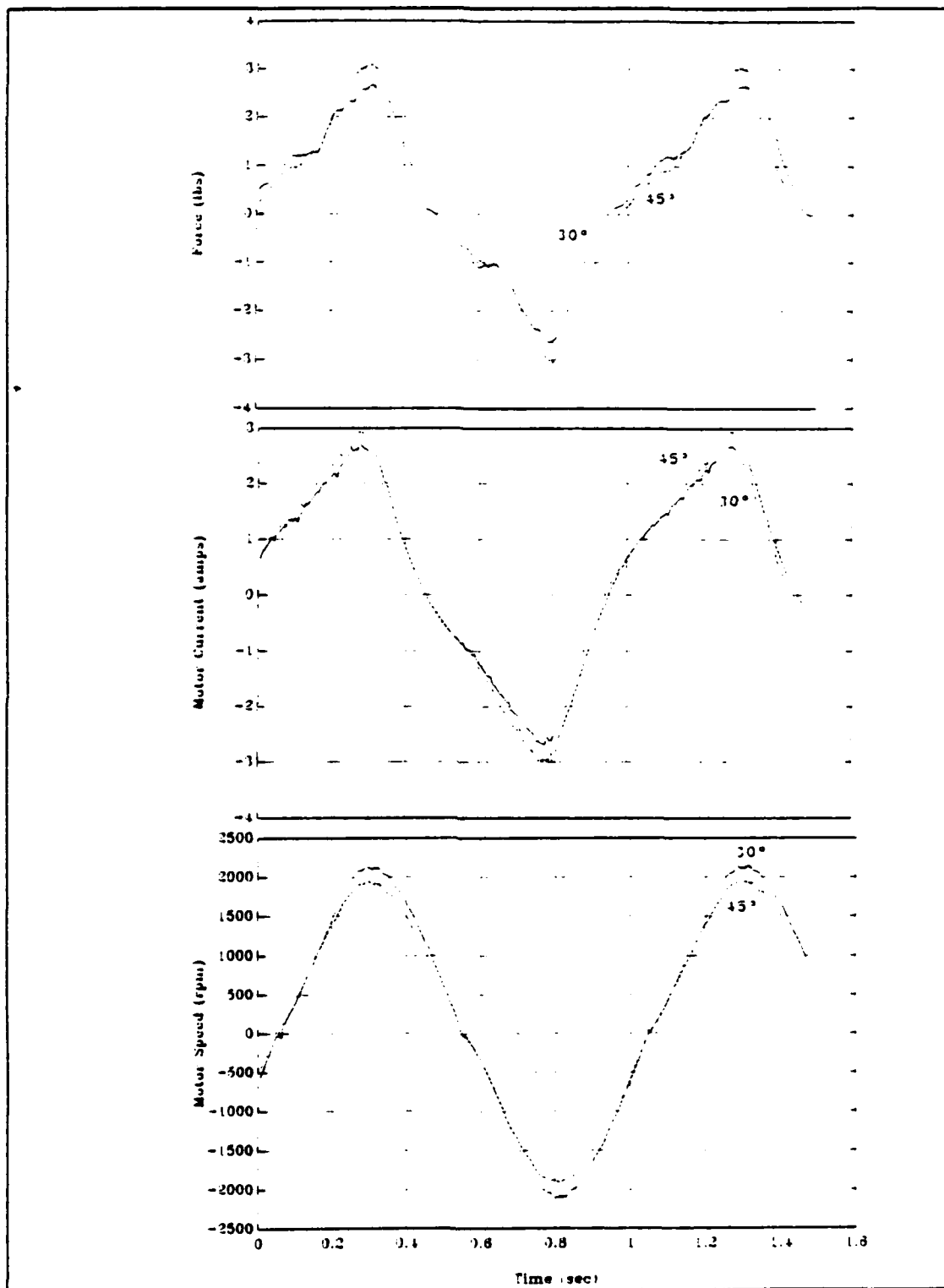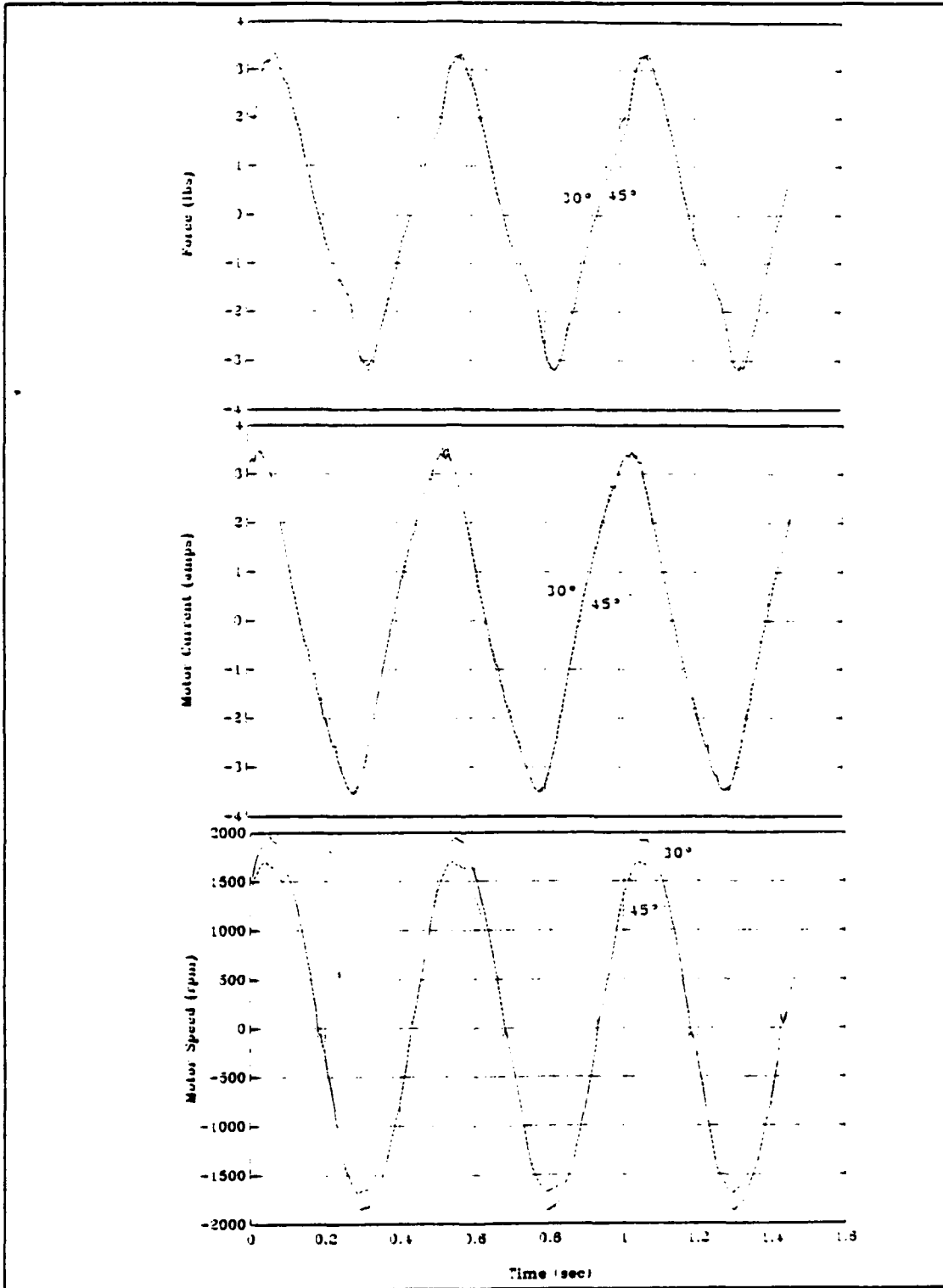
50
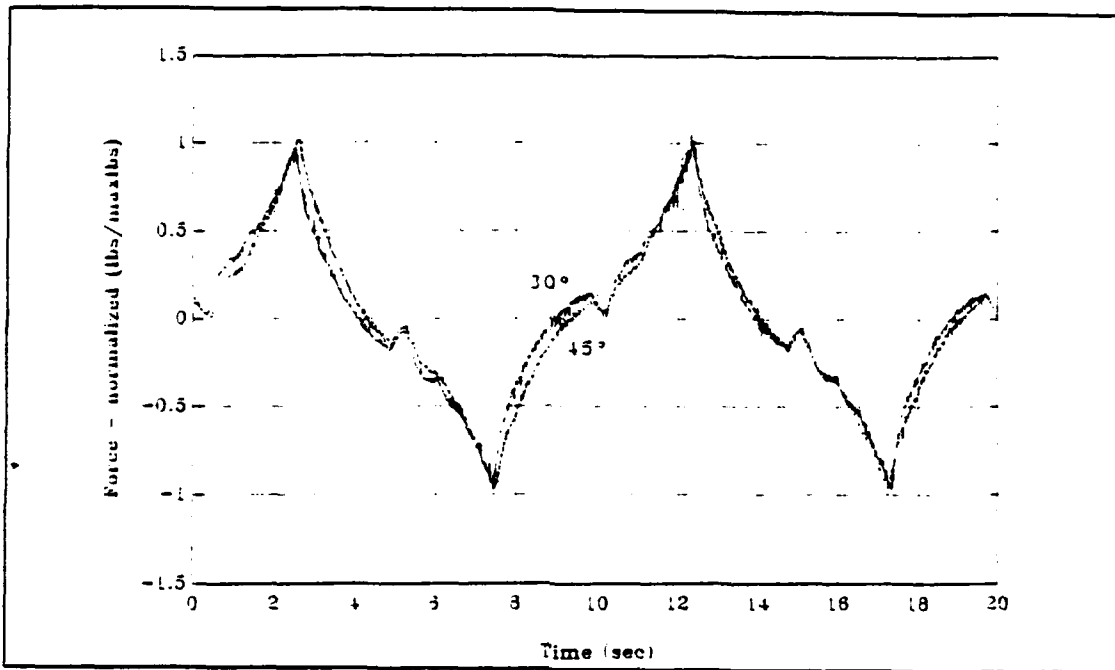
Figure 25 10 second period triangular wave, +/- 20.4 volts 30° & 45° pitch propellers, 16.5 inch tunnel length
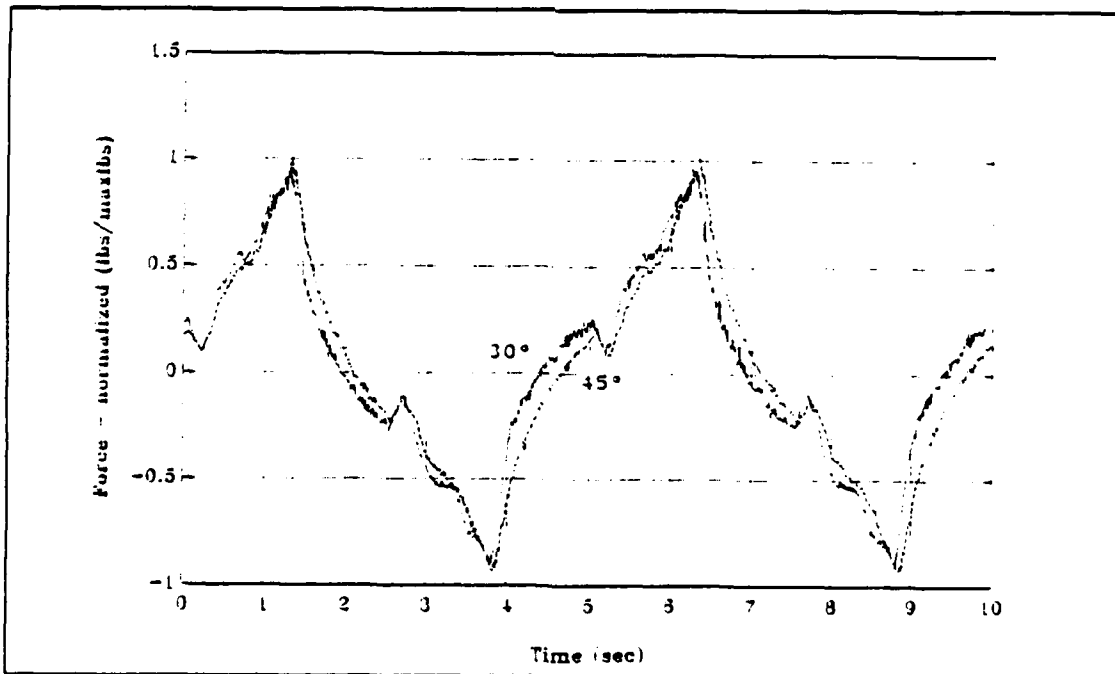
Figure 26 5 second period triangular wave, +/- 20.4 volts 30° & 45° pitch propellers, 16.5 inch tunnel length
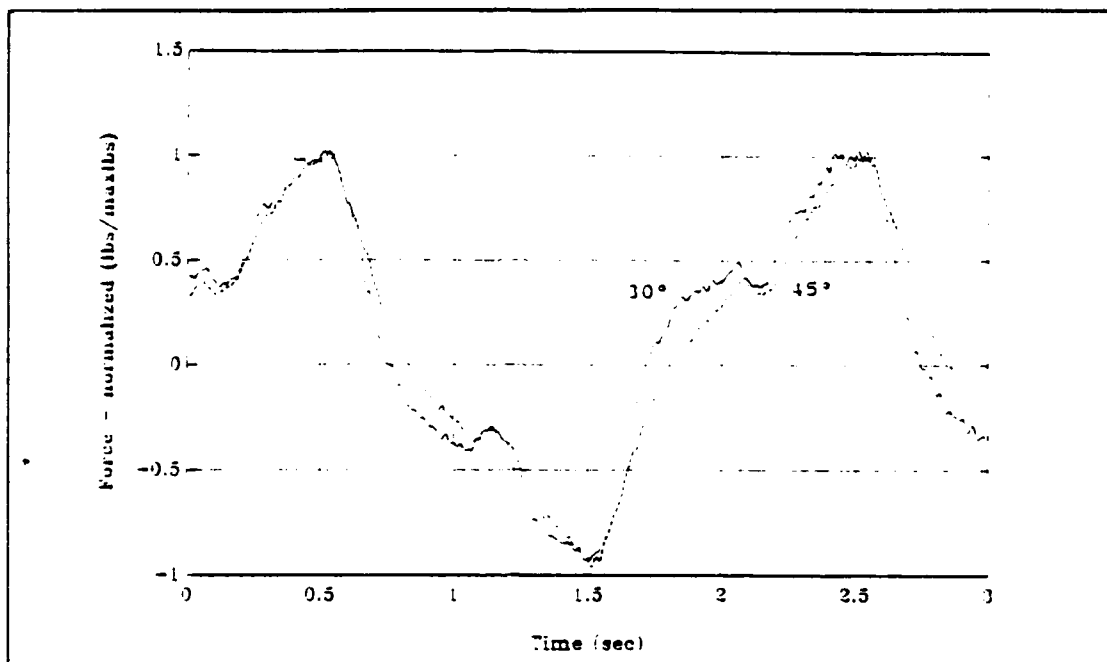
Figure 27 2 second period triangular wave, +/- 20.4 volts
30° & 45° pitch propellers, 16.5 inch tunnel length
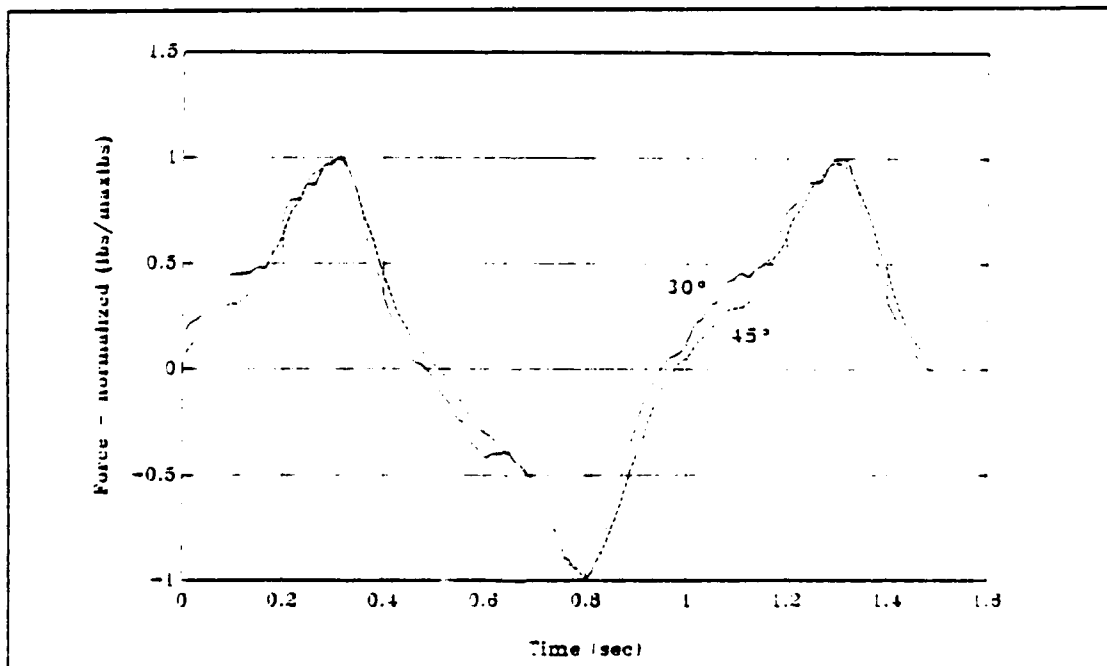
Figure 28 1 second period triangular wave, +/- 20.4 volts
30° & 45° pitch propellers, 16.5 inch tunnel length
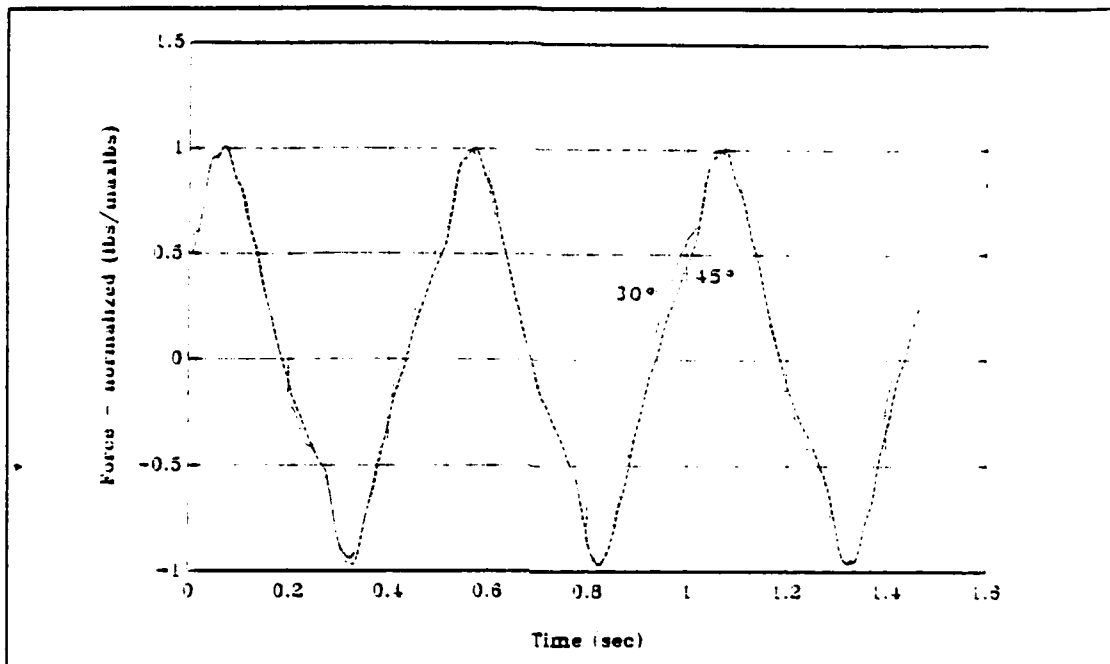
Figure 29 0.5 second period triangular wave, +/-20.4 volts 30° & 45° pitch propellers, 16.5 inch tunnel length

were adjusted from 2 seconds for the large amplitude signals to 8 seconds for the low amplitude signals in order to ensure the motor achieved steady state following the step change.

The evaluation of the square wave inputs will be broken down into two sub categories. The first will address the effects of varying propeller pitch and tunnel lengths while maintaining the same amplitude square wave input voltage. The second will analyize the effects of varying the amplitude the square wave input voltage signal with the propeller pitch and tunnel length remaining invariant.

1. Effects of Propeller Pitch and Tunnel Length

In order to determine the effects of propeller pitch and tunnel length on the thruster responses, data for different combinations, as stated above, was recorded for a square wave input signal of +/- 20.4 volts.

a. Thruster Force Response

The general shape of the force response that was observed for the various inputs following the step change was a large peak followed by a decay period to a steady state force level. In all cases, the steady state force levels observed were comparable in magnitude to the peak force levels observed for the long period (50 second) triangular wave, for the same propeller pitch and tunnel length combinations. Also, for each case a secondary peak during the decay period was observed. This coincided with an overshoot observed in the motor speed response.

Comparing the force response of the 45° and 30° propellers, at the same tunnel lengths, to the same magnitude square wave input, showed that both propellers provided the same magnitude of peak thrust for the 16.5 inch tunnel, of about 5 lbs. The peak forces for the 10.0 inch tunnels were slightly different from each other and lower than the 16.5 inch tunnel at about 4.5 and 4.0 lbs respectively. The elapsed time from step change to peak were roughly the same for all combinations. Following the peaks, the force

responses decayed to different steady state force levels over approximately the same elapsed time, with the 45° propeller providing higher steady state force than the 30° propeller, Figures 30 and 31 refer. The phenomena of both propellers providing the same magnitude peak thrust was comparable to that of the short period triangluar wave, where both propellers provided the same response. The two responses were of different peak magnitudes, however.

Comparing the force response of the same propeller at two different tunnel lengths showed that the longer tunnel provided a significantly larger magnitude peak thrust, at roughly the same time constant, than the shorter length. It then decayed to slightly less steady state force than the shorter tunnel, (Figures 32 and 33). This is consistant with the responses for the long period triangular waves where the peak forces were lower in the long tunnels due to fluid friction. Additionally, the peak thrust difference for the two different tunnel lengths is consistant with the extra inertia due to the larger volume of water being acted upon.

b. Motor Current Response

As seen before with the triangular waves, the current response follows that of the force response, as expected. Also as seen with the triangular waves, the steady state current responses appear to be affected by propeller pitch and unaffected by tunnel length, (Figures 30, 31, 32 and

33). The steady state current levels are consistant with the peak levels for the long period triangular waves for similar propeller configurations. This supports the earlier assumption that the long period triangular wave would approximate steady state conditions. Additionally, as seen in the force response, a secondary peak was observed in the decay period, which also concided with the overshoot observed in the motor speed response.

c. Motor Speed Response

The motor speed response was roughly the same for all cases, typical of a first order lag with a slight overshoot before settling out at steady state. As seen with the triangular waves, the speed response appeared to be affected by propeller pitch and unaffected by tunnel length, (Figures 30, 31, 32 and 33). The steady state speed was consistant with the long period triangular wave with the same propeller configuration, again validating the assumption stated above.

2. Effects of Amplitude of Applied Input Square Wave

For this section, the effects of varying the amplitude of the applied square wave input voltage, as described above, will be evaluated for a single propeller pitch and tunnel length combination of 30° and 16.5 inches. Other combinations produced similar results.

a. Thruster Force Response

As expected, the force response to the decreasing magnitude square wave input showed a decrease in both the peak and steady state magnitudes as can be seen in Figure 34. In all cases, the peak force was reached in approximately the same elapsed time and decayed to steady state in approximately the same elapsed time as well. Only the 20.4 volt signal exhibited a secondary peak during the decay. This was again coincident with an overshoot observed in the motor speed response for the 20.4 volt signal.

b. Motor Current Response

The motor current response followed the force responses as has been seen throughout this experiment. The peaks were reached within approximately the same elapsed time and the decay to steady state occurred over approximately the same elapsed time. Also, as seen in the force response, only the 20.4 signal exhibited a secondary peak during the decay period, coincident with the overshoot observed in the motor speed response.

c. Motor Speed Response

The motor speed response exhibited a standard first order lag response of approximately the same time constant, 0.05 seconds. As expected, the steady state speed was dependent upon the magnitude of the input signal. Only the 20.4 volt signal was observed to exhibit an overshoot.
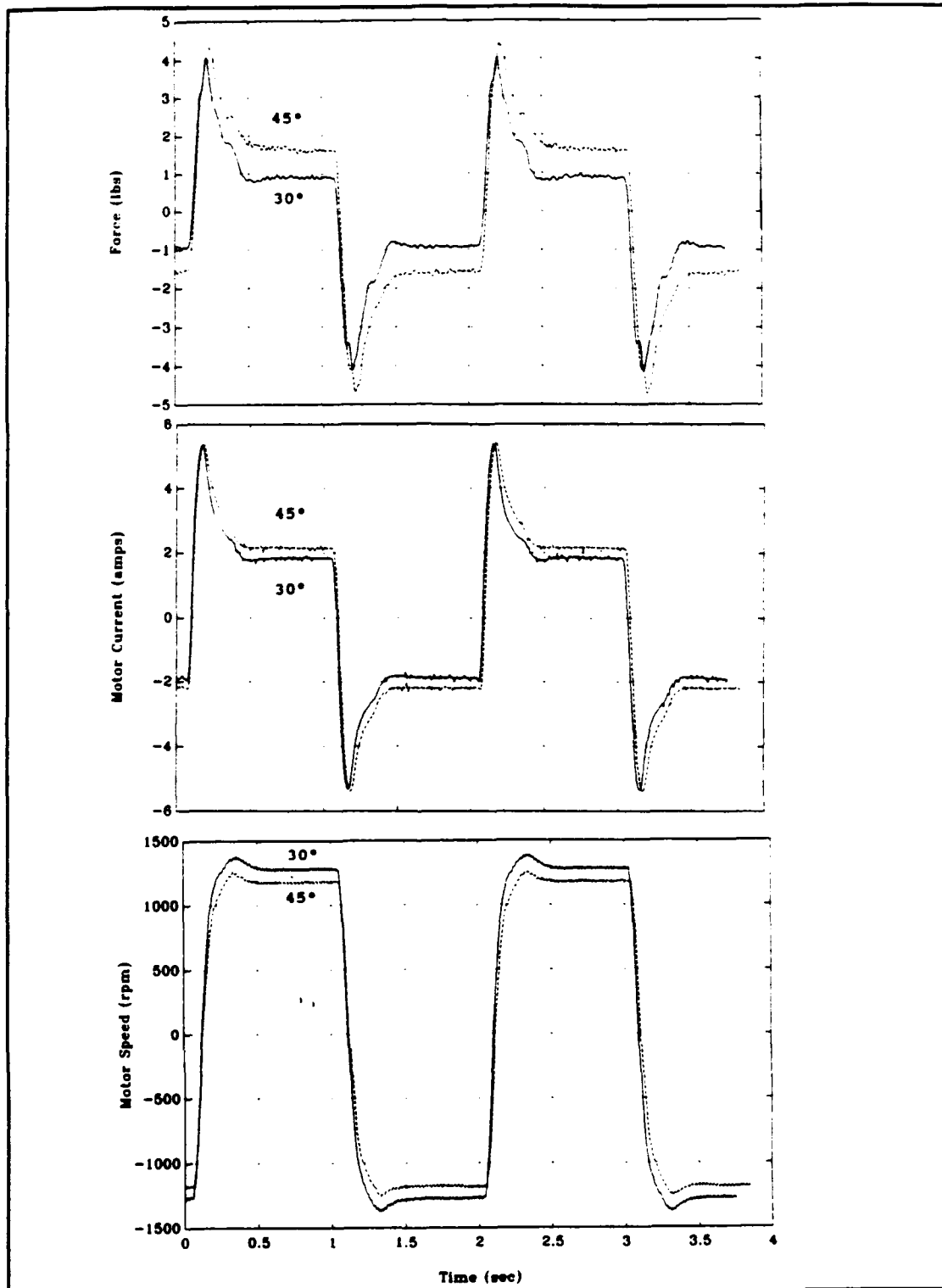
Figure 30 2 second period square wave, +/- 20.4 volts, 30° & 45° pitch propellers, 10.0 inch tunnel length
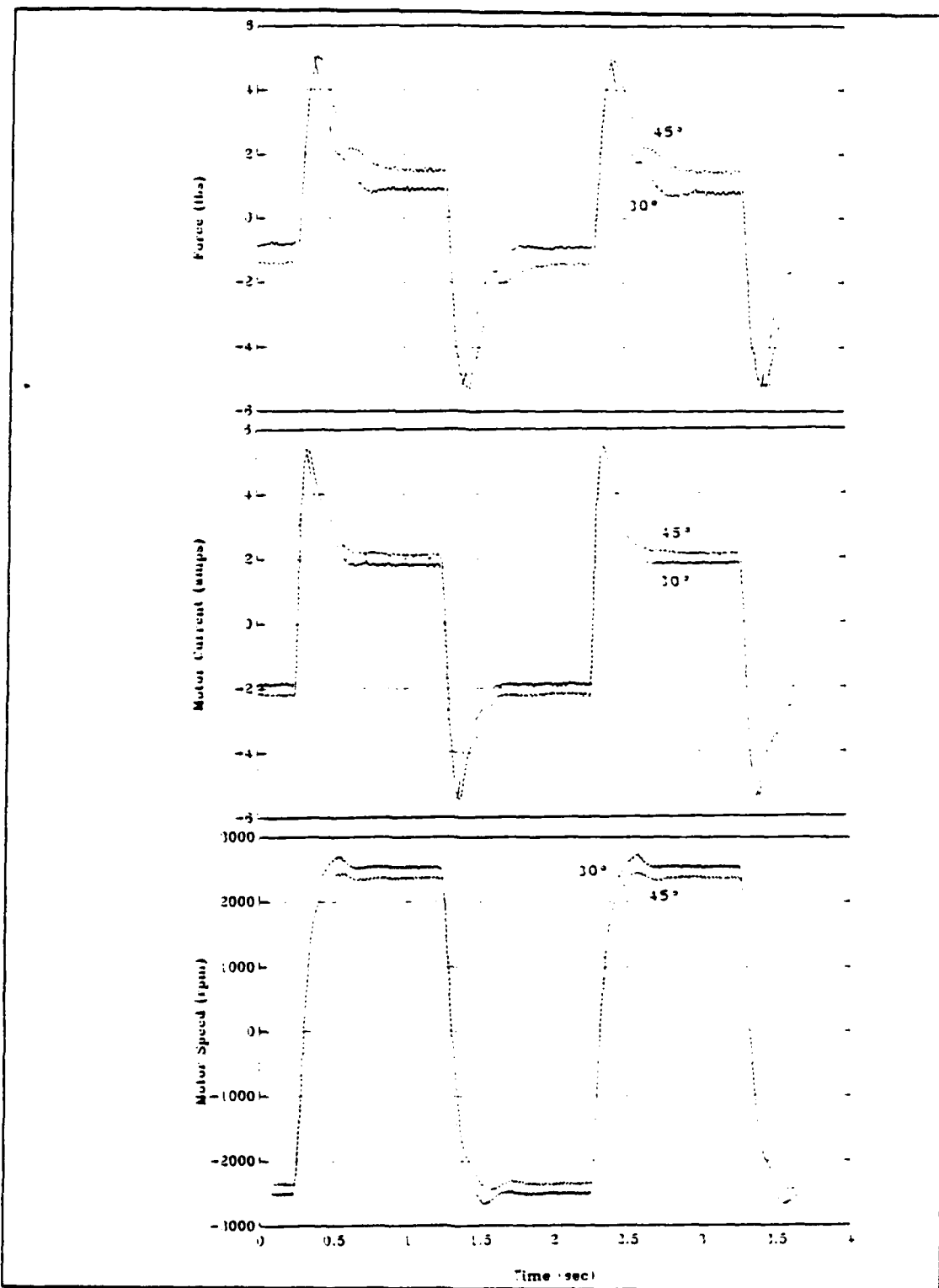
Figure 31 2 second period square wave, +/- 20.4 volts, 30° & 45° pitch propellers, 16.5 inch tunnel length

59
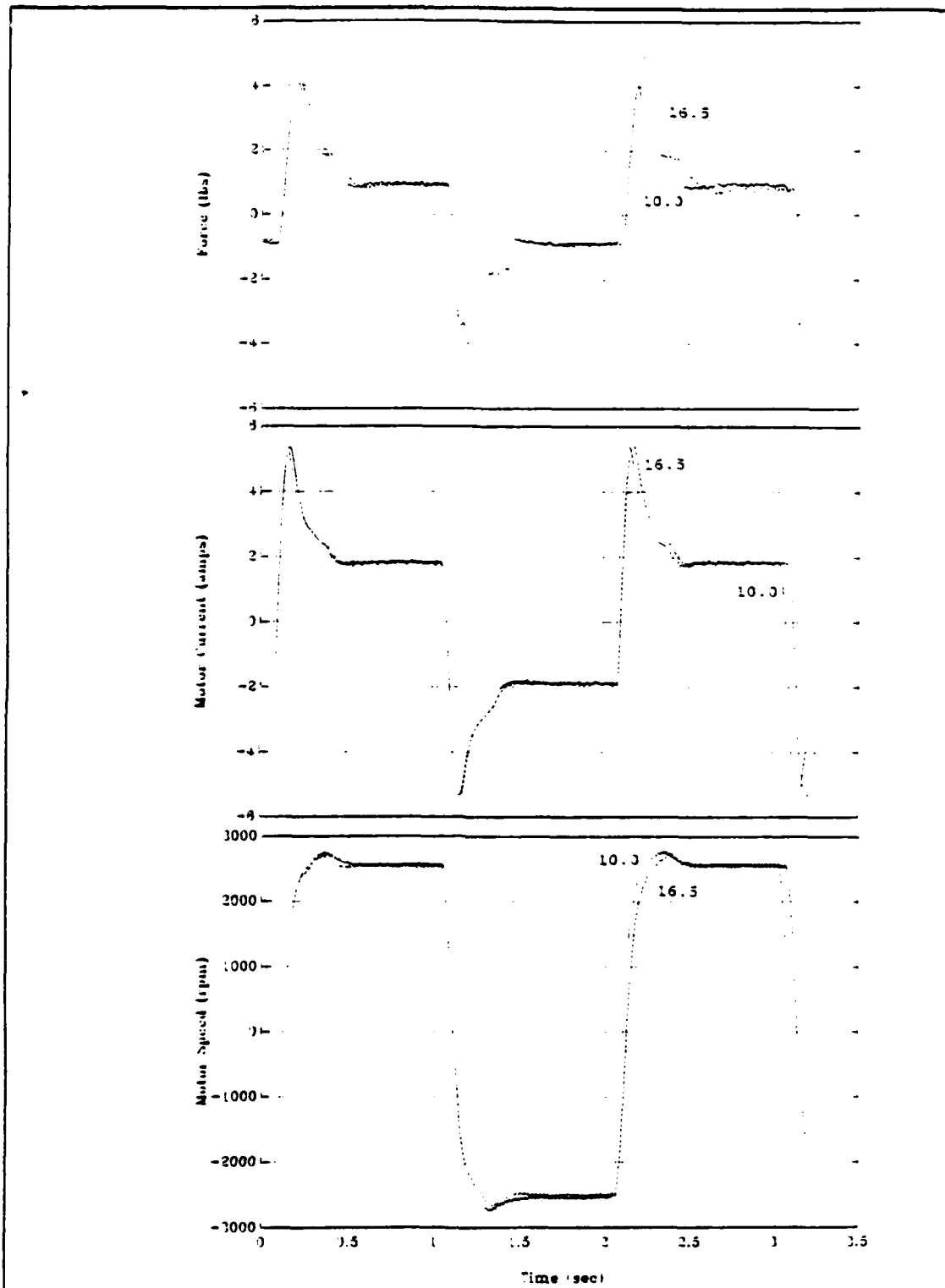
Figure 32 2 second period square wave, +/- 20.4 volts, 30° pitch propeller, 10.0 and 16.5 inch tunnel lengths
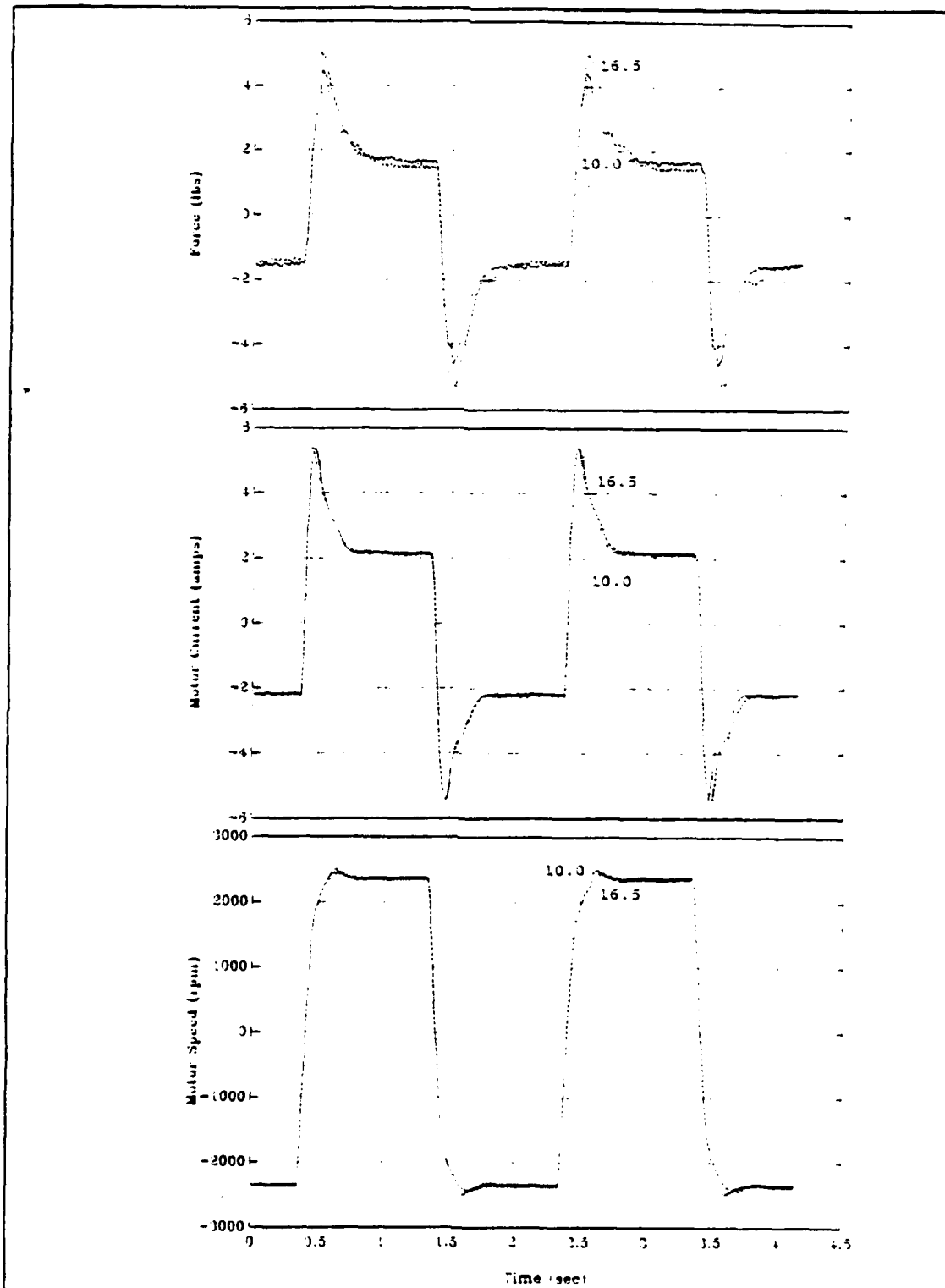
Figure 33 2 second period square wave, +/- 20.4 volts,
45° pitch propeller, 10.0 & 16.5 inch tunnel lengths

61
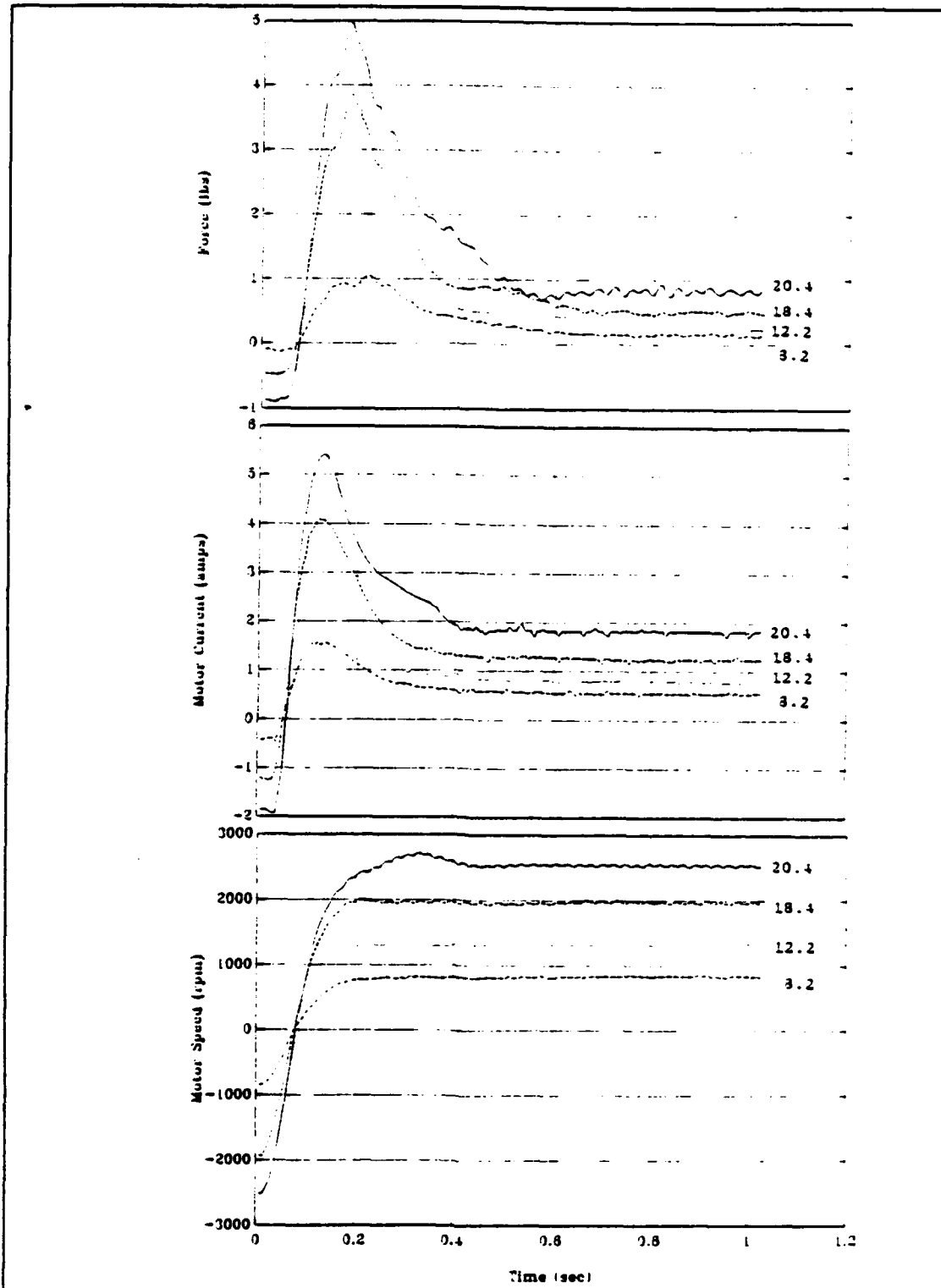
Figure 34 2 second period square wave, +/- 20.4, 18.4, 12.2, and 8.2 volts, 30° pitch propeller, 16.5 inch tunnel length

62

V. COMPARISON OF MODEL AND EXPERIMENTAL DATA

A. GENERAL

In this chapter the actual construction of the model, with emphasis on determining the numerical value of particular coefficients, and the comparison of simulated responses to the experimental data will be discussed.

B. DETERMINATION OF MODEL COEFFICIENTS

The model derived in Chapter II basically consisted of two coupled first order differential equations. One for motor angular velocity,

$$\dot{\omega}_M = \frac{-(C_{PM} + \frac{K_T K_M}{R})}{J_{PM}} + \frac{K_T}{R J_{PM}} Vs - \frac{\tau_H}{N J_{PM}}$$

where the hydrodynamic torque (τ_H) is related to the pressure or thrust on the propeller blades (T) by some efficiency factor (σ) and acting at some effective blade length (L_B),

$$\tau_H = \sigma L_B T$$

and where the thrust (T) is related to the acceleration of the mass of the water column and its momentum by,

$$T = \rho A (L + L_a) \dot{U} + \rho A \Delta \beta U |U|$$

Note that this equation for thrust differs from the one for McLean's model, in that the coefficient for the acceleration term is not a strictly linear relationship with respect to length of the tunnel. More likely, it is a combination of tunnel length and some other added length term resulting from added mass which is related to the cross sectional area of the tunnel.

The second equation is for the affected water column linear velocity (U) where the acceleration of the water column (U) is related to the angular velocity of the motor (ω_M) by some time constant (t_c), assuming that the axial flow velocity in the tunnel is proportional to propeller speed but does not respond instantaneously. Thus,

$$\dot{U} = \frac{(-U + (np) \frac{\omega_M}{N})}{t_c}$$

In order to be able to solve these equations for specific values, the particular coefficients for the thruster system had to be determined. Several of these coefficients were unique to the motor and provided by the manufacturer, others had to be calculated or measured and still others had to be

64

estimated and then refined through trial and error comparisons with the empirical data. Refer to Appendix A for a table of coefficients and their associated values.

1. Known and Calculatable Coefficients

The coefficients provided by the manufacturer of the motor consisted of the armature inertia (J_M), the motor resistance (R), the torque constant (K_T), and the motor constant for back EMF (K_M) [Ref. 6]. The inertia of the pinion (J_{DG}) and ring gear were calculated from their dimensions and material density. The inertia of the propeller (J_P) was approximated by determining the rotational inertia of a disk of the same size and material, and adding to that the inertia of the ring gear. The cross sectional area (A) was calculated from the inside diameter of the tunnel and the length of the tunnels (L) was determined by direct measurements. The reduction gear ratio (N) was calculated from the specifications provided by the manufacturer, specifically the number of teeth per gear [Ref. 7]. The pitch of the propeller, or the linear distance travelled per radian of rotation (assuming no slip conditions), was calculated by utilizing the angle of the blade and the radius of the propeller [Ref. 8]. This assumed that the blade had the same pitch for the entire length of the blade. Finally, the density of the water (ρ) was assumed to be at standard

temperature and pressure and constant throughout the course of these experiements.

2. Unknown Parameters

The remaining coefficients for the motor shaft (C_M) and the propeller shaft (C_p) friction, the added length (L_a), the propeller efficiency (η), and the momentum correction factor ($\Delta\beta$) were initially estimated. In order to begin the process by which these parameters were determined, the friction was set at zero, the added length was set to the length of the tunnel and the momentum correction factor was adjusted to obtain the best match to the experimental data. Next the efficiency term was adjusted to improve the match. The friction terms were increased to reduce the force and speed while increasing the current to make fine adjustments. Finally the added length term was adjusted while comparing combinations of the same propeller at two different tunnel lengths. Through these trial and error comparisons with experimental data, the coefficients were refined to consistant values for the friction and the added mass terms. These appeared to be independent of the propeller pitch, tunnel length or any other variables of this experiment. The propeller efficiency and the momentum correction factor proved to be dependent only upon the propeller used. This is consistant with propeller theory [Ref. 8].

3. Computer Simulation

In order to graphically observe the behavior of the model for applied input voltages, a MATLAB computer program was written to solve the above differential equations, utilizing the ODE45 solver function. The program was written to accept inputs interactively from the operator that tailored the program to a specific triangular or square wave input signal as well as a specific propeller and tunnel length combination. These adjustable inputs were the time period of the input signal (T), the maximum input control voltage (Vs), the tunnel length (L), the propeller efficiency (η), the propeller pitch (p) and the momentun correction factor ($\Delta\beta$). This allowed the operator to quickly and easily reconfigure the model for comparison with data from a different set of variables. Refer to programs MODELT.M and MODELS.M in Appendicies B and C respectively.

In Chapter II, during the development of the model, the inductance of the motor was ignored due to its seemingly insignificant value. However, in attempting to model the applied voltage signal to the motor, it was found that a small first order delay (tau) was necessary at abrupt voltage changes such as the steps for the square wave in order to avoid singularities arising from the ODE45 solver used. This was originally found to be necessary only for the square wave signal but was also applied to the triangular wave for consistency with successful results.

In both cases, for the triangular and square wave inputs, a function to simulate the regularly varying applied voltage signal was required. This was imbedded in the ODE solver function. The first order delay described above was incorporated into this function. Refer to programs OMEGAT.M and OMEGAS.M in Appendicies D and E for the voltage signal simulation.

C. COMPARISON OF MODEL TO EXPERIMENTAL DATA

The graphic comparison of the model simulation to the experimental data will be broken down into the responses to the triangular and the square wave inputs. The coefficients for a specific propeller and tunnel combination were held consistant for the simulations between both of the two different types of input signals.

It should be noted that the magnitude of the maximum voltage signal used as the control signal input to the PWM servo amplifier produced a simulation of significantly higher responses, most notably in the motor speed response. A simulated voltage signal that best represented the experimental responses was +/- 8.0 volts vice +/- 9.0 volts. This may be attributed to the fact that only the control voltage signal, not the voltage to the motor was recorded and that the output voltage from the 24 volt power supply to the PWM servo amplifier was set at a no load condition. Input control voltage signals of 8.0 volts were used in generating

the simulations presented in this chapter.

In order to provide a commonality between the simulation and the experimental data, the phase of the experimental motor speed reponse was adjusted to coincide with that of the simulation. As in Chapter IV, where the experimental data was compared to determine the effect of several variables, some phase differences between the experimental data and simulation existed due to the inaccuracies in the generated time counter.

For both the triangular and square wave inputs, the model simulations provided remarkably similar responses. However, fluid friction was not modeled and hence the result of increased tube length did not have the same effect as the experimental data of reducing the output thruster force. Also, the maximum motor speed for the simulation was noticably higher than the experimental data in all cases. This may be an extension of the disparity between the experimental and simulation control voltage input encountered above.

The simulated responses were generated utilizing the ODE function solver and required initial conditions for motor speed and water column velocity. These initial conditions were set at zero for a static environment. As such, the initial portion of each simulation does not reflect the dynamic conditions present in later data points, or the experimental data, for that matter. It does, however, provide good information pertaining to response from static conditions.

1. Triangular Wave Response Comparison

All combinations of propeller and tunnel length at varying periods were examined. As with the experimental data, the simulations provided responses consistant with a specific propeller and tunnel length combination. All four combinations will be addressed under the section for the long period (50 seconds) wave, for comparison to see the effects of the individual variables. Only one combination will be utilized to demonstrate the effect of reduced periods.

a. Long Period (50 second) Waves

As seen in Figures 35, 36, 37 and 38, the simulated responses for force, motor current and motor speed followed closely those of the experimental data. The simulations, however, did not show the effects of stiction and passed through the null condition in a smooth, continuous fashion as expected.

b. Shorter Period Waves

As the period of the triangular wave was reduced from 50 seconds, the simulated responses for force, motor current and motor speed again followed those of the experimental data extremely closely. Reflecting the influence of the increasing fluid inertia, the simulated responses of force and motor current became more skewed with decreasing period as seen in Figures 39, 40, 41, 42 and 43. Begining with the the five second period, however, the simulated

responses for force and motor current begin to 'lead' those of the experimental data. The effect became more noticable with the shorter periods, where the force response led by a comparatively larger amount than the motor current response. In all cases, however, the general shape of the three responses were similar to those of the experimental data with the major disparities appearing in the regions of stiction and the peaks. This may be attributable to modeling inaccuracies that resulted from ignoring the effect of inductance and complex added mass effects.

2. Square Wave Inputs

As seen with the triangular wave responses, the simulated responses of thruster force, motor current and motor speed to square wave input signals followed extremely closely to those of the experimental data. The steady state values for the force and motor current were utilized as one of the major benchmarks by which to gauge the selection of appropriate values for the variables and as such are almost identical with the experimental data. This carries over to the long period triangular wave responses as well since they are dominated by steady state conditions.

The simulations, however, did not exhibit an overshoot in the motor speed response and associated secondary peaks in the force and motor current responses as did the experimental data as seen in Figures 44, 45, 46 and 47. This may be

attributable to the complexities in modeling the added mass effects of the surrounding water.

The simulated responses for force and motor current also showed a tendency to 'lead' those of the experimental data, as they did with the shorter periods triangular wave input signals. This may be a combined result of the time constants associated with the input voltage signal and the water column velocity equations. It is important to note here that the parameters identified by matching were not changed in identifying the 'dynamic' effects.

Only one simulation for a reduced step voltage signal comparable to those seen in Chapter IV, Figure 34, was produced. A signal of +/- 6.0 volts versus +/- 6.75 (same ratio as 8.0 versus 9.0) was utilized and is provided as Figure 48. The simulation was consistant with those of the other simulations in that it followed the same general shape as that of the experimental data, that the magnitudes at both peak and steady state were almost identical and that the force and motor current responses 'lead' those of the experimental data.

The simulated responses did show a reduction in the peak and steady state values consistent with a reduction in the voltage signal as did the experimental data. This leads to the expectation that further reductions in input voltage signals would produce similar results.

Figure 35 50 second period triangular wave, +/- 20.4 volts, 30° pitch propeller, 10.0 inch tunnel length with model

73

Figure 36 50 second period triangular wave, +/- 20.4 volts, 30° pitch propeller, 16,5 inch tunnel length with model

Figure 37 50 second period triangular wave, +/- 20.4 volts, 45° pitch propeller, 10.0 inch tunnel length with model

75
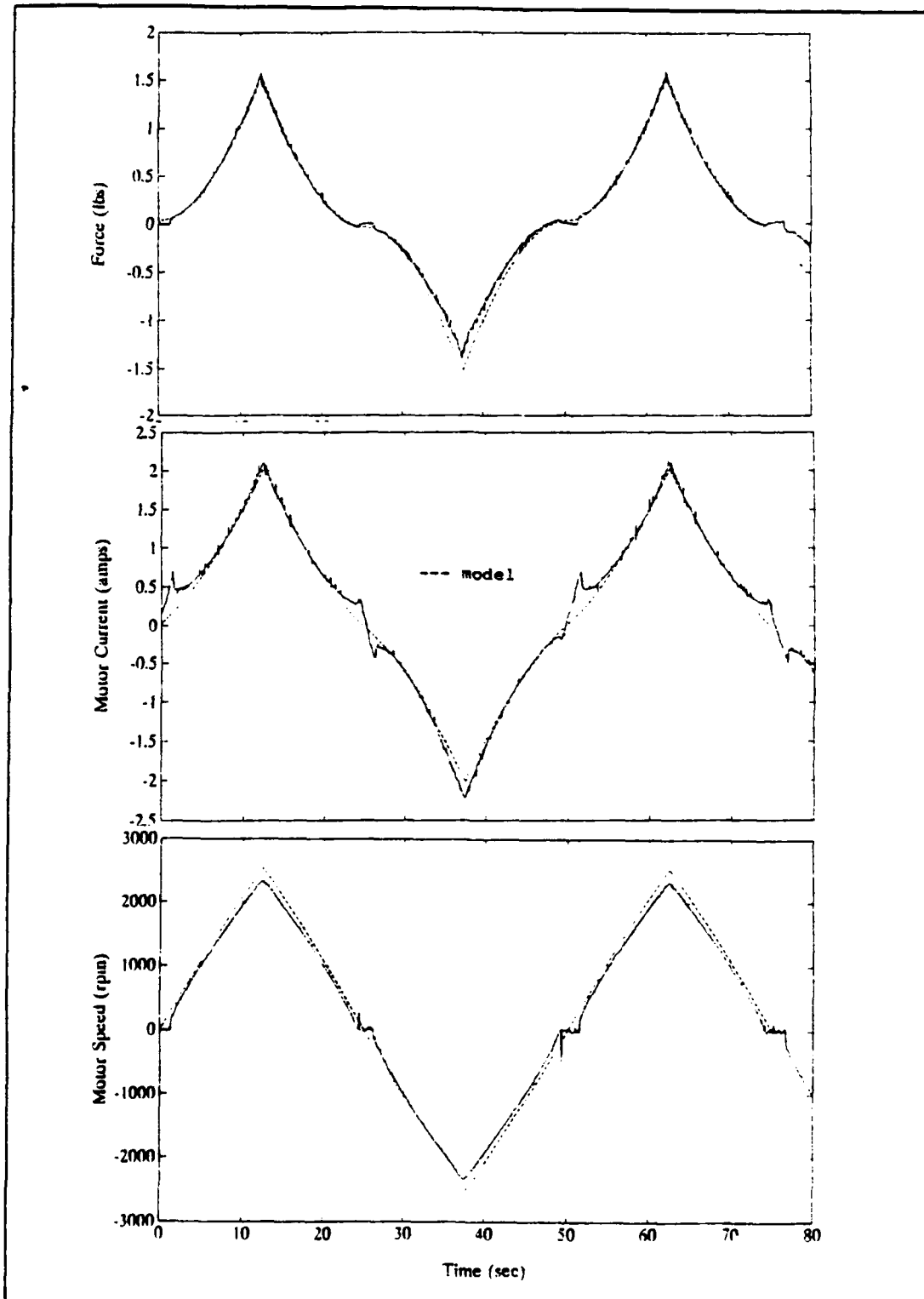
Figure 38 50 second period triangular wave, +/- 20.4 volts, 45° pitch propeller, 16.5 inch tunnel length with model

76
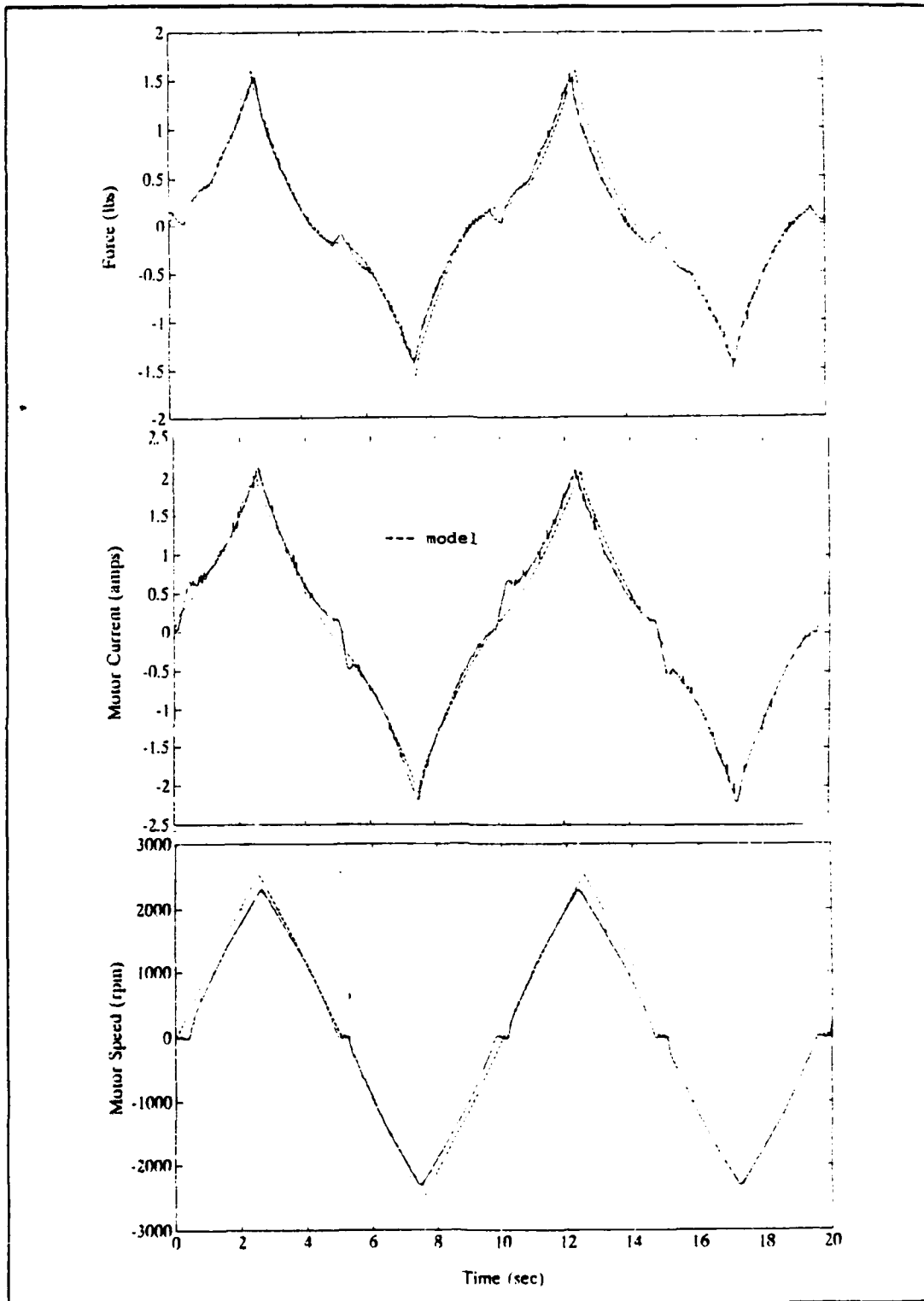
Figure 39 10 second period triangular wave, +/- 20.4 volts, 45° pitch propeller, 16.5 inch tunnel length with model
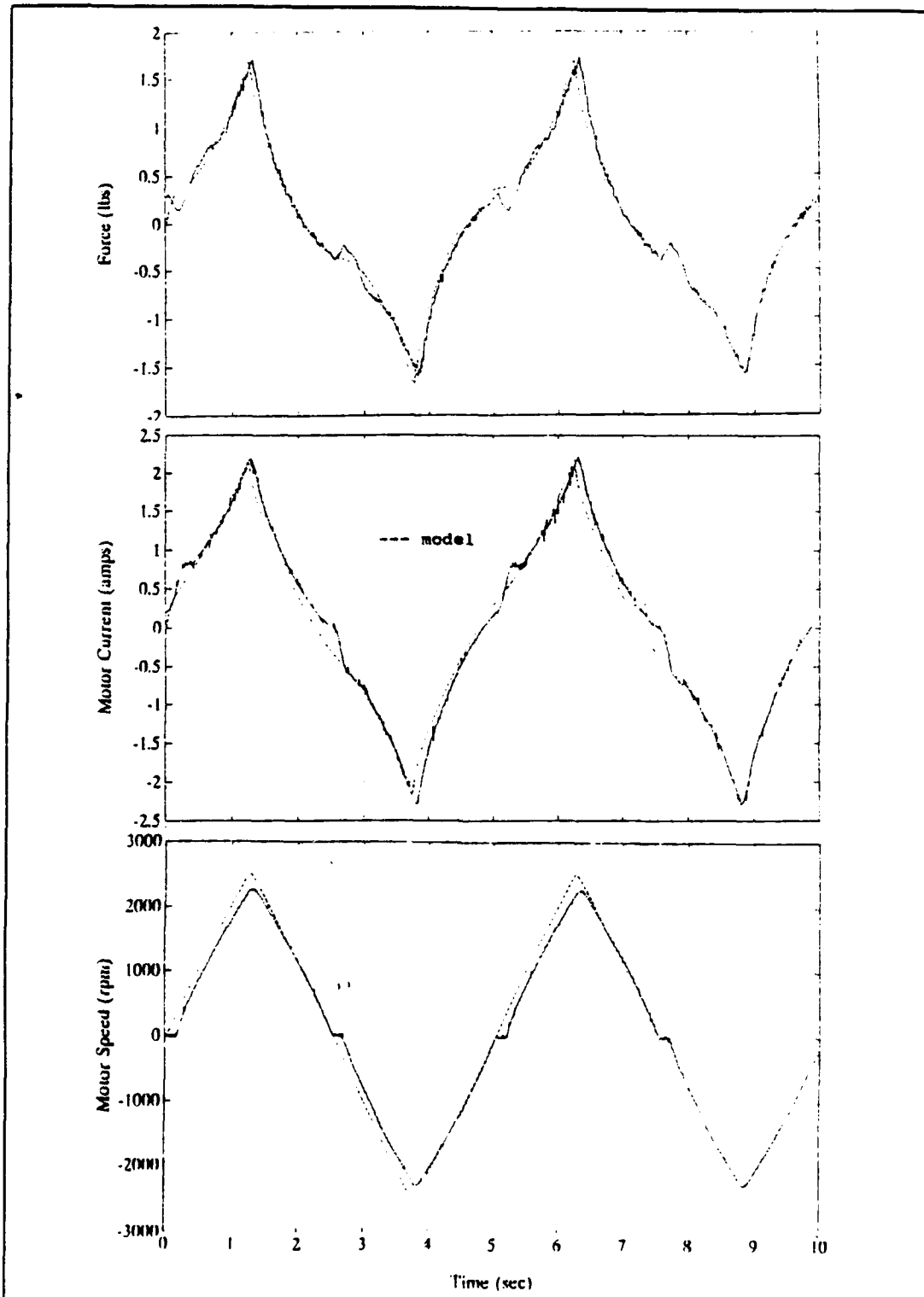
Figure 40 5 second period triangular wave, +/- 20.4 volts, 45° pitch propeller, 16.5 inch tunnel length with model

78
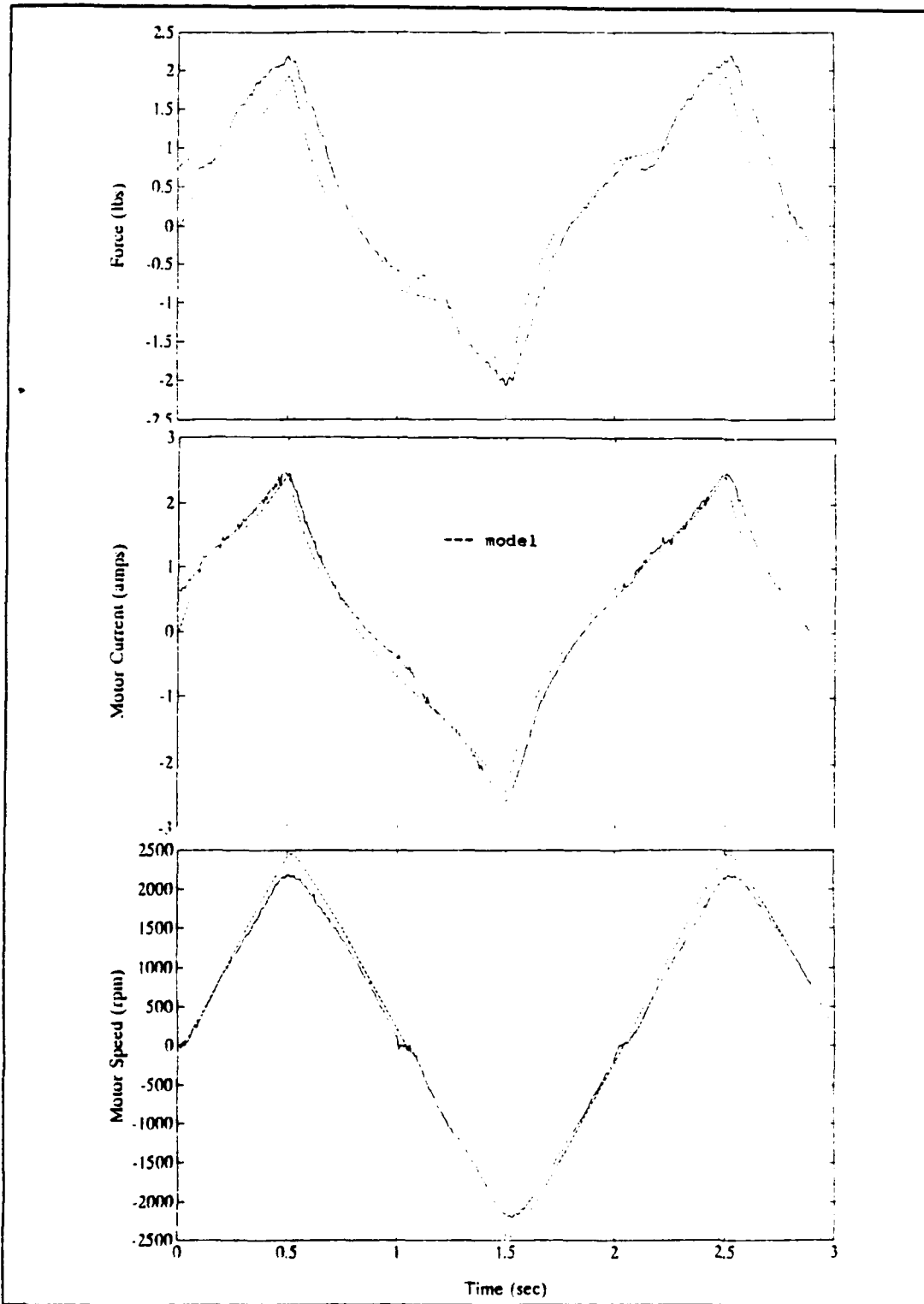
Figure 41 2 second period triangular wave, +/- 20.4 volts, 45° pitch propeller, 16.5 inch tunnel length with model
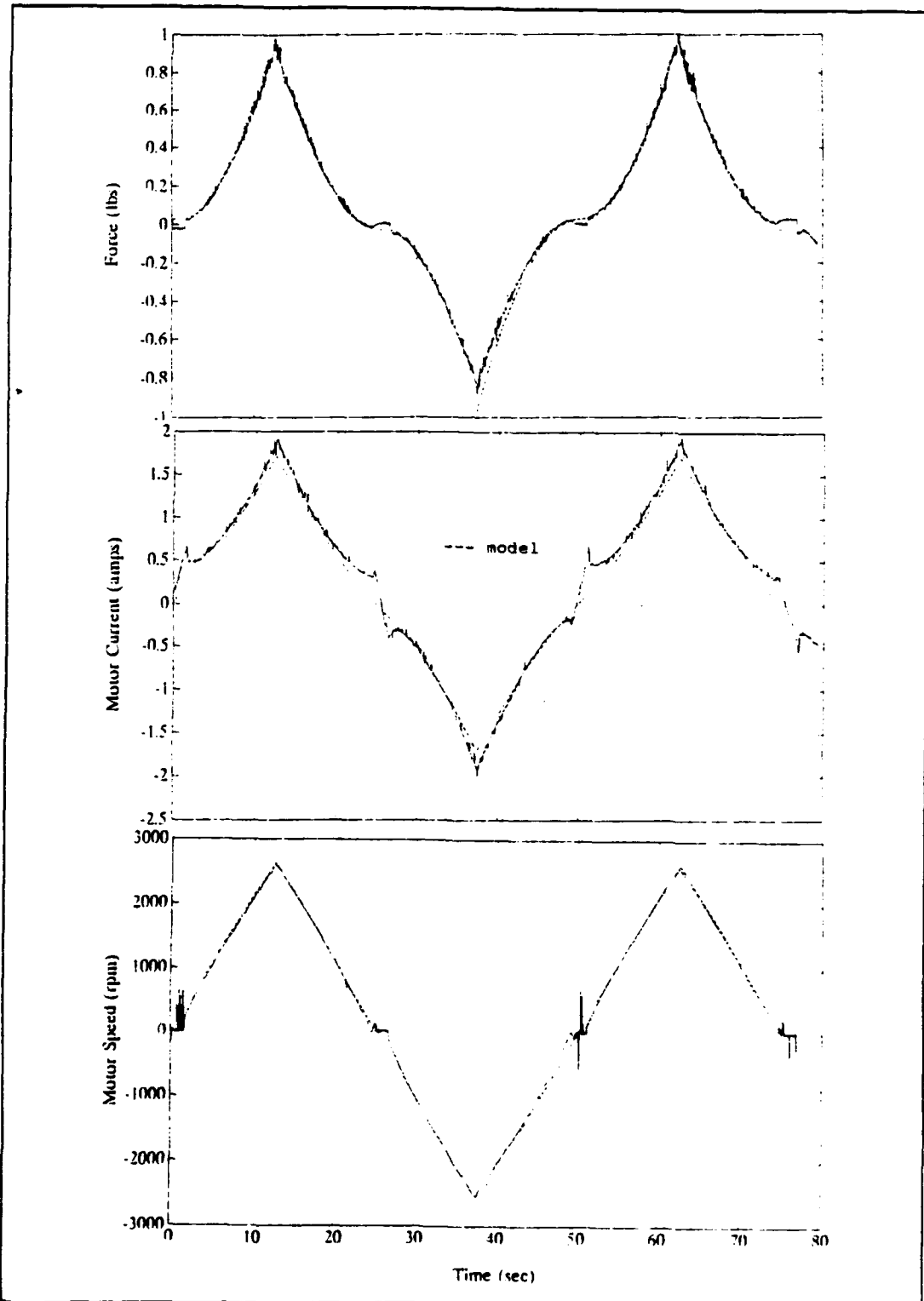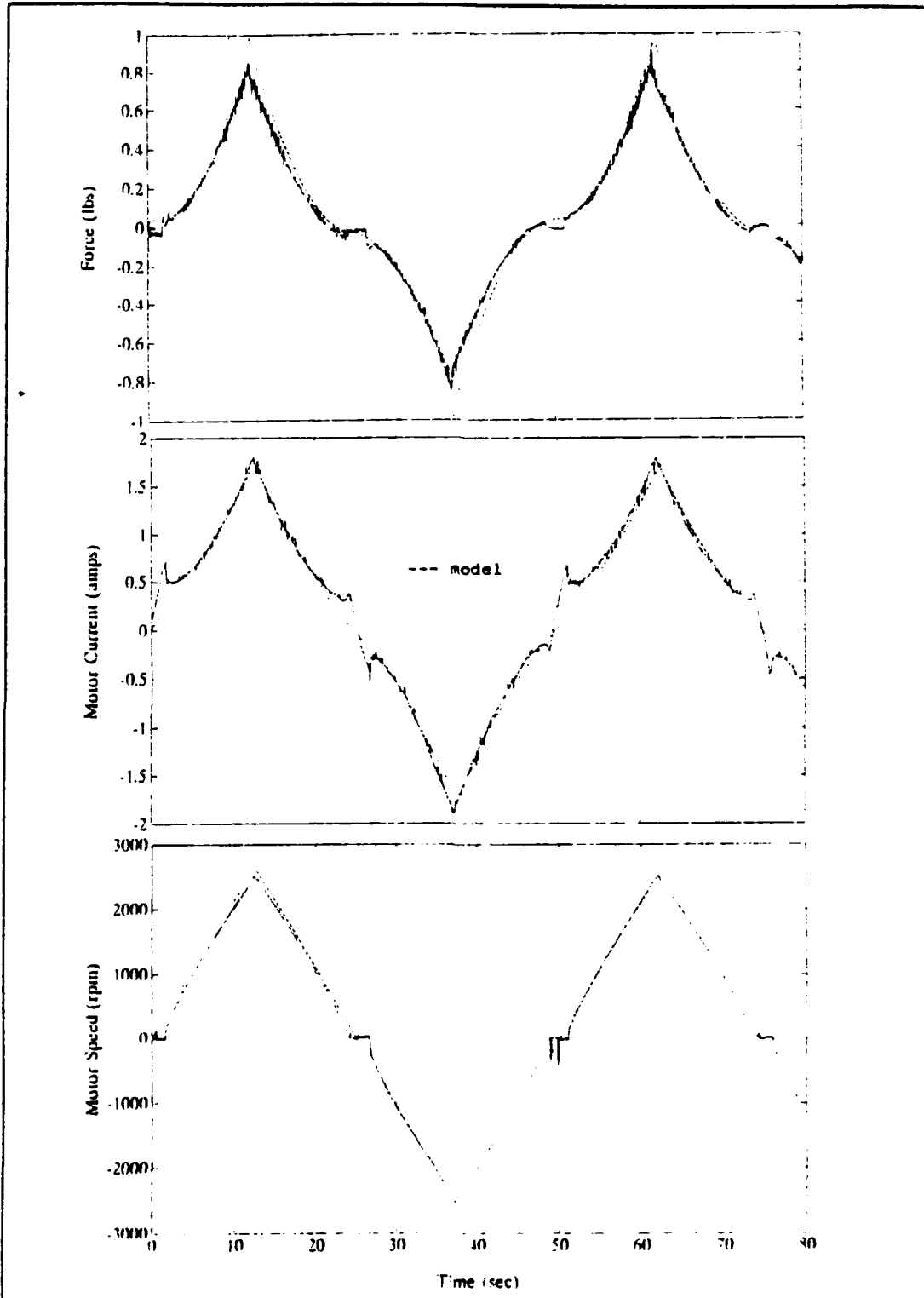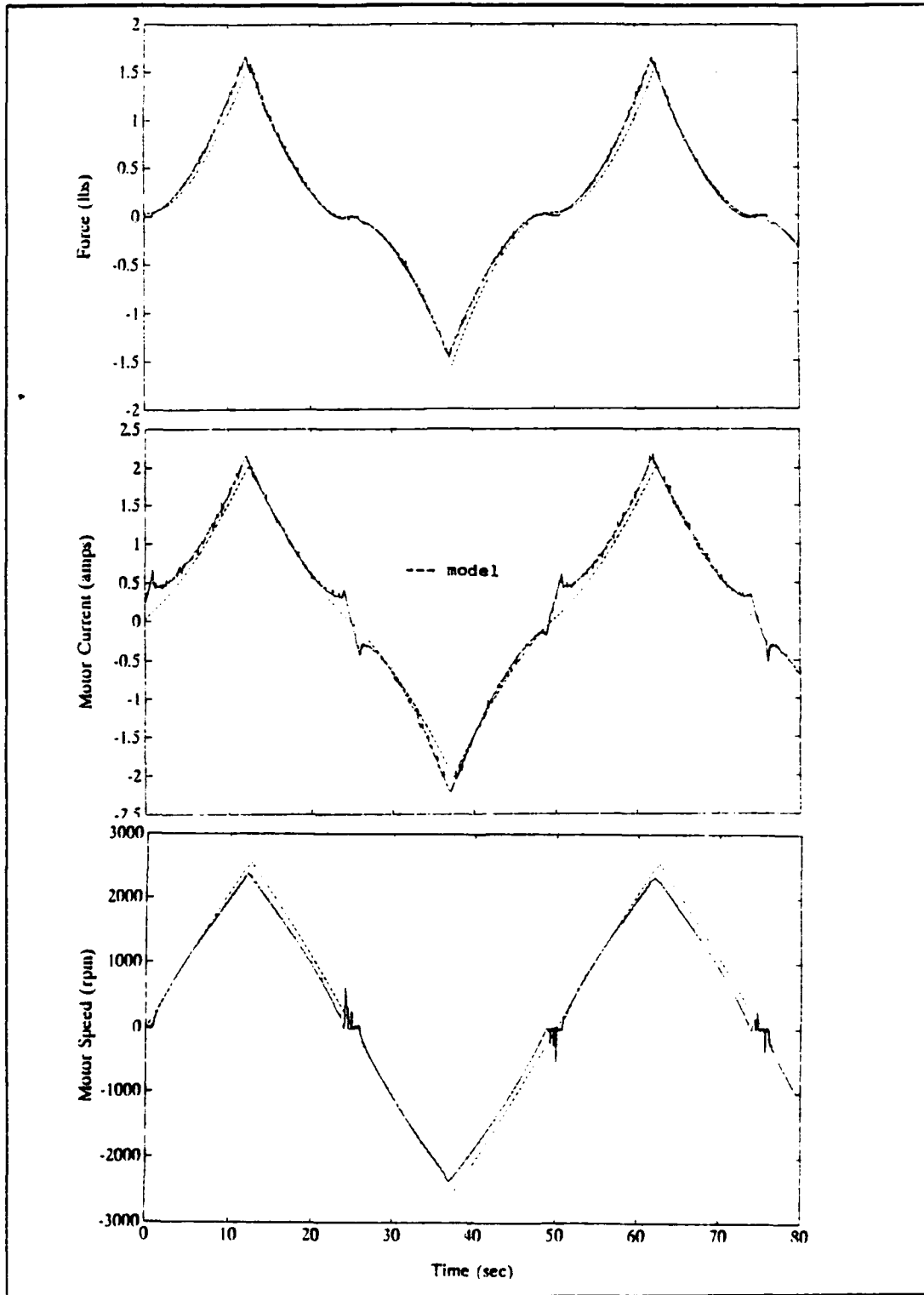
79
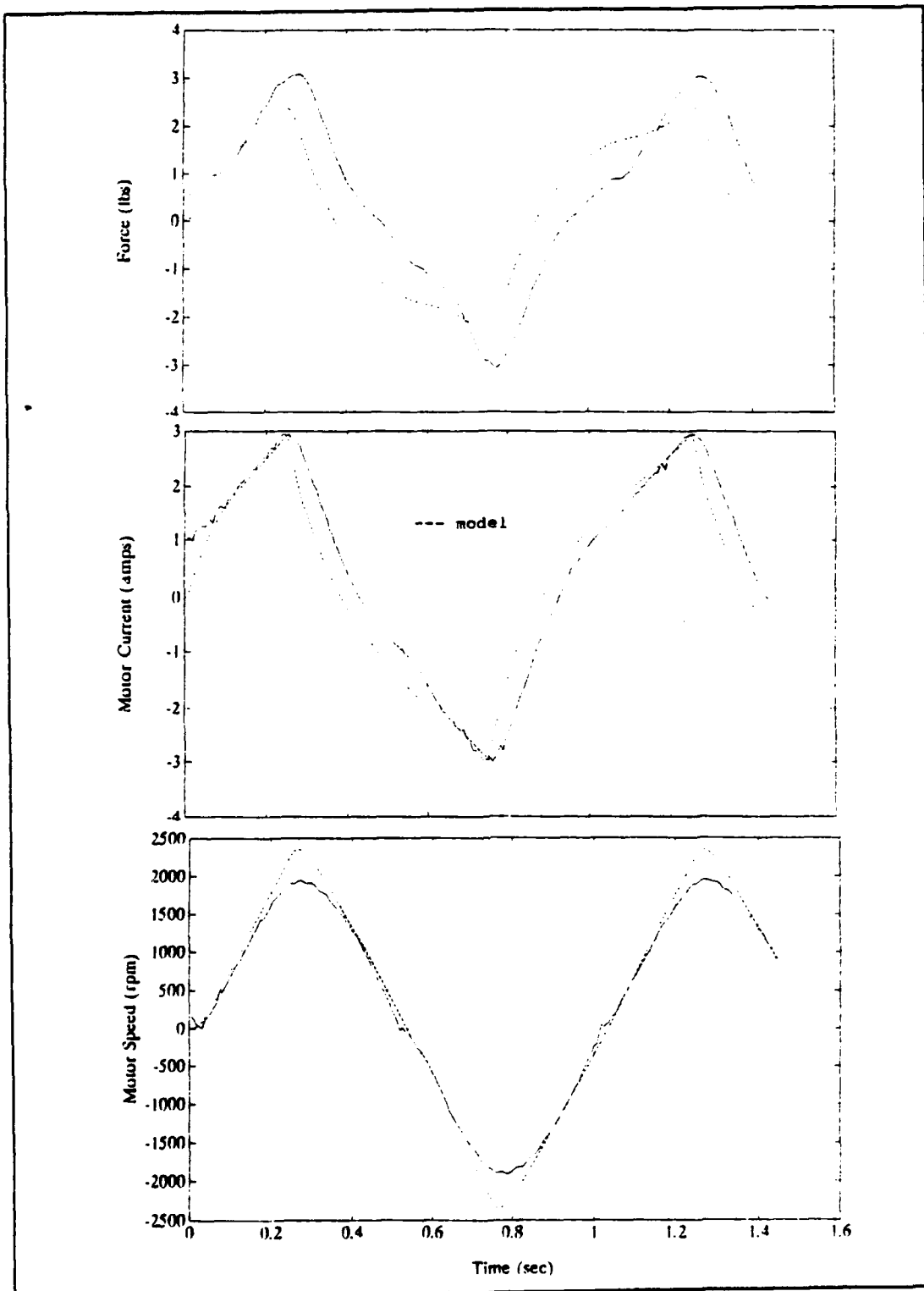
Figure 42 1 second period triangular wave, +/- 20.4 volts, 45° pitch propeller, 16.5 inch tunnel length with model

Figure 43 0.5 second period triangular wave, +/-20.4 volts, 45° pitch propeller, 16.5 inch tunnel length with model

81
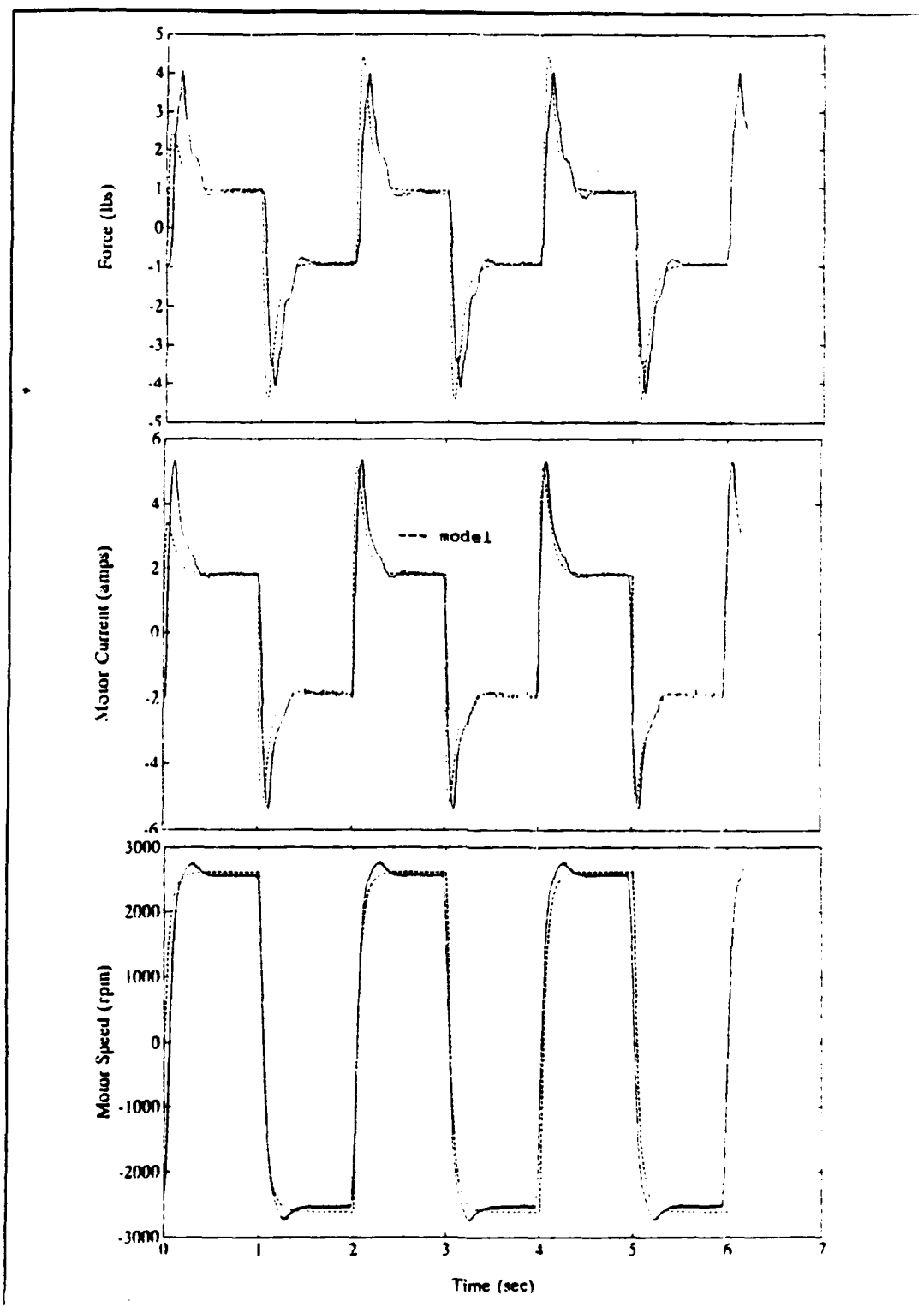
Figure 44 2 second period square wave, +/- 20.4 volts, 30° pitch propeller, 10.0 inch tunnel length with model
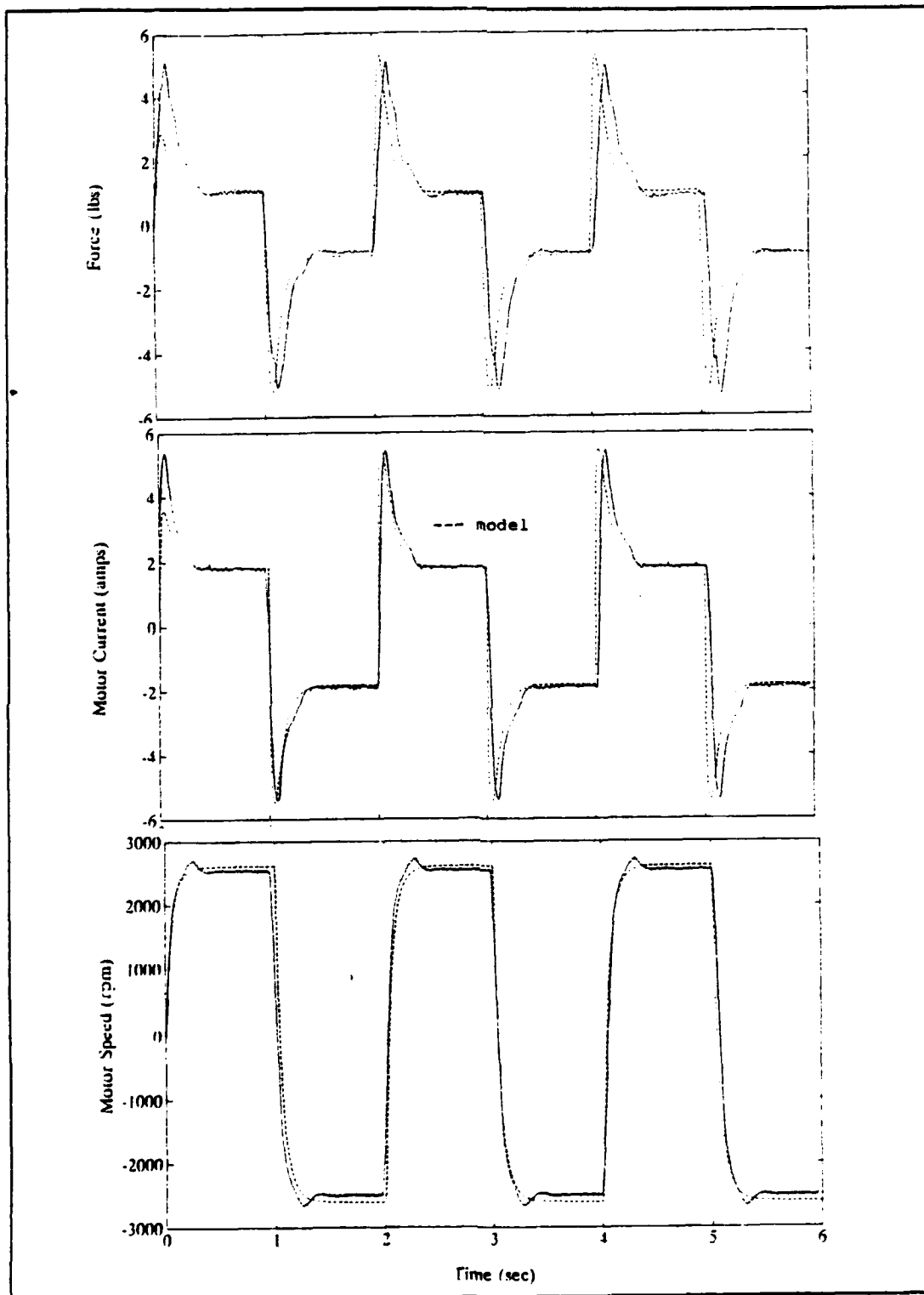
Figure 45 2 second period square wave, +/- 20.4 volts, 30° pitch propeller, 16.5 inch tunnel length with model

83
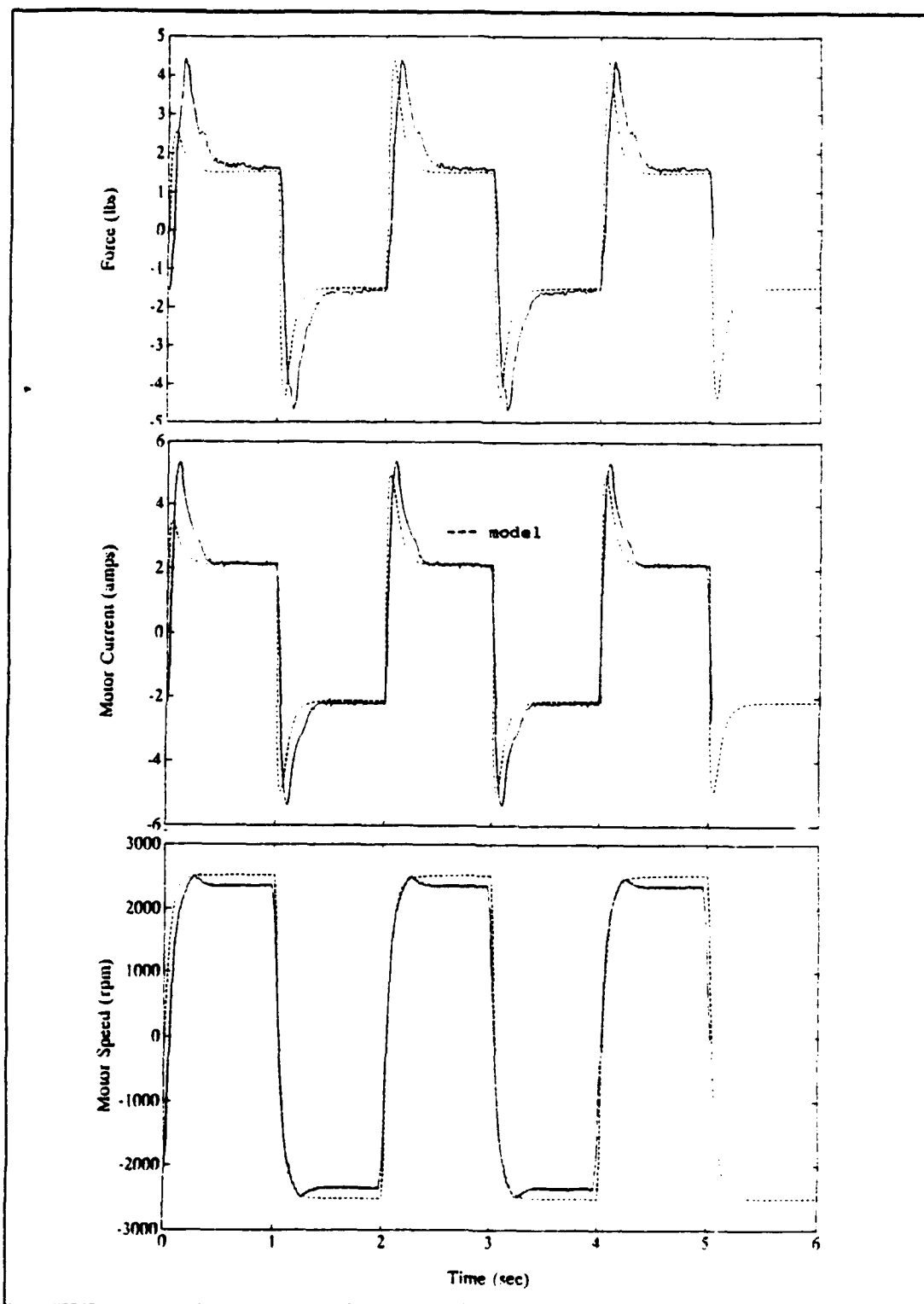
Figure 46 2 second period square wave, +/- 20.4 volts, 45° pitch propeller, 10.0 inch tunnel length with model
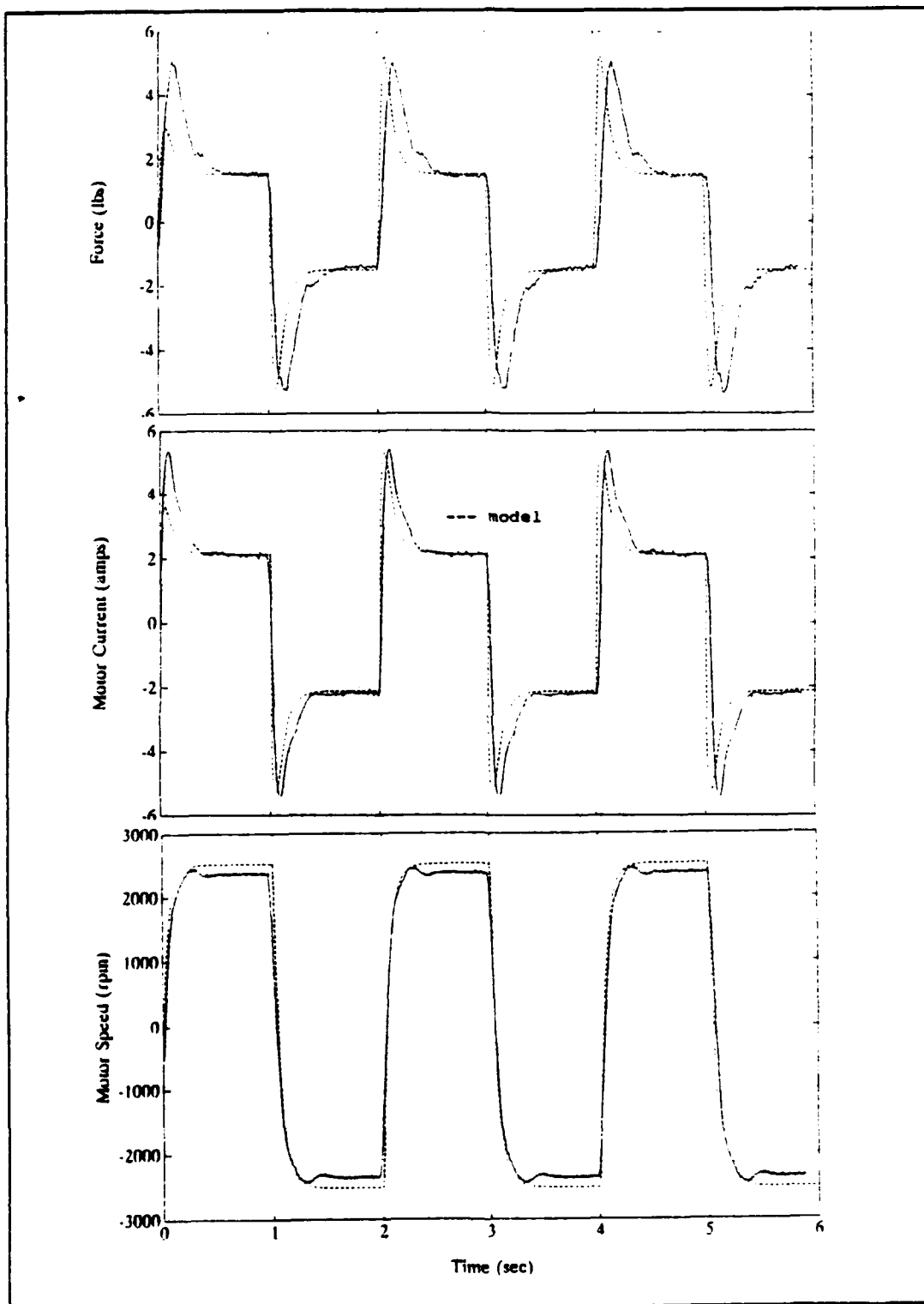
Figure 47 2 second period square wave, +/- 20.4 volts, 45° pitch propeller, 16.5 inch tunnel length with model

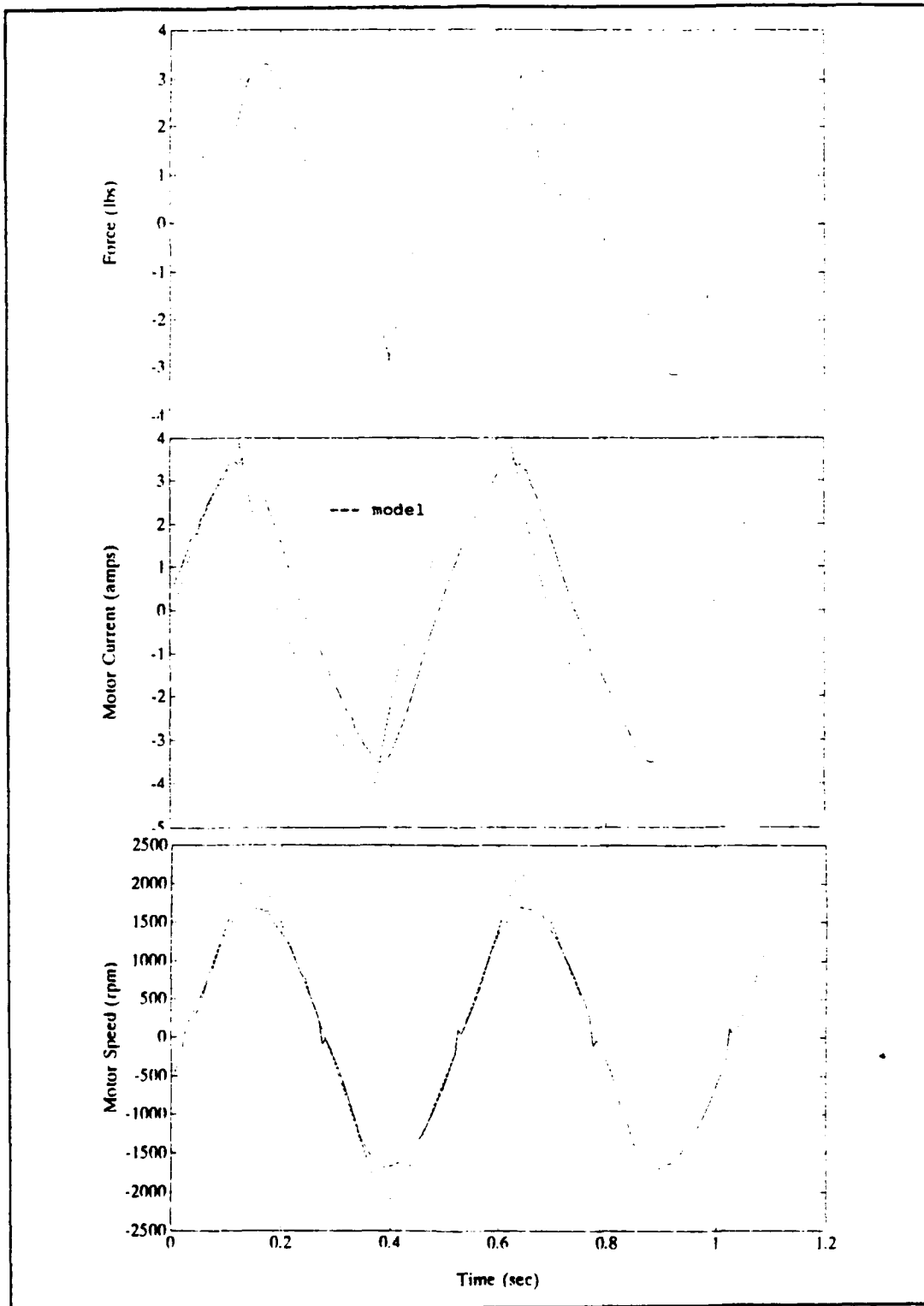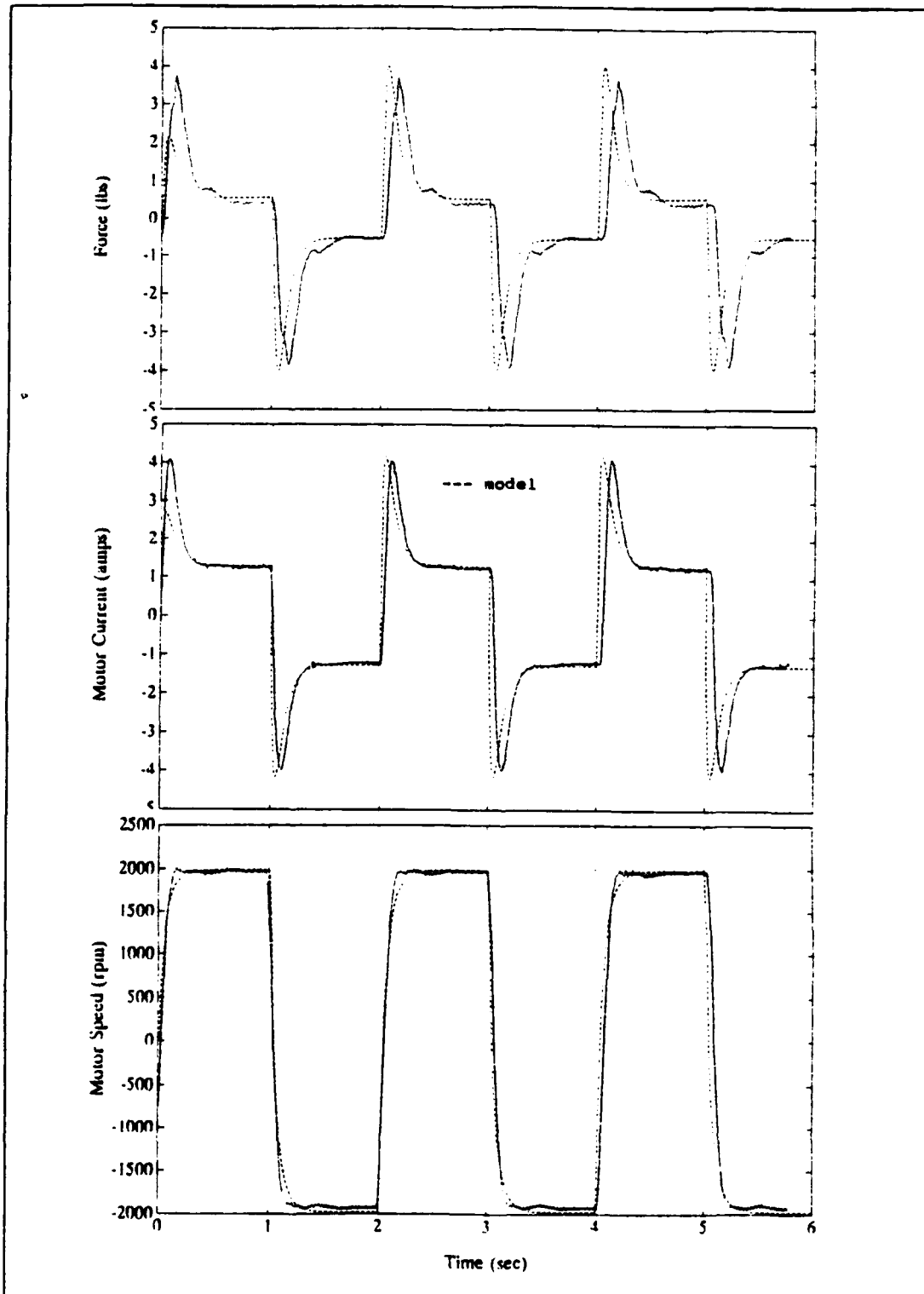**Figure 48** 2 second period square wave, +/- 18.4 volts, 30° pitch propeller, 16.5 inch tunnel length with model

VI. CONCLUSIONS

A. SUMMARY

From the experimental data it was seen that at steady state, the thruster force was proportional to the square of the motor (propeller) velocity, as expected. These steady state forces were also dependent upon the pitch of the propeller utilized and, to a lesser degree, the length of the thruster tunnel due to fluid friction. It was also shown that the choice of propeller influenced the motor current response due to the loading on the propeller. Tunnel length appeared to have no significant effect on the motor current response or the motor speed response.

As the conditions to which the thruster was subjected became more dynamic in nature, the influence of fluid inertia became more apparent, again, as expected. The effect of transient conditions dominated the force, motor current and motor speed responses during rapid changes in applied voltages.

Relating the hydrodynamic torque on the propeller to the thrust produced via the energy of the affected column of water, and including a propeller velocity/fluid velocity lag term, produced a model which accurately predicted the responses for thruster force, motor current and motor speed to

87

various input signals. Through trial and error comparison of the simulations generated by this model with experimental data, numerical values for the coefficients of the coupled, first order differential equations pertaining to the thruster system dynamics have been identified. Although the model does not reflect the effect of fluid friction or the effect of motor inductance, this model can reasonably be considered to represent the dynamics of tunnel thrusters.

B. RECOMMENDATIONS

As was seen in model simulation response to short period triangular waves and square wave input signals, the simulated force and motor current 'lead' those of the experimental data. It is conjectured that, increasing the time constant for the water column velocity (t_c) would have an effect of both reducing and delaying the peaks for the force and the motor current responses, while maintaining the response for the motor speed. Identifying the correct time constant would improve the overall accuracy of the model.

As alluded to in the introduction to this thesis, minimizing the limit cycling in underwater vehicle position control has been a problem for vehicle designers and operators. The use of this model for thrusters could reasonably be expected to improve thruster control, and ultimately, position control for ROVs and AUVs.

APPENDIX A

TABLE OF COEFFICIENTS

Coefficient	Symbol	Value	Units
Length	L	0.254 (10.0) 0.4191 (16.5)	meters
Propeller Efficiency (eta)	η	0.16 (30°) 0.095 (45°)	-
Propeller Pitch	p	0.0220 (30°) 0.0381 (45°)	m/rad
Momentum Correction Factor	$\Delta\beta$	4.0 (30°) 6.5 (45°)	-
Tunnel Cross Sectional Area	A	4.5604e-5	m^2
Motor Polar Moment of Inertia	J_M	1.63e-5	$kg\ m^2$
Pinion Polar Moment of Inertia	J_{DG}	0.3186e-5	$kg\ m^2$
Propeller Polar Moment of Inertia	J_P	3.4481e-5	$kg\ m^2$
Motor Shaft Friction	C_M	0.00025	-
Propeller Shaft Friction	C_P	0.0	-
Motor Electrical Resistance	R	1.73	ohms
Motor Back EMF Constant	K_M	0.055	volts/ (rad/sec)

Coefficient	Symbol	Value	Units
Motor Torque Constant	K_T	0.0551	Nm/A
Reduction Gear Ratio	N	2.0	-
Water Density	ρ	998.0	kg/m^3
Added Length	L_a	0.45	meters
Voltage Signal Time Constant	tau	0.03	-
Water Column Velocity Time Constant	t_c	0.06	-
Propeller Thrust Efficiency	σ	0.6	-
Propeller Blade Effective Length	L_B	0.0254	meters

APPENDIX B

```
%%%%%%%%%%%%%%%%%%%%%%%%%%%%%%%%%%%%%%%%%%%%%%%%%%%%%%%%%%%%%%%%%%
%
%
%   MATLAB PROGRAM: MODELT.M   (TRIANGULAR WAVE INPUT)
%
%   LCDR STEVEN E. CODY
%   NAVAL POSTGRADUATE SCHOOL, MONTEREY, CA.
%   DECEMBER 1992
%
%
%%%%%%%%%%%%%%%%%%%%%%%%%%%%%%%%%%%%%%%%%%%%%%%%%%%%%%%%%%%%%%%%%%

global T Vmax K0 K1 K2 K3 K4
global eta p N

%   Input Variables

T = input ('Enter desired time period "T" [e.g. 50.0]');
Vs = input ('Enter desired control voltage signal ...
            "Vs" [e.g. 9.0]');
L = input ('Enter 0.254 for 10.0 in. or 0.4191 for ...
            16.5 in. tube length (m)');
eta = input ('Enter 0.16 for 30 or 0.095 for 45 deg ...
            propeller efficiency (assumed)');
p = input ('Enter 0.0220 for 30 or 0.0381 for 45 deg ...
            propeller pitch (m/rad)');
delB = input ('Enter 4.0 for 30 or 6.5 for 45 deg ...
            propeller momentum correction (assumed)');

%   List Known Constants

Vmax = Vs * 2.272;
A = 4.5604e-3;
Jm = 1.63e-5;
Jdg = 0.3186e-5;
Jp = 3.4481e-5;
Cm = 0.00025;
Cp = 0.0;
R = 1.73;
Km = 0.055;
Kt = 0.0551;
N = 2.0:
Rho = 998.0;
Ma = 0.45;
```

```
%  Calculate Coefficients for Thruster System Dynamics

K0 = Cm + Cp/N^2 + Kt*Km/R;
K1 = Kt/R;
K2 = Jm + Jdg + Jp/N^2;
K3 = Rho*A*(L + Ma);
K4 = Rho*A*delB;

%  Calculate 'omega', 'F' and 'i'

t0=0.0; tf=T/2; x0=[0.0;0.0];
[t,x]=ode459'omegat',t0,tf,x0);
[m,n]=size(t);
        for i=1:m, t1(i)=t(i); x1(i,:)=x(i,:);
            [xdot,v]=omegat(t1(i),x1(i,:));
            Udot(i)=xdot(1); U(i)=x(i,1);
            wmdot(i)=xdot(2); wm(i)=x(i,2);
            vs(i)=v;
            F(i)=K3*Udot(i)+K4*U(i)*abs(U(i));
            a(i)=(vs(i)-Km*wm(i))/R;
        end;


t0=T/2; tf=T; x0=x1(i,:);
[t,x]=ode459'omegat',t0,tf,x0);
[l,n]=size(t);
        for i=(m+1):(l+m), t1(i)=t(i-m); x1(i,:)=x(i-m,:);
            [xdot,v]=omegat(t1(i),x1(i,:));
            Udot(i)=xdot(1); U(i)=x1(i,1);
            wmdot(i)=xdot(2); wm(i)=x1(i,2);
            vs(i)=v;
            F(i)=K3*Udot(i)+K4*U(i)*abs(U(i));
            a(i)=(vs(i)-Km*wm(i))/R;
        end;

t0=T; tf=T*1.5; x0=x1(i,:);
[t,x]=ode459'omegat',t0,tf,x0);
[k,n]=size(t);
        for i=(m+l+1):(k+l+m), t1(i)=t(i-m-l); ...
                                x1(i,:)=x(i-m-l,:);
            [xdot,v]=omegat(t1(i),x1(i,:));
            Udot(i)=xdot(1); U(i)=x1(i,1);
            wmdot(i)=xdot(2); wm(i)=x1(i,2);
            vs(i)=v;
            F(i)=K3*Udot(i)+K4*U(i)*abs(U(i));
            a(i)=(vs(i)-Km*wm(i))/R;
        end;
```

92

```
%%%%%%%%%%%%%%%%%%%%%%%%%%%%%%%%%%%%%%%%%%%%%%%%%%%%%%%%%%%%%%%%%%%%%
%
%
%   MATLAB PROGRAM: MODELS.M   (SQUARE WAVE INPUT)
%
%   LCDR STEVEN E. CODY
%   NAVAL POSTGRADUATE SCHOOL, MONTEREY, CA.
%   DECEMBER 1992
%
%
%%%%%%%%%%%%%%%%%%%%%%%%%%%%%%%%%%%%%%%%%%%%%%%%%%%%%%%%%%%%%%%%%%%%%

global T Vmax K0 K1 K2 K3 K4
global eta p N

%   Input Variables

T = input ('Enter desired time period "T" [e.g. 50.0]');
Vs = input ('Enter desired control voltage signal ...
            "Vs" [e.g. 9.0]');
L = input ('Enter 0.254 for 10.0 in. or 0.4191 for ...
            16.5 in. tube length (m)');
eta = input ('Enter 0.16 for 30 or 0.095 for 45 deg ...
            propeller efficiency (assumed)');
p = input ('Enter 0.0220 for 30 or 0.0381 for 45 deg ...
            propeller pitch (m/rad)');
delB = input ('Enter 4.0 for 30 or 6.5 for 45 deg ...
            propeller momentum correction (assumed)');

%   List Known Constants

Vmax = Vs * 2.272;
A = 4.5604e-3;
Jm = 1.63e-5;
Jdg = 0.3186e-5;
Jp = 3.4481e-5;
Cm = 0.00025;
Cp = 0.0;
R = 1.73;
Km = 0.055;
Kt = 0.0551;
N = 2.0:
Rho = 998.0;
Ma = 0.45;
```

```
%  Calculate Coefficients for Thruster System Dynamics

K0 = Cm + Cp/N^2 + Kt*Km/R;
K1 = Kt/R;
K2 = Jm + Jdg + Jp/N^2;
K3 = Rho*A*(L + Ma);
K4 = Rho*A*delB;

%  Calculate 'omega', 'F' and 'i'

t0=0.0; tf=T/2; x0=[0.0;0.0];
[t,x]=ode459'omegaS',t0,tf,x0);
[m,n]=size(t);
     for i=1:m, t1(i)=t(i); x1(i,:)=x(i,:);
         [xdot,v]=omegat(t1(i),x1(i,:));
         Udot(i)=xdot(1); U(i)=x(i,1);
         wmdot(i)=xdot(2); wm(i)=x(i,2);
         vs(i)=v;
         F(i)=K3*Udot(i)+K4*U(i)*abs(U(i));
         a(i)=(vs(i)-Km*wm(i))/R;
     end;
```

APPENDIX D

```
%%%%%%%%%%%%%%%%%%%%%%%%%%%%%%%%%%%%%%%%%%%%%%%%%%%%%%%%%%%%%%%%%%%
%
%
%   MATLAB PROGRAM: OMEGAT.M (SPEED FUNCTION FOR MODELT.M)
%
%   LCDR STEVEN E. CODY
%   NAVAL POSTGRADUATE SCHOOL, MONTEREY, CA.
%   DECEMBER 1992
%
%
%%%%%%%%%%%%%%%%%%%%%%%%%%%%%%%%%%%%%%%%%%%%%%%%%%%%%%%%%%%%%%%%%%%

function [xdot,v] = omegat(t,x)

%   List Constants

tau = 0.03; tc = 0.06; sigma = 0.6; Lb = 0.0254;

%   Generate Triangular Wave Voltage Signal

if t<T/4,    v=(Vmax*(1-exp(-t/tau))/(T/4))*t; end;
if T/4<=t,   v= Vmax-(2*Vmax*(1-exp(-(t-T/4)/tau)) ...
                *(t-T/4)/(T/2); end;
if 3*T/4<=t, v=-Vmax+(2*Vmax*(1-exp(-(t-3*T/4)/tau)) ...
                *(t-3*T/4)/(T/2); end;
if 5*T/4<=t, v= Vmax-(2*Vmax*(1-exp(-(t-5*T/4)/tau)) ...
                *(t-5*T/4)/(T/2); end;

%   Initialize the Velocity Vectors

U=x(1); wm=x(2); wp=x(2)/N;

%   Calculate the Acceleration Vectors

Udot=(-U+(eta*p)*wp)/tc;

F=K3*Udot+K4*U*abs(U);

wmdot=-(K0/K2)*wm+(k1/K2)*v-(sigma*Lb*F)/(N*K2);

%   Return the acceleration terms

xdot=[Udot;wmdot];
```

APPENDIX E

```
%%%%%%%%%%%%%%%%%%%%%%%%%%%%%%%%%%%%%%%%%%%%%%%%%%%%%%%%%%%%%%%%%%%%%%%%
%
%
%   MATLAB PROGRAM: OMEGAS.M (SPEED FUNCTION FOR MODELS.M)
%
%   LCDR STEVEN E. CODY
%   NAVAL POSTGRADUATE SCHOOL, MONTEREY, CA.
%   DECEMBER 1992
%
%
%%%%%%%%%%%%%%%%%%%%%%%%%%%%%%%%%%%%%%%%%%%%%%%%%%%%%%%%%%%%%%%%%%%%%%%%

function [xdot,v] = omegas(t,x)

%   List Constants

tau = 0.03; tc = 0.06; sigma = 0.6; Lb = 0.0254;

%   Generate Square Wave Voltage Signal

if t<T/2,      v=(Vmax*(1-exp(-t/tau))); end;
if T/2<=t,     v= Vmax-(2*Vmax*(1-exp(-(t-T/2)/tau))); end;
if T<=t,       v=-Vmax+(2*Vmax*(1-exp(-(t-T)/tau))); end;
if 3*T/2<=t,   v= Vmax-(2*Vmax*(1-exp(-(t-3*T/2)/tau))); end;
if 2*T<=t,     v= Vmax-(2*Vmax*(1-exp(-(t-2*T)/tau))); end;
if 5*T/2<=t,   v=-Vmax+(2*Vmax*(1-exp(-(t-5*T/2)/tau))); end;
if 3*T<=t,     v= Vmax-(2*Vmax*(1-exp(-(t-3*T)/tau))); end;

%   Initialize the Velocity Vectors

U=x(1); wm=x(2); wp=x(2)/N;

%   Calculate the Acceleration Vectors

Udot=(-U+(eta*p)*wp)/tc;

F=K3*Udot+K4*U*abs(U);

wmdot=-(K0/K2)*wm+(k1/K2)*v-(sigma*Lb*F)/(N*K2);

%   Return the acceleration terms

xdot=[Udot;wmdot];
```

LIST OF REFERENCES

1. Yoerger, D.R., Cooke, J.G., and Slotine, J.-J.E., "The Influence of Thruster Dynamics on Underwater Vehicle Behavior and Their Incorporation into Control System Design," _IEEE Journal of Oceanic Engineering_, Volume 15, Number 3, pp. 167-177, July 1990.

2. Cooke, J.G., _Incorporating Thruster Dynamics in the Control of an Underwater Vehicle_, Master's Thesis, Massachusetts Institute of Technology, Cambridge, Massachusetts, September 1989.

3. McLean, M.B., _Dynamic Performance of Small Diameter Tunnel Thrusters_, Master's Thesis, Naval Postgraduate School, Monterey, California, March 1991.

4. Miles, D., Burton, D., Lee, M., and Rock, S., _Closed Loop Force Control of an Underwater Thruster_, Monterey Bay Aquarium Research Institute/Stanford Aerospace Robotics Laboratory, Monterey/Palo Alto, California, October 1992.

5. Adams, J.C., Burton, D., and Lee, M., _Dynamic Characterization and Control of Thrusters for Underwater Vehicles_, Monterey Bay Aquarium Research Institute/Stanford Aerospace Robotics Laboratory, Monterey/Palo Alto, California, September 1991.

6. Pittman Division of Penn Engineering and Manufacturing Corporation Bulletin 14000, _PITMO D--C Servo Motors_, June 1987.

7. Winfred M. Berg, Incorporated, Catalog, _BERG Precision Mechanical Components B8_, 1988.

8. _Principles of Naval Architecture_, E. V. Lewis, editor, 2ND Rev., Vol. 2, pp. 131-143, Society of Naval Architects and Marine Engineers, 1988.

INITIAL DISTRIBUTION LIST

1. Defense Technical Information Center   2
   Cameron Station
   Alexandria, VA   22304-6145

2. Library, Code 052   2
   Naval Postgraduate School
   Monterey, CA   93943-5000

3. Chairman, Code ME/KK   1
   Department of Mechanical Engineering
   Naval Postgraduate School
   Monterey, CA   93943-5000

4. Naval Engineering Curricular Office, Code 34   1
   Naval Postgraduate School
   Monterey, CA   93943-5000

5. Dr. Anthony J. Healey, Code ME/HY   2
   Department of Mechanical Engineering
   Naval Postgraduate School
   Monterey, CA   93943-5000

6. LCDR Steven E. Cody   1
   4613 Ware Creek Road
   Williamsburg, VA   23188

7. Dr. Dana Yoerger   1
   Woods Hole Oceanographic Institute
   Woods Hole, MA   02543

8. Chris Agoras/Chris Hellenbaum   1
   Naval Underwater Systems Center (NUSC)
   Newport, RI   02841-5047

9. RADM Evans, Code SEA92   1
   Naval Sea Systems Command
   Washington, DC   20362

10. Dick Blidberg   1
    Marine Systems Engineering Lab
    SERB Building 242
    University of New Hampshire
    Durham, NH   03824

11. Mr. Mike Lee   1
    Monterey Bay Aquarium Research Institute
    160 Central Avenue
    Pacific Grove, CA   93950

12. Mr. Gary Trimble   1
    Lockheed Marine Systems Division
    P.O. Box 3504
    Sunnyvale, CA   94088